INFORMATION TO USERS

This manuscript has been reproduced from the microfilm master. UMI films the text directly from the original or copy submitted. Thus, some thesis and dissertation copies are in typewriter face, while others may be from any type of computer printer.

The quality of this reproduction is dependent upon the quality of the copy submitted. Broken or indistinct print, colored or poor quality illustrations and photographs, print bleedthrough, substandard margins, and improper alignment can adversely affect reproduction.

In the unlikely event that the author did not send UMI a complete manuscript and there are missing pages, these will be noted. Also, if unauthorized copyright material had to be removed, a note will indicate the deletion.

Oversize materials (e.g., maps, drawings, charts) are reproduced by sectioning the original, beginning at the upper left-hand corner and continuing from left to right in equal sections with small overlaps.

Photographs included in the original manuscript have been reproduced xerographically in this copy. Higher quality 6" x 9" black and white photographic prints are available for any photographs or illustrations appearing in this copy for an additional charge. Contact UMI directly to order.

ProQuest Information and Learning
300 North Zeeb Road, Ann Arbor, MI 48106-1346 USA
800-521-0600

Modeling and Control of Antilock Braking Systems Utilizing Dynamic Friction Tire Model

By

Xiang Gao

A Thesis
in
The Department
of
Mechanical and Industrial Engineering

Presented in Partial Fulfillment Of the Requirements
for the Degree of Master of Applied Science at
Concordia University
Montreal, Quebec, Canada

November 2001

ABSTRACT

Modeling and Control of Antilock Braking Systems Utilizing Dynamic Friction Tire Model

Xiang Gao

The development of high-performance antilock braking systems that provide reliability, steerability, and stability during braking in different road conditions, i.e., wet, icy or dry road surface, has attracted much attention in the automobile industry. This thesis addresses the controller designs for antilock braking systems (ABS) in vehicles. Simplified quarter vehicle models with special emphasis on the modeling of tire and dynamic tire-road interaction is utilized to develop and test the proposed controllers.

The novelty of the present research is in the utilization and formulation of a new dynamic friction tire model for the development and testing of designed controller. Due to complex mechanics of tires, the dynamic friction tire model is significantly more realistic than that of commonly used static friction tire model. A detailed comparison of dynamic friction tire model with that of well-known magic formula and experimental data is carried out to demonstrate the effectiveness of the proposed formulation. Using this dynamic tire model, two methods for control of ABS system are proposed in this thesis, i.e., proportional-plus-integral (PI) control and the sliding mode control. Utilizing the PI controller design, the difficulty associated with on-line search of the optimal longitudinal slip can be easily overcome with the help of the dynamic friction tire model, which solves a commonly existed problem in the PI controller design. To show the advantage of the new dynamic tire model, a robust sliding mode control algorithm is also developed for the quarter vehicle model. The global stability of this control scheme is established by using the stability theory. Extensive simulation studies have been conducted for the developed controllers to demonstrate the effectiveness of the proposed control schemes. The investigation further demonstrates the effectiveness and convenience of utilizing dynamic friction tire model for the development of ABS controllers.

ACKONWLEDGEMENTS

The author wishes to express his sincere gratitude and appreciation to his supervisors, Dr. C.-Y. Su and Dr. A. K. W. Ahmed, for their wisdom, constant encouragement, and continuous guidance throughout the research. The author thanks Dr. C.-Y. Su and Dr. A. K. W. Ahmed for the financial support that enabled the author to pursue his graduate studies.

The author would like to thank his parents for their love and enlightening education during his early years in the countryside of China. The author also thanks his wife, Yang Sui, for her endless love, limitless energy, and support.

Special thanks go to all the friends at Concave Research Center for their friendship, help, and the good times they have spent together.

TABLE OF CONTENTS

LIST OF TABLES

Table

LIST OF FIGURES

Figure

LIST OF ABBREVIATIONS AND SYMBOLS

Symbol	Description
ABS:	antilock braking system
A_f :	vehicle frontal area
C_d :	vehicle drag coefficient
C_i :	parameters that characterize the magic formula $(i = 1, 2, 3, 4)$
F, F_x, F_t :	longitudinal force at tire-road interface
F_a :	aerodynamic drag force
F_f :	tire rolling resistance
F_L :	load transfer between axle under deceleration
F_n, F_z:	normal tire force
$F(s)$:	friction force as a function of slip (skid)
f_0 :	basic coefficient
f_s :	speed effect coefficient
g :	gravitational acceleration
h_{cg}:	center of gravity height
i_s :	definition for braking skid
J_e :	engine inertia
J_t :	wheel inertia
J_w, J :	effective wheel inertia
K_a :	control gain in slide mode
K_b :	brake coefficient gain

K_{mph}:	speed scaling constant
l :	wheel base
L :	tire/road contact length
m :	quarter vehicle mass
m_t :	tire mass
m_{car}:	vehicle mass
P_b :	braking pressure
R_w , r :	wheel radius
s :	longitudinal slip
$\tilde{s}$:	sliding surface
T_b :	Braking torque
v :	forward velocity of the vehicle
v_r :	relative velocity
v_s :	stribeck velocity
z :	internal state in dynamic tire model
ξ	transmission gear ratio
ρ :	air density
σ_0 :	rubber longitudinal stiffness
σ_1 :	rubber longitudinal damping
σ_2 :	viscous relative damping
σ_ω :	viscous resistance moments experienced by the wheels
μ_s :	normalized static friction coefficient

μ_c : normalized Coulomb friction

$\mu(\lambda)$: tire/road adhesion coefficient as function of skid

λ : longitudinal skid

λ_{max} : maximum longitudinal skid

λ_{peak} : longitudinal skid at peak adhesion

λ_{ref} : reference longitudinal skid in PI controller

ω : angular velocity of the wheel

θ : road condition parameter

CHAPTER I
INTRODUCTION

1.1 Problem statement

Automobile braking performance is the most important vehicle characteristics that affect its safety. Since the braking force is developed at the tire/road interface, tire mechanics and tire/road friction play a major role in the braking performance of the road vehicles. Braking efficiency is commonly defined as the extent to which the vehicle utilizes the available coefficient of road adhesion. For pneumatic tires, the maximum utilization corresponds to around 20% skid condition of the tire. If the wheels are, however, locked causing 100% skid, the coefficient of road adhesion falls to its sliding value which is lower. Furthermore, the mobilization of available adhesion by the braking effort leads to loss of lateral or cornering force that may be needed for handling of the vehicle. Brake designers are, therefore, challenged to develop systems that will prevent wheels from locking and ideally keep the tire skid within desired level regardless of the road condition. State-of-the-art technology in the brakes, backed-up by electronic control engineering provides for reliable steerability and stability when braking provided that the physical limits are not exceeded.

Today's modern automobiles and commercial vehicles are equipped with reliable, high-performance brake systems which ensure efficient braking even at very high speeds. However, the behavior of a vehicle has to be carefully considered when a driver brakes in an emergency in an attempt to avoid an accident, where the driver applies his brakes as

hard and as rapidly as possible. It has been shown that even the best brakes cannot prevent a driver from hitting the brake pedal too hard when faced by severe road conditions or a panic situation. Moreover, for low road adhesion coefficient, such as those corresponding to snow or wet road, proper control the braking forces applied to each tire to prevent them from locking becomes vitally important.

Under above circumstances, the antilock braking system (ABS) controls the braking force at each wheel to ensure that the driver not only retains steerability, but also full control of the vehicle. According to the statement of ABS in [1], "The antilock braking system is the aggregate of all those components within the service-brake system responsible for providing closed-loop control of wheel-slip rates at one or several wheels during braking manoeuvres." Therefore, it is obvious that ABS contributes to keeping the vehicle stable and steerable.

The primary components in a base brake system include the master cylinder, the brake assist boost, brake force valve, and brake calipers or slave cylinder. The driver's commanded brake pedal force assisted by brake boost develops pressure in the system: The brake force valve proportions the brake pressure to the front and rear wheels to compensate for differing axle loadings; The pressure is transmitted to force through calipers or slave cylinders to achieve brake at the wheels. Antilock braking systems (ABS) supplement this base system with an electro-mechanical hydraulic modulator, four wheel speed sensors, and an electronic controller as shown in Figure 1.1. The controller monitors each wheel speed signal for the onset of wheel lockup during braking maneuvers, and if present, regulates the brake pressure to that wheel.

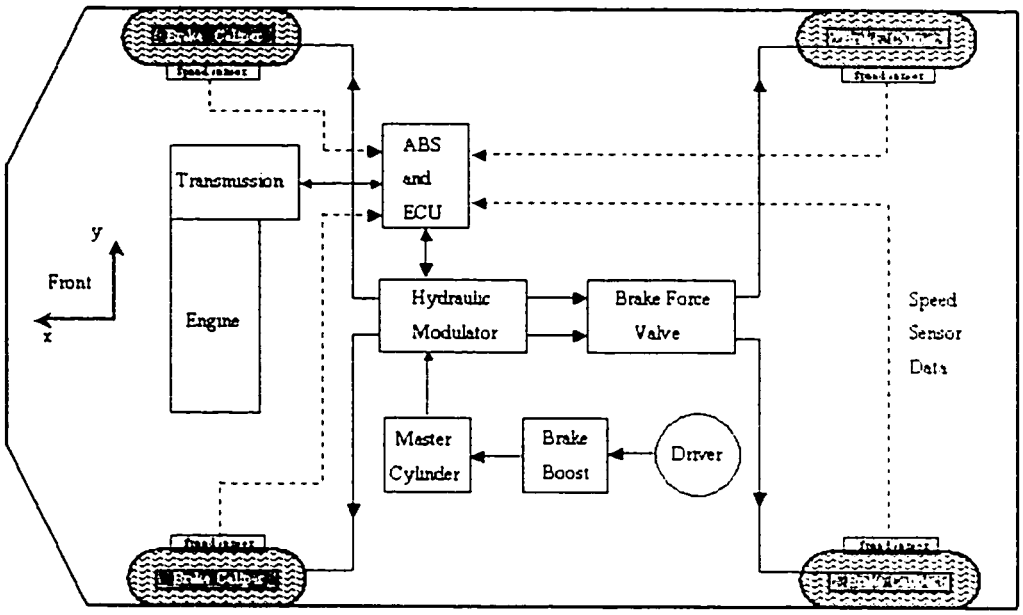

Fig. 1.1 Light to medium-duty vehicle with ABS

In fact, ABS has to be a closed-loop control system which can adjust the control variable (brake pressure) frequently based on the feedback that can be easily achieved on-line. If wheel lock is detected, the pressure in one or more of the cylinder is reduced until the wheel speed exceeds a predetermined value, at which time the pressure is increased. And the system continues this cycle until the vehicle comes to a total stop or close to a stop. Typical ABS control loop is shown in Fig. 1.2 and consists of the following component [1]:

Controlled system: vehicle with wheels, wheel brakes and braking force between tires and road surface.

Disturbance factors: road-surface conditions, brake condition, vehicle load and tires.

Controller: wheel-speed sensors and ABS control unit.

Controlled variables: wheel-speed, and the data derived from it on deceleration at the tires' periphery, peripheral wheel acceleration and brake skid.

Reference input variable: pressure applied to brake pedal (driver's brake-pressure input.

Manipulated variable: braking pressure at wheels

.

Selection of suitable controlled variables is a major factor in deterring the efficiency of ABS control. The basis is provided by the signals from the wheel-speed sensors, which the control unit (ECU) employs to calculate the wheel's peripheral deceleration, tire skid, and reference speed. The skid of the tire (i_s), which is the difference between the forward velocity and velocity due to rolling, can be easily defined as:

$$i_s = (1 - \frac{r\omega}{v}) \times 100\%$$

where, r is the effective radian of the wheel, ω is the angular velocity of the wheel, and v is the linear velocity of the wheel or vehicle. In practice, the skid of the tire is difficult to determine accurately, primarily due to the lack of a practical and cost-effective means to directly measure the linear speed of the tire center during braking. The control logic of an antilock device, therefore, is usually formulated based on some easily measurable parameters, such as the angular speed and angular deceleration or acceleration of the tire and linear deceleration of the vehicle.

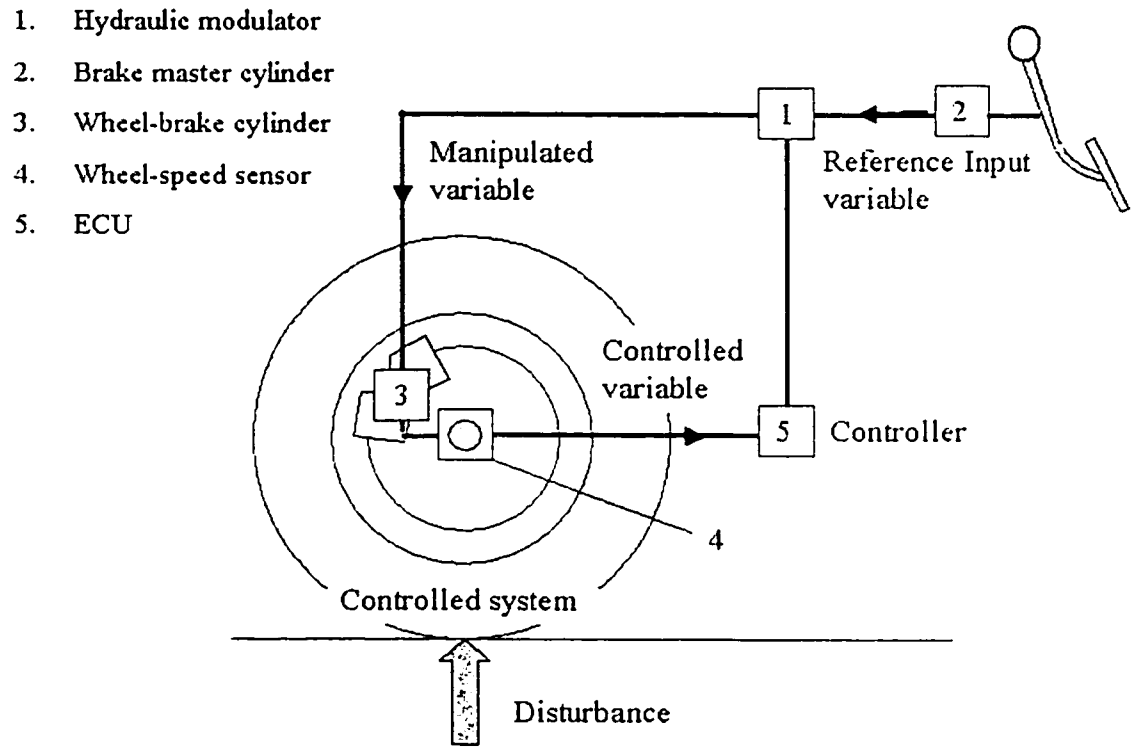

Fig. 1. 2 ABS Control Loop

Since both skid and braking forces are developed by the tire and tire/road interaction, a reliable and accurate tire model is an essential element in all ABS design and analysis. One of the most well-known tire model is Pacejka's "magic formula" model. This model has been shown to suitably match experimental data, and has been used in most of the investigation of the ABS. The F(s) map in the "magic formula", however, is a static function that has some limitations in the dynamic tire model analysis. As an alternative to the static F(s) maps, a dynamic tire model was developed that can suitably describe the road/tire contact friction. Dynamic models can be formulated as a lumped and distributed models, and is suitable for design and analysis of ABS controllers. The detailed description of the tire model will be given in Chapter III.

Other than a reliable and realistic tire model, the scheme for the controllers largely dictates the realization and reliability of a designed ABS system. The three common approaches to develop ABS controller are: a) Common Phase Plane; b) Sliding Mode Control methods, also named Variable Structure Control (VSC or VSS); c) Modified Sliding Mode Control methods. These controllers using the static friction tire model have limitation that can be overcome by utilizing dynamic friction tire model. The detailed review for the three methods will be given in Chapter II.

1.2 Objectives and organization of the thesis

The goal of this thesis is to design an on-line scheme for ABS controller to estimate the vehicle's tire/road friction characteristics and the overall gain of the braking system. The wheel relative velocity that achieves maximum braking effort in a quasi-static LuGre friction model solution is estimated on line. This information is used to design a controller that achieves near-maximum braking effort. Two methods, namely PI and Sliding Mode Control method, are used in this thesis to develop the ABS controllers. The speed-dependent, dynamic friction models are also introduced in this thesis that can be used to describe the tire/road interaction.

The work carried out and the results obtained are organized in this thesis as follows:

Chapter II gives the literature review that consists of seven parts: a) historical overview; b) basic ABS; c) control algorithms of ABS; d) tire model; e) vehicle model; f) test and simulation techniques. The first two parts give the brief review of ABS, from

the first introduction of ABS to current state of the art. In part 3, the development of three common ABS control algorithms are reviewed. The different type of tire models used for different purposes are described in part 4. Finally, the review of the vehicle model along with simulation techniques are presented in part 5.

Chapter III fully analyzes the dynamic friction tire model and vehicle model used in this thesis. The relationship between the dynamic friction model and "magic formula" is also given in this chapter. From the curve of the friction coefficient via longitudinal slip, it is shown that the dynamic friction model can match with "magic formula" and experimental data perfectly. Furthermore, it is convenient to develop control algorithm by using mathematical method based on this type of tire model. This chapter finalizes the vehicle and tire models that are utilized in the controller design discussed in Chapter IV and Chapter V.

In Chapter IV, the PI controller for the ABS system is developed. In the PI designing process, a simple vehicle model with dynamic tire model is utilized, which permitted a search for optimal longitudinal skid value at each step, while braking force remained a function of the longitudinal skid. Furthermore, the controlled variables in the vehicle dynamics are linear velocity and angular velocity of the vehicle. The performance of ABS with PI controller developed in this section is evaluated through simulations and the results are discussed in this chapter.

In Chapter V, Sliding Mode Control method for the system is developed. In the slide mode controller, the dynamic friction tire model is incorporated into the vehicle model, where the braking force is not taken as a common function of the longitudinal skid. In this case, the braking force is related to an introduced internal state while the

controlled variables are changed to velocity and relative velocity. This presents an opportunity to design controllers of ABS based on new variables. In this design, the selection of the proper sliding surface for the controller is very important as it dictates the efficiency of the controllers. This part of the study considers velocity and relative velocity as variables to build sliding surface for the controllers. The performance achieved through ABS controllers presented here is demonstrated through simulations. The results of simulations are finally discussed in this chapter.

Finally, Chapter VI presents highlight of the present investigations, important conclusions and a list of recommendation for further work in this area.

CHAPTER II

LITERATURE REVIEW

2.1 Historical Overview

The concept of anti-lock brake systems (ABS) dates back to the 1930s, but has only become truly practical with development of electronics for modern vehicle system. ABS are now used on more and more passenger cars and light trucks. They are optionally available on some commercial vehicles equipped with air brakes.

Development of ABS brakes, one of the few truly outstanding safety features in the history of the motor vehicle, resulted in the Dunlop "Maxaret" fitted to aircrafts in 1952. In 1972 in England, the Jensen Interceptor automobile became the first production car to offer a Maxaret-based ABS using a propeller shaft speed sensor and viscous coupling. In the U.S., vehicle manufacturers worked with various brake manufacturers to develop ABS systems. In 1969, a rear-wheel-only ABS developed by Ford and Kelsey Hayes was offered on the Thunderbird. Chrysler and Bendix produced a four-wheel ABS offered on the 1971 Imperial. General Motors likewise offered the feature on some of their luxury models by the mid-1970s.

The basic shortcomings of the early ABS brakes revolved around low reliability of system electronics, and to some extent slow cycles rates due to limitations associated with the vacuum source. These reasons, and probably low public awareness and additional cost to the buyer, led to their quiet withdrawal from the market in the mid-1970s.

In the early 1970s the National Highway and Traffic Safety Administration (NHTSA) of the U.S. Department of Transportation issued a regulation (FMVSS121) which indirectly required the installation of ABS brakes on air-brake-equipped trucks and trailer by 1975 [2].

In Europe during the early and mid-1970s, brake and electronics suppliers had developed digital electronics changing from analog to integrated circuits and microprocessors which resulted in the introduction of the first Bosch ABS systems on Mercedes passenger vehicles in 1978 [2].

In 1984, an integrated ABS produced by ITT-Teves was introduced on the Lincoln Mark VII in the U.S. and , in 1985, as standard equipment on the Ford Scorpio in Germany [2].

Since the late 1980s and early 1990s, ABS started to appear on nearly all top models of every manufacturer including four-wheel systems for four-wheel-drive vehicles developed by Bendix and others.

By the year 1991, automobile manufacturers offered ABS brakes on approximately one-third of their passenger vehicles. With the development of economical sensors and electric processors, practically all passenger cars and light trucks are now equipped with four-wheel ABS.

2.2 Basic ABS

The primary function of an antilock brake system is to prevent the tire from locking, and ideally to keep the skid of the tire within a desired range. This will ensure

that the tire can develop a sufficiently high braking force for stopping the vehicle, and at the same time it can retain an adequate cornering force for directional control and stability. Under normal braking conditions the driver operates the brakes as usual; however, on slippery roadways or during severe braking, as the driver causes the wheels to approach lockup, the ABS takes over and modulate brake line pressure and hence braking force, during braking.

From the above statement, one may see that ABS must satisfy a wide range of requirements, with particular emphasis on safety considerations regarding dynamic braking response on a very wide range of operating and environmental conditions [1]:

- The closed-loop brake control system must be capable of maintaining steering response and vehicle stability at all times, regardless of road conditions (extending from dry, high-friction surfaces to glare ice).
- ABS should be capable of exploiting the adhesion between tires and road surface to maximize its effect, with the proviso that vehicle stability and maintenance of steering response have a higher or equal priority to that of minimizing stopping distances. These requirements must be fulfilled regardless of whether the driver applies full force immediately, or gradually increases the pedal pressure up to the wheel-lock limit.
- The brake control system must remain operational throughout the vehicle's entire speed range. It must be effective down to walking speed (after which wheel lock is no longer a critical factor in the final distance until the vehicle stops).
- The brake control system must be capable of rapid adaptation to changes in surface traction. For example, on dry roads with occasional ice patches, any wheel lock must

be restricted to such brevity that vehicle stability or steering response cannot be impaired. The adhesion on the dry road sections must simultaneously be fully exploited for maximum effectiveness.

- When the brakes are applied on road surfaces affording different traction levels on the two sides of the vehicle (e.g., right tire on ice, left tire on dry asphalt, referred to as "μ-split"), the unavoidable yaw effect (rotational forces centered at the vehicle's vertical axis tending to turn the vehicle sideways) should be slowed to the point where it will be no problem for an average driver to initiate compensatory countersteer.
- During cornering, the vehicle should retain stability and steering response while also braking in the shortest possible distance, the proviso here being that the vehicle's speed remains sufficiently below the cornering limit velocity (the cornering limit velocity is defined as the highest speed at which a vehicle can negotiate a curve of a defined radius without throttle input, and without leaving the defined circle).

2.3 Control Algorithms of ABS

Design of ABS controllers is a difficult task from the traditional approaches of intuitive design, test evaluation and analytical derivation. Some reasons for this are uncertainty in measured inputs, the wide variety of performance conditions that must be addressed, and sample intervals for sensor measurements that are greater than 5 milliseconds. The control algorithms of existing ABS were mostly developed through iterative laboratory experiments and engineering tests. There are some theoretical and

systematic studies that addresses conventional ABS. Guntur [3] and Ouwerkerk [4] listed and studied several criteria used in ABS: some for predicting the occurrence of lock-up of wheels and others for reapplying brakes while the danger of lock-up is averted. On the other hand, frequency domain methods such as the describing function method by Flin and Fenton [5] and a classical feedback control approach by Zellner [6] were used to analysis and design ABS. The ABS dynamics, however, are inherently nonlinear as can be identified from the frequency domain investigations. Trade-offs among a large number of design criteria must therefore be studied and optimized. A Quasi-Monte Carlo multi-criteria optimization method recently introduced in [7], and [8] is used to optimize and compare ABS control strategies.

A variety of ABS control algorithms have been published. Most algorithms utilize the wheel speed, vehicle velocity, and deceleration as state variables; some measure vehicle deceleration while others estimate it. Some algorithms also include estimated line pressures and steering input as state variables. The three algorithms used in the present study are :

Common Phase Plane;

Sliding Mode Control methods;

Modified Sliding Mode Control methods.

The algorithms are adapted to a simulated controller capable of five outputs:

fast pressure release;

slow pressure release;

fast pressure apply;

slow pressure apply;

pressure hold.

The algorithms can use either instantaneous input values, as measured at each sample time, or averaged over the period between sample times. The three algorithm are discussed under the following sub-headings.

Phase Plane

A representative response for the Phase Plane control might be " IF wheel slip is less than ten percent AND less than its previous value AND IF wheel deceleration is negative AND IF line pressure was not increased in the previous step THEN increase line pressure." The essence of phase plane design is generation of a desirable dynamic balance. The control system is designed to move the state variables to a curve in the phase plane where they cycle around and do not leave (stable limit cycles). Dozens of design variables may be involved. Tan and Tomizuka [9] note that a system of this kind retains intuitive understanding, with design performed more experimentally than analytically. Tuning and calibration of such algorithm rely upon trial and error, and robustness is not explicitly addressed.

Sliding Mode Control

Variable structure control system are characterized by a discontinuous control on an appropriate switching surface in the state space. Control algorithm structure is changed during operation to obtain a desired system behavior, in response to state errors and their time derivatives. When the velocity vectors of the state trajectory are in the vicinity of the switching surface they are desired towards that surface. Switching surface

stability requirements can be found in [10]. The control strategy moves the state variables towards the chosen switching surface and then "slides" them along the surface, hence the term sliding mode control.

Several results have been published coupling the ABS problem and the variable structure control system design technique [11], [12]. In these papers the authors design sliding mode controllers under the assumption of knowing the optimal value of the target skid. A problem of concern here is the lack of direct slip measurements. In all previous investigations the separation approach has been used. The problem was divided into the problem of optimal skid estimation and the problem of tracking the estimated optimal value. Drakunov, Özgüner, Dix, and Ashrafi [13] developed a control algorithm which allows the maximal value of the tire/road friction force to be reached during emergency braking without a priori knowledge of the optimal slip. The developed algorithm allowed one to track an unknown optimal value even in the case of value changing in real-time.

A sliding mode controller to maintain the wheel skid at any given value is designed by Kachroo and Tomizuka [14]. This longitudinal traction controller is found to give better results than the conventional controllers. On the other hand, a typical ABS can only sense the angular wheel velocity and/or acceleration of the vehicle to estimate the wheel slip. The design of traction controller is based on the assumption that vehicle and wheel angular velocities are both available on-line by direct measurement and /or estimations. As angular wheel velocity is directly measured, only vehicle velocity is needed to estimate wheel skid. Two of the many methods for estimating the vehicle velocity are using magnetic markers imbedded in the pavement and the use of an

accelerometer to calculate velocity by integration [15]. Both methods have drawbacks: one requires an accurate sensing system and infrastructure, the other requires updating because of accumulation of integration errors. Ünsal, and Kachroo [16] proposed a sliding mode measurement feedback control that described a nonlinear-based design. The sliding observer is found promising while the extended Kalman filter is unsatisfactory due to unpredictable changes in the road conditions. Drakunov, Ashrafi, and Rosiglioni [17] proposed a yaw control algorithm via sliding mode control which is based on the variations of right-left distribution of the braking torque. The main challenge of this approach is that the uncertainty in the friction forces on different wheels result in the lack of a priori information about the direction of the applied torque. The periodic switching function approach is used to overcome this uncertainty and achieve the desired yaw.

The variable structure controller in the present study uses the description by Tan [18] that does not explicitly consider implementation with discrete controllers. Therefore, Tan's algorithm was adapted by defining four bands parallel to the sliding mode surface, as suggested by Gibson's "Dual Mode Switching"[19]. Five design variables were chosen for optimization. The sliding surface is defined as

$$S\left(\frac{\delta\lambda}{\delta t},\lambda\right)=\frac{\delta\lambda}{\delta t}+\varsigma(\lambda-\lambda_{peak}) \qquad (3)$$

Where λ is wheel skid, λ_{peak} is wheel skid at peak adhesion, and ς is a control parameter. The four bands have constant S values, which are design variables during optimization. As a computed value for S falls in a relative band position, the following rules apply: (i) below the lowest band use fast apply rate; (ii) between the lowest band and one higher use low apply rate; (iii) between bands adjacent to S=0 (one on either side) hold pressure

unchanged; (iv) above the first positive band but below the highest band use slow release; (v) above the highest band use fast release. The fifth design variable is the control parameter ς in Equation (3).

The algorithm activates ABS control the first time when estimated wheel skid exceeds the estimated value for wheel skid at peak traction. The latter estimate is calculated by a traction identification estimation algorithm described later in this section.

Recently, Kawabe et al. [20] of Nissan Diesel Motor proposed a new sliding surface using frequency shapping concept. They also introduced wheel acceleration feedback to ABS and conducted hardware-in-the-loop simulations and experiments. The sliding surface proposed in [20] has considerable limitation in practical implementation. It also has the problem that the wheel acceleration feedback is not theoretically related to sliding mode control.

Modified Sliding Mode Control

In a scheme proposed by Tomizuka and Tan, [9], the bounded or slow-varying uncertainties of the brake system are grouped together and treated as disturbances, estimated by a derivative feedback. The resultant system is locally linearized by a nonlinear prefilter, and linear digital control theory is used to determine the controller design variables. This modified sliding mode (MSM) scheme allows for a small number of control variables. Will, Hui, and Zak [21] proposed a hybrid wheel skid controller that contained a sliding mode module coupled with PID control module. The proposed controller does not require a prior knowledge of the surface type nor the relation between

the coefficient of adhesion and the wheel skid, and could be implemented to compute the optimal skid rate on-line using data obtained from commonly available longitudinal accelerometers and wheel speed sensors. Choi, and Cho [22] developed a longitudinal four-wheel vehicle model with a solenoid-solenoid valve type brake actuator and applied the sliding mode controller with pulse width modulation method (PWM) to the control of ABS. In applying the sliding mode control to the proposed system, the dynamics of solenoid-solenoid valve type actuator was introduced in system equations. The pulse width modulation method was proposed to be used in conjunction with the sliding mode control to compensate for the discrete nature of actuator dynamics by duty control.

2.4 Tire Model

Apart from aerodynamic and gravitational forces, all other forces and moments affecting the motion of the vehicle are applied through the tires. The tire forces during lateral maneuvering, acceleration, and braking dominate vehicle handling performance. Over the years, many braking and steering control systems were developed by using linear or linearized tire models. The linear tire model simplifies the analysis of vehicle dynamic performance. However, the linear tire model is only valid for small steering angle and braking inputs and only adequate for evaluating the lateral force of the tire with small slip angle and camber angle.

A real pneumatic tire is a very complex nonlinear mechanical system as shown in Figure 2.1. The basic tire input variables for a maneuvering vehicle include tire velocity, normal load, slip angle, longitudinal skid, and chamber angle. The output variables

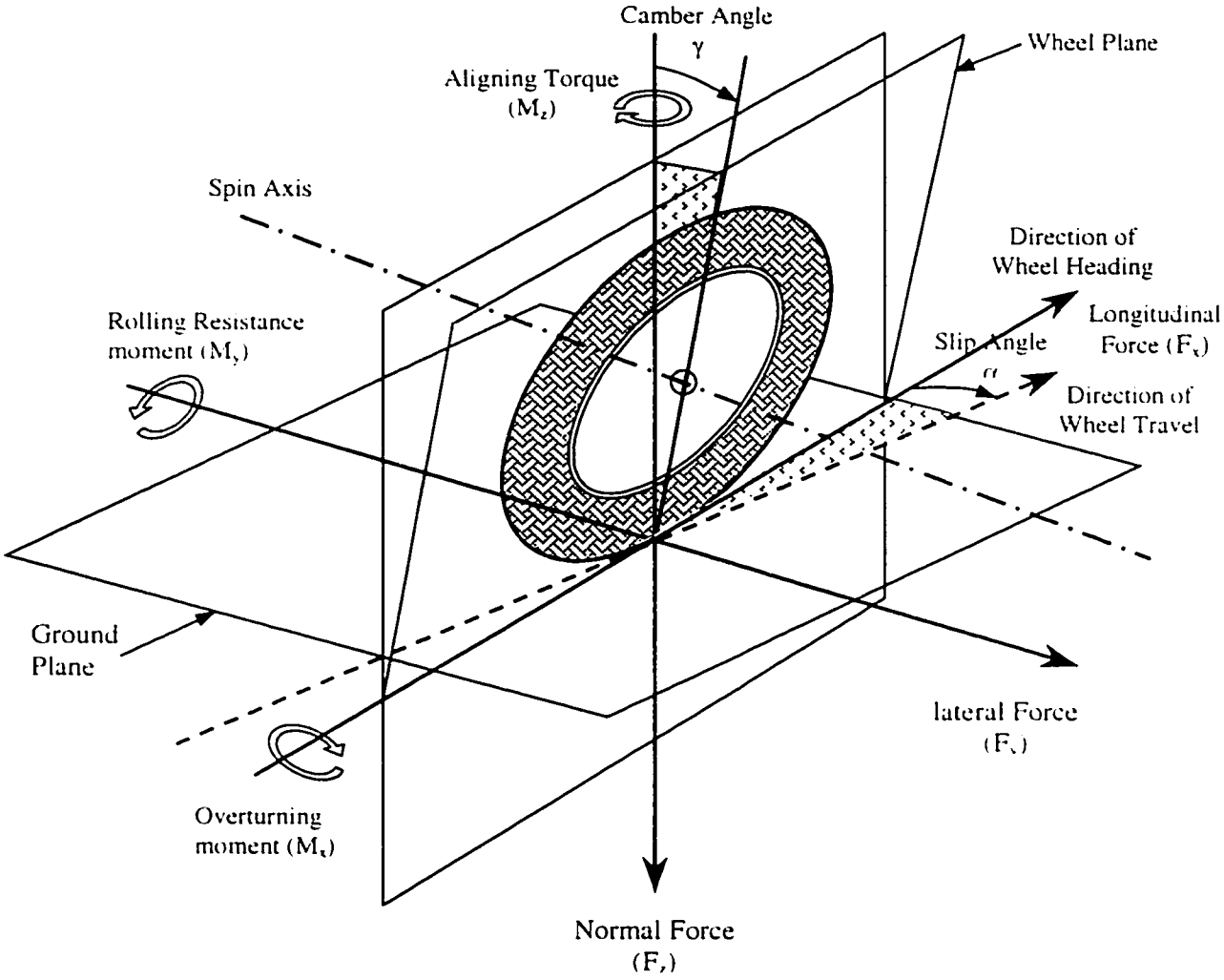

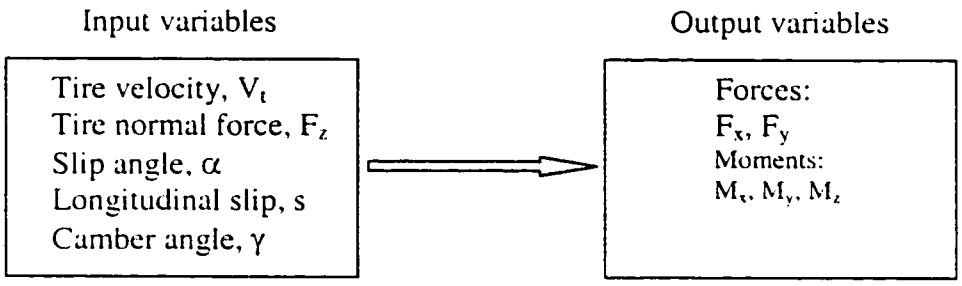

Figure 2.1 Tire axis system and input/output quantities

are three dimensional force and moment vectors. For large control inputs, i.e., large steering and braking commands, the tire force characteristics become highly nonlinear. In such situations the longitudinal and lateral motions of the vehicle are strongly coupled through the tire forces. Therefore, a realistic tire model is required to properly represent tire forces and moments throughout the full maneuvering range from low acceleration to limit performance. Limit performance means that the force generating capacity of the tire is at or beyond saturation. Hence, to develop a more comprehensive brake system, especially for adverse road conditions, a nonlinear tire model should be used.

In the last few decades, a number of nonlinear tire models have been developed by using various approaches. Each of them is developed for a specific purpose and has its limited application. Several researchers have investigated the lateral and longitudinal dynamics of tires [23-24]. Usually a "relaxation length" or similar metric is used to characterize a first order lag in lateral shear force buildup; traditional kinematic relationships relating wheel spin to longitudinal slip, and longitudinal slip to shear forces at the tire road interface provide an adequate model for most simulation purpose. Zanten [25] presented an experimental result with "unexpected" oscillations in wheel spin just after rapid application of braking torque. It was hypothesized that these oscillations would likely influence the performance of antilock braking systems. An insightful overview of tire and vehicle modeling, calls for further elaboration of the tire shear forces and moments that are generated under time varying lateral and longitudinal slip by Segel [26].

Szostak, et al [27] and Allen et al [28] carried out comprehensive works in the development of a nonlinear tire models. The work in [28] was based on work done by

previous investigators in [29] and [30]. As explained in [28], the "...basic objective was not to develop a new tire model, but to consolidate the work of others into a convenient computational form which could be easily applied in a vehicle dynamics simulation. They had no desire to invent new unmeasurable parameters, but instead strived to work with parameters available from the tire test data such as the comprehensive Calspan model and data [31], [32]."

The basic input parameters to the tire model described in [28] are: tire normal load , tire camber angle, tire velocity, lateral slip angle, and longitudinal slip ratio. The outputs of the model are aligning torque and the normalized lateral and longitudinal forces. The general structure of tire model described in [28] is shown in Figure 2.2. The model is capable of estimating longitudinal and lateral forces from small levels through saturation and could be used to simulate tire forces over a wide range (i.e., lateral and longitudinal acceleration). The details for the simulation of nonlinear tire forces and moments are summarized in a flow chart presented in Fig. 2.3. The nonlinear tire force characteristics for a given tire and speed are shown in Fig. 2.4 to demonstrate the trend of lateral force as a function of slip angle for different longitudinal slip, as well as longitudinal force as a function of slip for different slip angles. This model is also able to analyze perturbation vehicle dynamics at high tire force output regions (e.g., braking-in-turn) where side force coefficients are significantly reduced, which may, in turn, lead to instability.

Even though the tire force and aligning torque generated by Szostak et al.'s nonlinear tire model as shown in Fig. 2.4 perfectly match the experimental data, the

calculation procedures and the mathematical calculation formulas are extremely complex, and hence, its utilization is not convenient in the development of the ABS controller.

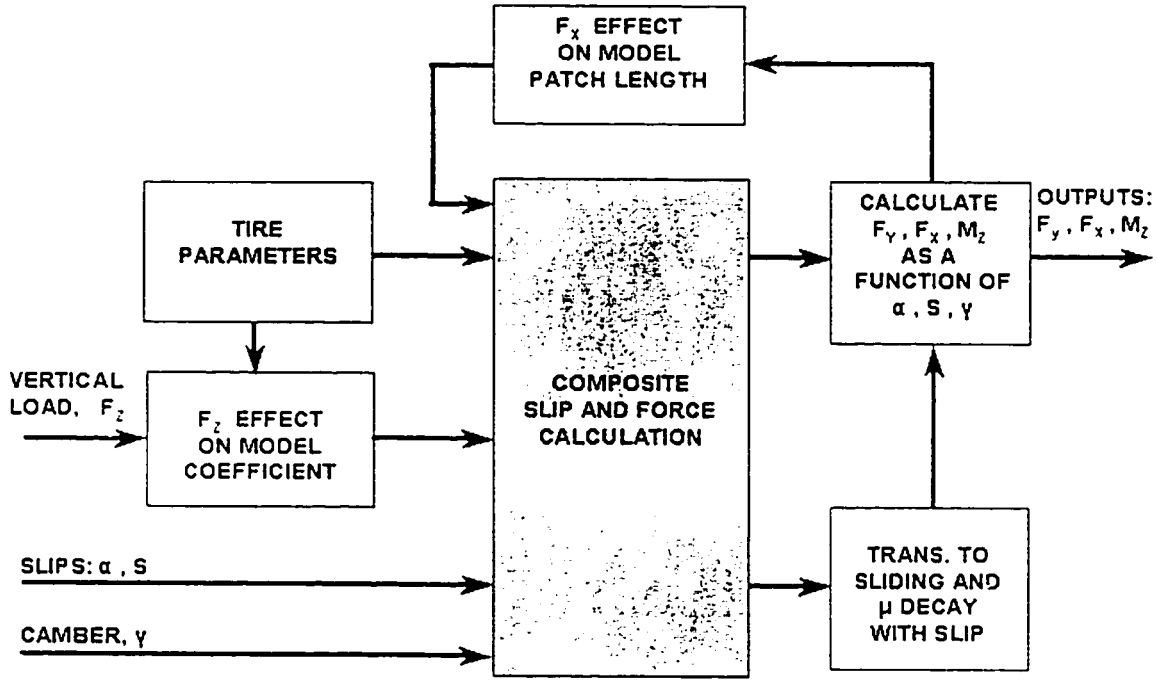

Fig. 2.2 General tire mode structure described in [28]

As we have known, the friction potential between tire and road is a function of many parameters, related to the tire (such as construction compound, tread type, tread depth, inflation pressure, temperature), to the road (such as type of surface, texture, drainage capacity, temperature, lubricant such as water or snow), and to the vehicle state (such as speed, brake skid). Most of these parameters, especially the tire and road related

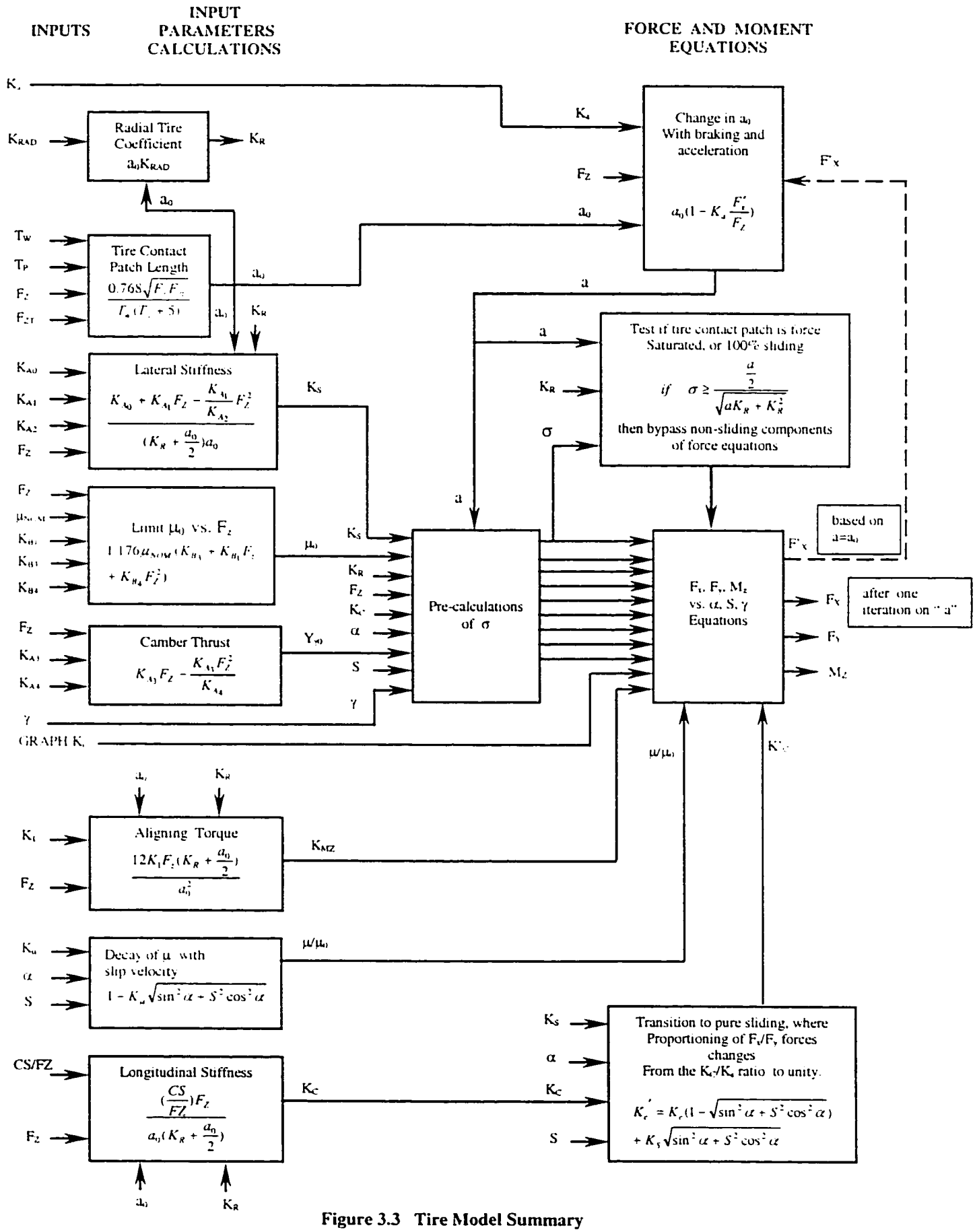

Figure 3.3 Tire Model Summary

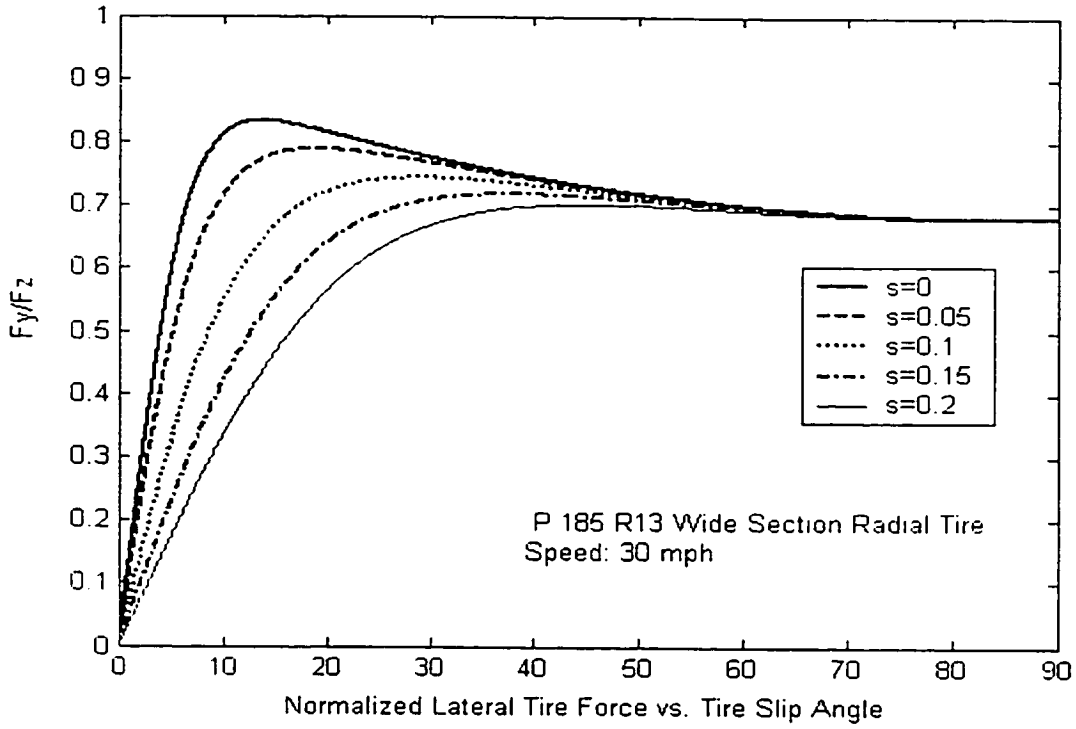

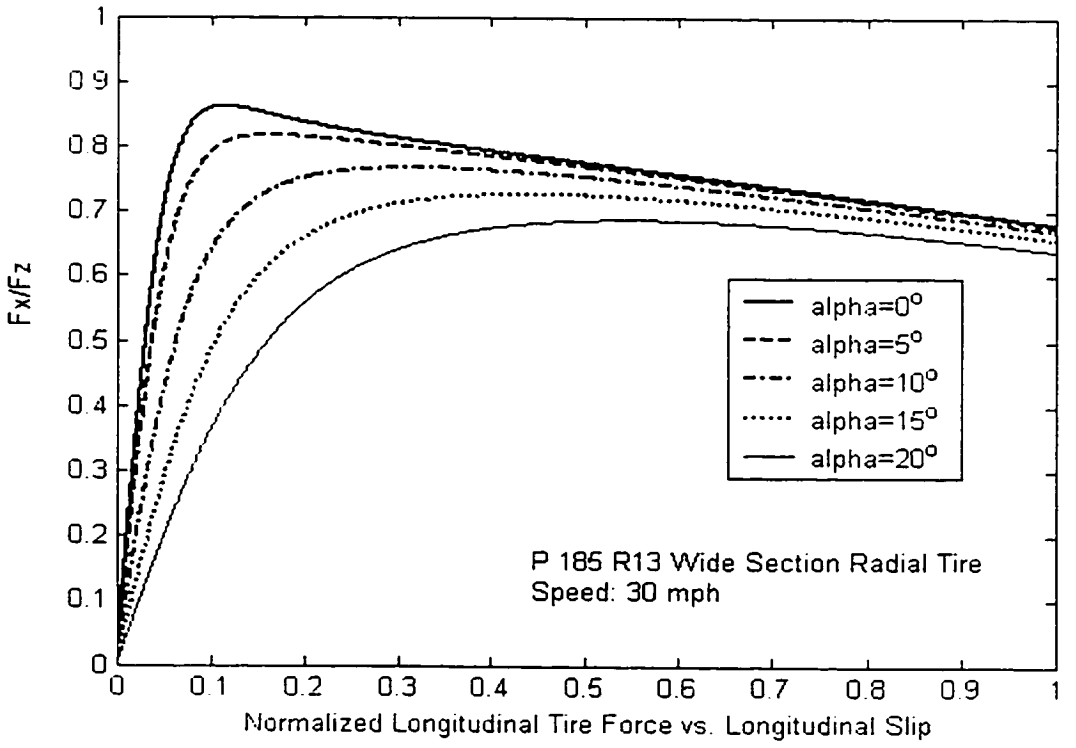

Fig. 2.4 Nonlinear tire force characteristics from Szostak et al.'s tire model

parameters, are uncontrollable from the driver's point of view; furthermore, a change in a parameter tends to influence other parameters in the frictional process. Over the last ten years, much research effort has been spent to estimate the friction coefficient between tire and road, either by monitoring effects of the frictional process itself on the vehicle or the tire, or by monitoring some parameters influencing the frictional process [33-34].

Literature on tire/road friction model is numerous. Tire/road friction model are usually described as a curve (or set of curves) of the wheel slip s, and the normalized friction force i.e.

$$\mu = \frac{F}{F_n} = \frac{Friction\ force}{Normal\ force}$$

Bakker et al. [35] describe two analytical models for tire/road behavior that are intensively used by researchers in the field. In the two models, μ is mainly determined based on the wheel slip s and some other parameters like speed and normal load. One of the most well-known model of this type is Pacejka's model [36], also known as the "magic formula". This model has been shown to suitably match experimental data, obtained under particular conditions of constant linear and angular velocity. The Pacejka model has the form

$$F(s)=c_1 sin(c_2 arctan(c_3 s - c_4(c_3 s - arctan(c_3 s)))),$$

where the subscript ci's are the parameters that characterize the model. These parameters can be identified by matching experimental data, as shown in Bakker et al. [35]. The parameters c_i depend on the tire characteristics (such as compound, tread type, tread depth, inflation pressure, temperature), on the road conditions (such as type of surface

texture, drainage, capacity, temperature, lubricant, i.e., water or snow), and on the vehicle operational conditions (velocity, load) [37].

Van and Parsons [38] described a method using the "magic formula" tire model to introduce correction of laboratory test data to be more like road data. They used two additional coefficients to the "magic formula" tire model in order to achieve a high degree of correlation between instrumented test and simulation results on different road surface. It was indicated that this new method is very effective in predicting correct lateral force data for a specific road surface and high degree of correlation is often desired to validate vehicle dynamic models.

As an alternative to the static F(s) maps, a dynamic model has been developed and analyzed by many researchers for the various control tasks. The dynamic model describing the spring-like behavior during stiction was proposed by Dahl [39]. The Dahl model is essentially Coulomb friction with a lag in the change of friction force when the direction of motion is changed. The model has many affricative features, and is also well understood theoretically. Questions such as existence and uniqueness of solutions and hysteresis effects were studied in an interesting paper by Bliman [40]. The Dahl model does not, however, include the Stribeck effect. An attempt to incorporate this into the Dahl model was carried out in [41] where the authors introduced a second-order Dahl model using linear space invariant descriptions. The Stribeck effect in this model is however only transient after a velocity reversal, and is not present in the steady-state friction characteristics. The Dahl model has been used for adaptive friction compensation [42], [43], with improved performance as a result. There are also other models for dynamic friction. Armstrong-Hélouvry proposed a seven parameter model in [44]. This

model does not combine the different friction phenomenon but is in fact one model for stiction and another for sliding friction. Another dynamic model suggested by Rice and Ruina [45] has been used in connection with control by Dupont [46]. This model is not defined at zero velocity. Canudas de Wit, Olsson, Åström, and Lischinsky [47] proposed another dynamic friction model that combines the stiction behavior, i.e., the Dahl effect, with arbitrary steady-state friction characteristics which can include the Stribeck effect. This dynamic friction model based on the dynamic friction model of Dahl is useful for various control tasks.

The dynamic models in [13], can be adapted to suitably describe the road-tire contact friction, which can be formulated as a lumped or distributed model.

The lumped friction model proposed by Canudas-de-Wit and Tsiotras [48] is based on a similar dynamic friction model for contact developed previously for contact-point friction problems, called LuGre model (Canudas de Wit et al. [47]). The model proposed in [48] is given by the following set of equations:

$$\dot{z} = v_r - \theta \frac{\sigma_0 |v_r|}{g(v_r)} z$$

$$F = (\sigma_0 z + \sigma_1 \dot{z} + \sigma_2 v_r) F_n$$

with,

$$g(v_r) = \mu c + (\mu s - \mu c) e^{-|v_r / v_s|^{1/2}}$$

where, σ_0 is the normalized rubber longitudinal lumped stiffness, σ_1 is the normalized rubber longitudinal lumped damping, and σ_2 is the normalized viscous relative damping. μ_c and μ_s are the normalized Coulomb and static friction coefficient, respectively

$(\mu_c \le \mu_s,\ \ \in [0,1])$. v_s is the Stribeck relative velocity, F_n is the normal force, $v_r = (r\omega - v)$ is the relative velocity, and z is the internal friction state. The parameter 0 is introduced to capture the changes in the road characteristics. It can be interpreted as being the coefficient of road adhesion.

Dynamic friction models specifically for tires have been reported in the work of Clover and Bernard [13], where they developed a differential equation for the slip coefficient, starting from a simple relationship of the relative deflections of the tire elements in the tire contact patch. They, however, use the semi-empirical static force/slip models to compute the corresponding friction force. In that respect, such models can be best described as quasi-dynamic models.

From above discussion of the tire models, one can group the different tire models into three of types:

a) Experimental tire model

b) "Magic formula" tire model

c) Dynamic friction tire model

Among these, the first two types of tire models try to present the relationship between the tire forces and longitudinal slip, whereas the last one can determine the tire force using relative velocity.

2.5 Vehicle Model

The dynamic response of a vehicle is determined by the inertia properties (e.g., mass distribution), suspension, tire properties, and externally applied forces. As mentioned previously, the nonlinear tire force significantly influence vehicle response during large magnitude maneuvers.

The simplest linear model used to investigate lateral vehicle response is the linear 2 DOF "bicycle model" [7]. This model lumps the left and right tires at the front and rear of the car into equivalent tires located at the car center line. The DOFs for such model at constant forward speed are lateral and yaw motion. The tire force nonlinearity, suspension effects and weight shift are neglected. This model can be used for preliminary investigation into the effects of different steering and braking control strategies [49]-[53].

In addition, a nonlinear refined "bicycle model" has been applied to study the limit performance of a vehicle during emergency maneuvers combining steering with braking commands [54]. The DOFs included are lateral and longitudinal velocity, yaw rate, and rotational speed of each of the wheels. The model includes a comprehensive, nonlinear tire model and is capable of simulating large control inputs. However, suspension effects and lateral weight shift are ignored in the refined "bicycle model". Generally, a realistic four wheel vehicle model [36][55] is a three dimensional model consisting of a sprung mass and unsprung masses for the front and rear suspension systems. The masses are interconnected through the vehicle roll axis. Such models may include the roll DOF of the vehicle, suspension effects and both lateral and longitudinal weight shifts.

The mathematical models of vehicle dynamics have been described through many papers [24-25]. The quality of a vehicle dynamics model, in general, relies upon the modeling methodology, characterization of properties of the vehicle and its components, and the validation of the model. The basic methodologies of modeling a vehicle include both analytical and experimental tasks. The analytical approach usually establishes the equations of motion of the vehicle and its components, which are considered valid under certain assumed conditions, while the experimental approach generally involves evaluations of the vehicle system or subsystem and estimation of vehicle parameters.

Most of vehicle subsystems are frequently designed and developed independently of each other. The dynamics of these subsystems, however, often interact. The dynamic coupling between the braking and steering systems has considerable effect on the stability, controllability and stopping distance of the vehicle [26][33]. For example, the maximum available longitudinal and lateral forces at the tire depend on each other. A vehicle combined cornering and braking or acceleration maneuver is a transient phenomenon and has no steady-state equilibrium conditions as those used in a constant speed turning behavior. However, by neglecting the effects of the change of vehicle speed in short periods of time, a quasi-steady-state condition can be assumed. The equilibrium equations of the vehicle motion with constant lateral and longitudinal accelerations then can be developed and solved. The characteristic descriptions of the vehicle turning behaviors in acceleration or in braking can be also derived [34][35]

Vehicle characteristics over full range of motions, including the nonlinear region and transient states, can be described in a single diagram by conducting analysis based on the side slip angle at center of gravity of the vehicle when yaw and lateral motions of the

center of gravity point are fixed [50]. The characteristics of yaw and lateral directional dynamic response for different vehicle combinations have been extensively investigated through development and analysis of simplified yaw-plane models. While majority of the reported yaw-plane models assume linear cornering characteristics of tires, some studies have incorporated nonlinear cornering properties of tires based upon regression functions and Magic formula. Bernard et al. [38] examined the yaw stability of a vehicle with four-wheel steering through analysis of a linear yaw plane model. Xia and Law [27] investigated analytically both the steady state and transient response characteristics of a linearized yaw-plane model. A nonlinear, four-wheel eight DOF model used slip control braking system [28] for body roll, longitudinal, and lateral weight transfer, tire force generation lag, roll steer, and steering compliance. Nonlinear yaw-plane four wheel models for vehicle braking system were developed by many researchers (Kazunori [29], Huei [30], His-Fu [31]). The yaw-plane models provide effective assessment of rearward amplification, dynamic off-tracking, yaw and lateral stability limits of vehicle combinations, while the contributions due to pitch and roll motions and suspension dynamics can not be evaluated. Such models offer considerable advantages in which relatively fewer number of parameters are required to evaluate the directional performance with reasonably good accuracy.

The static roll stability limit of a vehicle is frequently characterized by its rollover threshold, defined as the maximum lateral acceleration to which the vehicle can withstand without rolling over in a steady turning maneuver. The roll instability is attained whenever the overturning moment, generated by the centrifugal forces, exceeds the net stabilizing moment. Conventional designers have long appreciated the influence

of specifying a roll moment distribution for vehicle dynamics. Such a study carried out by Williams and Haddad [52] describes the effect of roll moment distribution. The directional dynamics of heavy vehicles under simultaneous applications of braking and steering have been investigated through development of variable speed three-dimensional models. The Phase IV program [25] perhaps represents the most comprehensive vehicle dynamics model for analysis of yaw, roll and lateral stability of heavy vehicles subject to braking and steering. The model integrates the properties of braking and anti-lock brake system, nonlinear cornering properties of tires under braking and steering using lookup tables, nonlinear force-deflection properties of suspension springs, static properties of the articulation mechanism, and the combination of steering (open-loop and closed-loop), and driving/braking torque. The vehicle model is developed to analyze different vehicle combinations comprising up to three units and ten axles, with a maximum 71-DOF. The phase IV model is thus considered as a complex model, which requires extensive vehicle parameters. The study through the reviewed vehicle models showed that more sophisticated simulation models, such as the Phase IV model, do not necessarily yield more accurate predictions in quantitative terms than the simpler models, such as the nonlinear yaw plane model [72].

2.6 Simulation and Test Techniques

Like most investigations, computer simulation is a necessary step in the process of ABS controller design, and it has been explored widely in many areas of mechanical engineering. It is a powerful tool to visualize the results of designed ABS controllers

before they are advanced to further test and practical application. Some researchers used the existing computer software, such as Matlab, MatrixX, Adams, and some developed their own simulation codes. Olson and Milacice developed the simulation codes of Dynamic Analysis and Design System[56], which allows one to study and observe factors such as the acceleration and braking performance of a vehicle. Another is the use of graphical modeling environment for real-time hardware-in-the-loop simulation of automotive ABS systems [57]. Schneider [58] provided an example HAZOP for examination of simplified ABS logic element that is representative of part of an ABS control strategy.

To verify and evaluate the designed ABS control algorithms, some braking measurement test techniques have been performed. Srinivasa et al [59] presented test results of two commercially available antilock devices to illustrate the utility of the test facilities. From the results shown, it appears that the laboratory testing facilities indeed provide most effective means to compare and to evaluate the slip performance and braking effectiveness of various antilock devices. The results obtained could provide the vehicle braking systems designer with guidance to optimize the design of antilock devices. Some laboratory test methods tried to simulate the real road condition as the input to ABS systems, which has been proven very useful to verify the designed controller for practical application. Tan, and Tomizuka, [9] conducted a comprehensive antiskid brake testing experiment as shown in Fig. 2.5. Mechanically, the test cell contains a large aluminum drum driven by a dynamometer. The inertia of the drum set is approximately half the inertia of a midsize car. Pressed against the drum are two production wheel assemblies, one front and one rear. The two wheels are thus driven by

the drum, which simulates a road surface. Each wheel is equipped with a production brake hardware and a toothed wheel for sensing the wheel speed. A brake pedal,

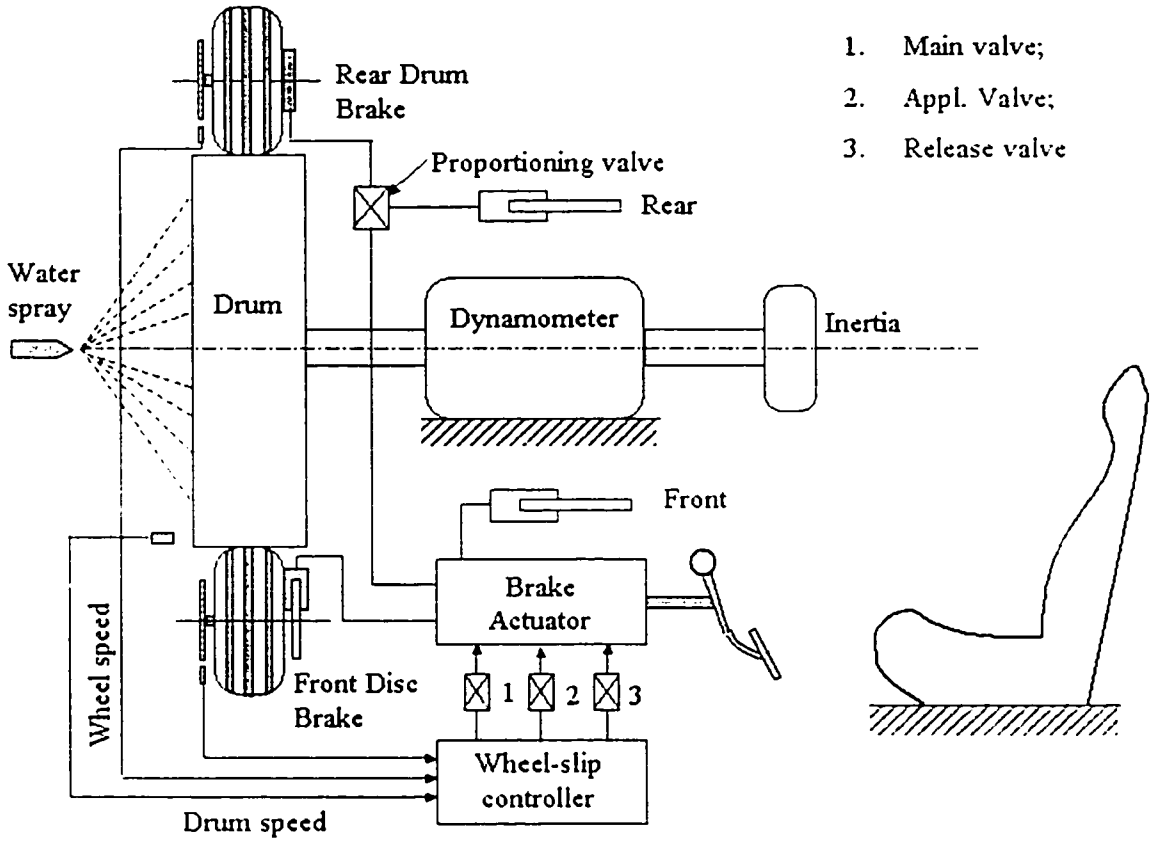

Fig. 2.5 Brake dynmometer test cell

depressed by the person acting as the test driver, actuates the brakes. The drum can be water-sprayed to simulate a road surface with a low friction coefficient .

Similar to the ABS test method as in [9], Choi, and Cho [22] set up an in-door test bench to test their control algorithm as shown in Fig. 2.6. Both the setup used a big drum

to simulate different types of the road surface, along with this individualize controllers for the setup to realize the simulations.

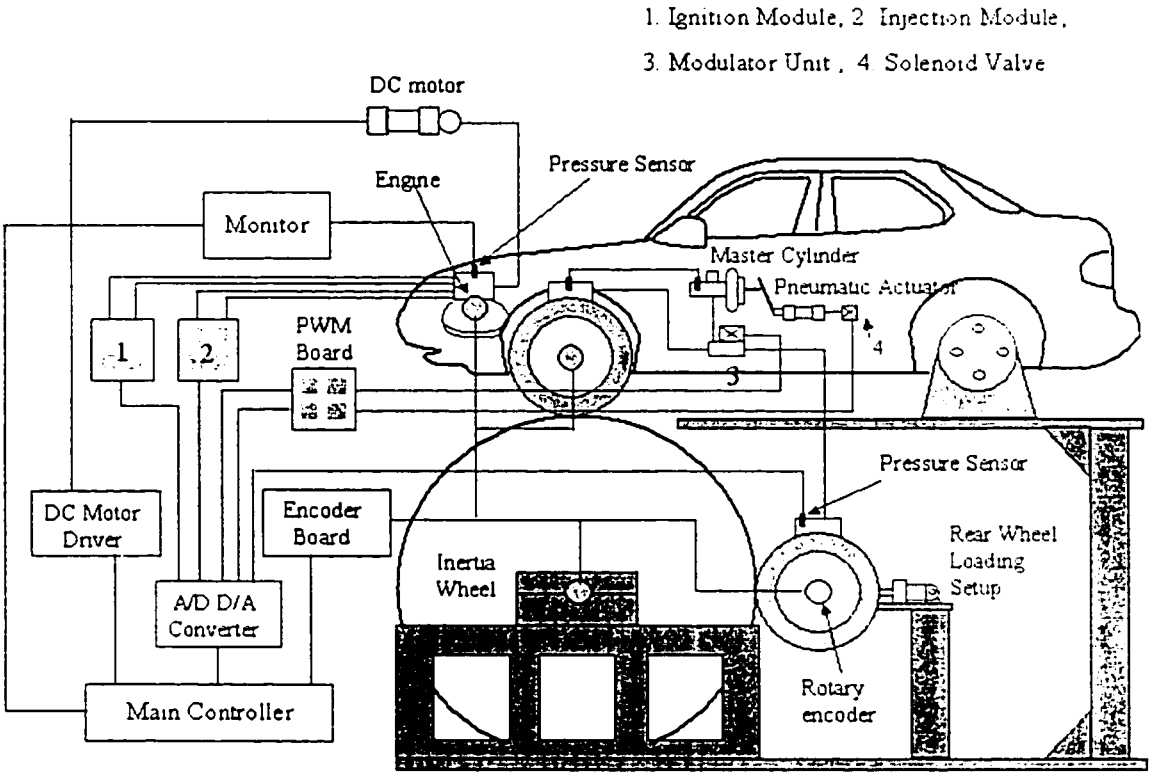

Fig. 2.6 Schematic diagram of the in-door test bench

2.7 Summary and Scope

As discussed in the literature review, a large number of vehicle models have been proposed with varying degrees of complexities. While comprehensive three-dimensional models permit analyses under wide range of design and operating conditions, they require more tedious characterization of a large number of vehicle parameters. Simplified

nonlinear yaw-plane models, on the other hand, yield lateral and yawing directional response in a reasonably accurate manner, assuming negligible contributions due to roll dynamics and braking of the vehicle. For the development of vehicle brake model and identification of vehicle design parameters, it is desirable to develop a simpler, yet credible vehicle model, which can be effectively interfaced with a more elaborate driver model, tire model and ABS controllers. In this investigation, a simplified quarter vehicle models with 2 and 3-DOF are utilized where major emphasis is placed on the nonlinear dynamic tire model and controller design.

Furthermore, as discussed in the literature review, static friction tire models, including "magic formula" and experimental tire model, can only give one-to-one maps between the friction force and the longitudinal slip rate. Such tire models cannot give the resulting optimal longitudinal slip under dynamic environment as the reference to the ABS controller. Dynamic friction tire model, therefore, is developed in this study to overcome such drawback of static tire model. Since the optimal slip at each constant velocity is known, the design of the controller can there be simplified significantly.

The three common approaches to the ABS controller design discussed in the literature review utilize static friction tire model and control methods are adapted to optimize the longitudinal slip at each step. This introduces complexity for the controllers and are prone to introduce errors in the optimization. In this study, the dynamic tire model is utilized for the designed two controllers, namely PI controller and sliding mode controller, and are expected sto function simply and reliably to achieve a stable and steerable performance of the controlled braking systems.

Section 2.6 illustrated the extent of elaborate tests that may be carried out to test new approaches and design ideas. Such test, however, is beyond the scope of he present investigation. This investigation being first phase of a design process, only focuses on detailed model development and computer simulations to demonstrate the effectiveness of the concept.

It should be noted that the present investigation is aimed at designed controllers for the ABS and is not applicable for comprehensive evaluation of the dynamic performance of the vehicle. For this a more comprehensive vehicle models capable of exhibiting dynamic behavior of vehicle under combined braking and steering maneuvers should be adapted with the proposed ABS system as recommended for further investigation.

CHAPTER III
FRICTION TIRE MODEL AND VEHICLE MODEL

3.1 Introduction to Friction Model

Friction is an important aspect of many control systems both for high quality servo mechanisms and simple pneumatic and hydraulic systems. Friction can lead to tracking errors, limit cycles and undesired stick-slip motion [44]. Control strategies that attempt to compensate for the effects of friction, without resorting to high gain control loops, inherently require a suitable friction model to predict and to compensate for the friction. These types of schemes are therefore named model-based friction compensation techniques. A good friction model is also necessary to analyze stability, predict limit cycles, find controller gains, perform simulations, etc. Most of the existing model-based friction compensation schemes use classical friction models, such as Coulomb and viscous friction. In applications with high precision positioning and with low velocity tracking, the results are not always satisfactory. A better description of the friction phenomena for low velocities and especially when crossing zero velocity is necessary. Friction is a natural phenomenon that is quite hard to model, and it is not yet completely understood. The classical friction models used are described by static maps between velocity and friction force. Typical examples are different combinations of Coulomb friction, viscous friction, and Stribeck effect [44]. The classical models explain neither hysteresis behavior when studying friction for nonstationary velocities nor variations in the break-away force with the experimental condition nor small displacements that occur

at the contact interface during sticktion. The latter very much resembles the behavior of a connection with a stiff spring with damper and is sometimes referred to as the Dahl effect. The following dynamic friction model combines the sticktion behavior, i.e., the Dahl effect, with arbitrary steady-state friction characteristics which can include the Stribeck effect. This model is useful for various control task.

Before proceeding, several definitions are needed in order to understand the friction model properly. A detailed analysis of friction model is presented in [44].

Static Friction (Sticktion):

The torque (force) necessary to initiate motion from rest. It is often greater than the kinetic friction.

Dahl Effect:

A friction phenomenon that arises from the elastic deformation of bonding sites between two surfaces which are locked in static friction. The Dahl effect causes a sliding junction to behave as a linear spring for small displacement.

Stribeck Effect:

A friction phenomenon that arises from the use of fluid lubrication and gives rise to decreasing friction with increasing velocity at low velocity. The Stribeck effect is a name given to decreasing friction with increasing velocity, it is recognized to produce a destabilizing effect at very low velocities.

Dynamic Friction

The qualitative mechanisms of friction are fairly well understood. Surfaces are very irregular at the microscopic level and two surfaces therefore make contact at a number of asperities. This can be visualized as two rigid bodies that make contact through elastic bristles. When a tangential force is applied, the bristles will deflect like springs which gives rise to the friction force as shown in Figure 3.1 [47].

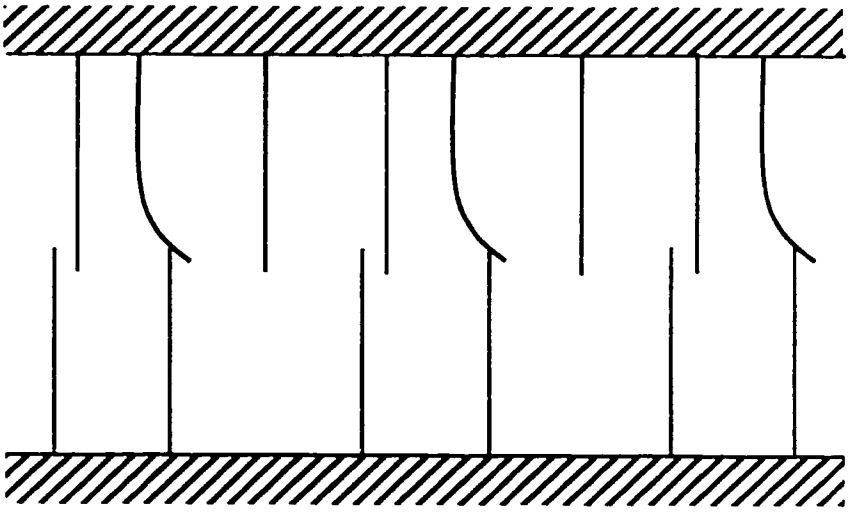

Fig. 3.1 The friction interface between two surface is thought of as a contact between bristles. For simplicity the bristles on the lower part are shown as being rigid.

If the force is sufficiently large, some of the bristles deflect so much that they will slip. The phenomenon is highly random due to the irregular forms of the surfaces. The average deflection of the bristles is denoted by z and is modeled as

$$\frac{dz}{dt} = v - \frac{|v|}{g(v)} z \qquad (3.1.1)$$

where v is the relative velocity between the two surfaces. The first term gives a deflection that is proportional to the integral of the relative velocity. For steady state motion, the second term asserts that the deflection z approaches the value

$$z_{ss} = \frac{v}{|v|} g(v) = g(v)\mathrm{sgn}(v) \qquad (3.1.2)$$

The function g in above equation is positive and depends on many factors such as material properties, lubrication, temperature, and it need not be symmetrical. Direction dependent behavior can therefore be captured. For typical bearing friction, g(v) will decrease monotonically from g(0) when v increases. This corresponds to the Stribeck effect. The friction force generated from the bending of the bristles is described as:

$$F = \sigma_0 z + \sigma_1 \frac{dz}{dt} \qquad (3.1.3)$$

where σ_0 is the stiffness and σ_1 is the damping coefficient. A term proportional to the relative velocity can be added to the friction force to account for viscous friction so that

$$F = \sigma_0 z + \sigma_1 \frac{dz}{dt} + \sigma_2 v \qquad (3.1.4)$$

The model given by (3.1.1) and (3.1.4) is characterized by the function g and the parameters σ_0, σ_1, and σ_2 . The function $\sigma_0 g(v) + \sigma_2 v$ can be determined by measuring

the steady state friction force when velocity is held constant. A parameterization of g that has been proposed to describe the Stribeck effect is

$$\sigma_0 g(v) = F_c + (F_s - F_c)e^{-(v/v_s)^2} \qquad (3.1.5)$$

where F_c is the Coulomb friction level, F_s is the level of the sticktion force, and v_s is the Stribeck velocity. With this description the model is characterized by six parameters σ_0, σ_1, σ_2, F_c, F_s, and v_s. It shows from (3.1.2) to (3.1.5) that for steady-state motion the relation between velocity and friction force is given by

$$F_{ss} = \sigma_0 g(v)\mathrm{sgn}(v) + \sigma_2 v = F_c\,\mathrm{sgn}(v) + (F_s - F_c)e^{-(v/v_s)^2}\,\mathrm{sgn}(v) + \sigma_2 v \qquad (3.1.6)$$

3.2 Lumped Model and Distributed Model

Based on the friction model described in section 3.1, also known as LuGre model, in [47], the dynamic friction models are adapted to suitably describe the road-tire contact friction. A potential advantage of such models is their ability to describe closely some of the physical phenomena found in road/tire friction (i.e. hysteresis loops, pre-sliding displacement, etc.), which in turn depend on parameters directly related with the phenomena to be observed, like for instance the change on the road characteristics (i.e.

dry wet, etc.). Dynamic models can be formulated as a lumped or distributed model, as shown in Fig. 3.2.

A lumped friction model assumes punctual tire-road friction contact, and the distributed model assumes the existence of an area of contact or patch between the tire and the road as illustrated in Fig. 3.2. The lumped friction model starts from a simple relationship of the relative deflections of the tire elements in the tire/road contact patch (punctual contact). When the braking torque is applied to a pneumatic tire, a shear deformation of the sidewall of the tire is developed, and a braking force is developed at this tire-ground contact patch. The lumped friction model is therefore a fundamental dynamic friction tire model. The distributed model further takes this contact patch into the consideration. A lumped friction model that can be readily derived from the friction model presented in subsection 3.1, can be extended to the distributed model. Therefore,

An example of a lumped friction model has been derived from the LuGre model [48] in subsection 3.1., i.e.

$$\begin{aligned} \dot{z} &= v_r - \frac{\sigma_0 |v_r|}{g(v_r)} z \\ F &= (\sigma_0 z + \sigma_1 \dot{z} + \sigma_2 v_r) F_n \\ &\textit{with,} \\ g(v_r) &= \mu_C + (\mu_S - \mu_C) e^{-|v_r / v_s|^{1/2}} \end{aligned} \qquad (3.2.1)$$

where, σ_0 is the normalized rubber longitudinal lumped stiffness, σ_1 the normalized rubber longitudinal lumped damping, σ_2 the normalized viscous relative damping, μ the normalized Coulomb friction, μ_s the normalized static friction, ($\mu \le \mu_s$, $\in [0.1]$).

v_s the Stribeck relative velocity, F_n the normal force, $v_r=(r\omega - v)$ the relative velocity, and z the internal friction state.

The basic dynamic model in Eq. (3.2.1) is a lumped parameter model with only one internal state z which is the function of relative velocity (v_r). A distributed friction dynamic model can be achieved by assuming the existence of a contact patch between the tire and the road [48]. This patch represents the projection of the part of the tire that is in contact with the road. The contact patch is associated to the frame O_p, with ζ as the axis coordinate, where the patch length is L.

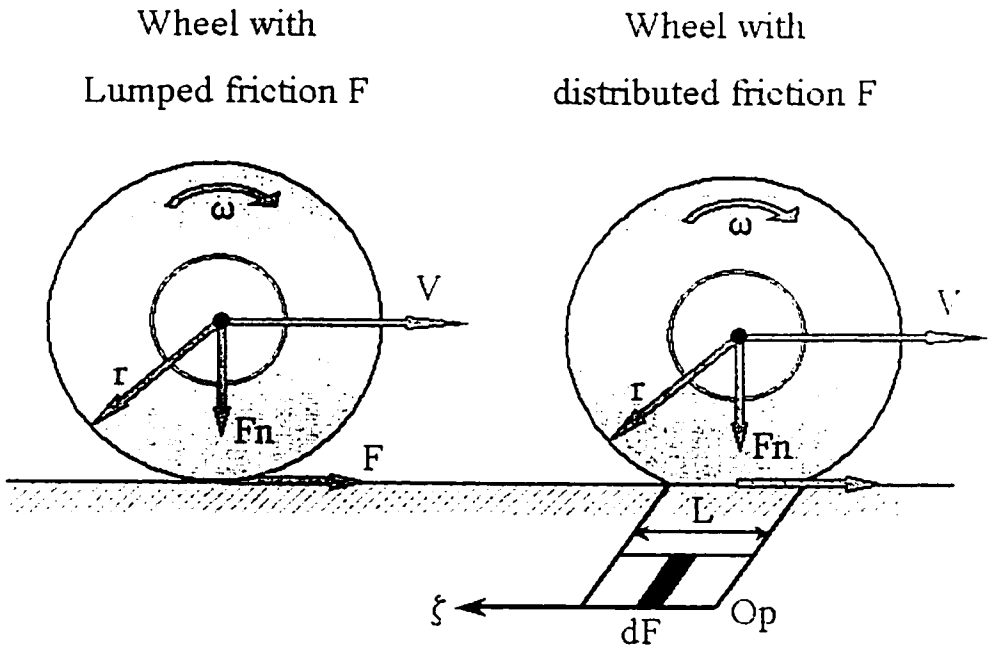

Fig. 3.2 A schematic of one vehicle wheel with lumped friction (left) and distributed friction (right) representation

Distributed dynamical models, have been studied previously, for example, in the works of Bliman et al. [60]. In this model, the contact patch area is discretized to a series of elements, and the microscopic deformation effects are studied in detail. In particular, Bliman et al. characterize the elastic and Coulomb friction forces at each point of the contact patch, but then give the aggregate effect of these distributed forces by integrating over the whole patch area. They propose a second order rate-independent model, and show that, under constant v and ω, there exists a choice of parameters that closely match a curve similar to the one characterizing the magic formula.

Similar results can be obtained by using a model based on the first-order LuGre friction model, i.e.

$$\frac{d\delta z}{dt}(\varsigma,t) = v_r - \frac{\sigma_0|v_r|}{g(v_r)}\delta z \qquad (3.2.2)$$

$$F = \int_0^L \delta F(\varsigma,t)d\varsigma \qquad (3.2.3)$$

with $g(v_r)$ *defined as before and*

$$\delta F = (\sigma_0\delta z + \sigma_1\dot{\delta z} + \sigma_2 v_r)\delta Fn$$

where δF is the differential friction force, δFn = Fn/L the differential normal force, v_r=rω-v the relative velocity, and δz the differential internal friction state. This model assumes that:

a. the normal force is uniformly distributed

b. the contact velocity of each differential state element is equal to v_r

Nevertheless, it is also possible to include different normal force distribution if necessary, i. e. δFn=f(ζ).

Note that Eq. (3.2.2) describes a partial differential equation (PDE), i.e.

$$\frac{d\delta z}{dt} = \frac{\partial \delta z}{\partial \varsigma}(\varsigma,t) r\omega + \frac{\partial \delta z}{\partial t}(\varsigma,t) = v_r - \frac{\sigma_0 |v_r|}{g(v_r)} \delta z \qquad (3.2.4)$$

where $\frac{\partial \varsigma}{\partial t} = r\omega$.

The above equation should therefore be solved in both time and space.

3.3 Representation of distributed model in the form of magic formula

The linear motion of the differential δF in the patch frame Op is $\dot{\varsigma} = r\omega$, for positive ω, and $\dot{\varsigma} = -r\omega$ for negative ω (the frame origin changes location when the wheel velocity reverses). Hence $\dot{\varsigma} = r|\omega|$. We can thus rewrite Eq. (3.2.2) in the ς coordinates as:

$$\frac{d\delta z}{d\varsigma} = -\frac{\sigma_0 |s|}{g(v_r)} \delta z + |s| \operatorname{sgn}(r\omega - v) \qquad (3.3.1)$$

where $s=v_r/r\omega=1-v/r\omega$. Assuming that v, and ω are constant (hence also v_r and s), the above equation describes a linear space-invariant system having the sign of the relative velocity as its input.

The solution of the above equation over the space interval $[\zeta(t_0), \zeta(t_1)]$, or equivalent over $[\zeta_0, \zeta_1]$, with $\delta z(\zeta_0)=\zeta_0=0$ is:

$$\delta\dot{z}(\varsigma) = \mathrm{sgn}(v_r)\frac{g(v_r)}{\sigma_0}\left(1 - e^{-\frac{\sigma_0|s|}{g(v_r)}\varsigma}\right)$$

Introducing this solution together with Eq. (3.3.1) in Eq. (3.2.3), and integrating, one can obtain:

$$\int_0^t \delta\dot{z}(\varsigma)d\varsigma = \mathrm{sgn}(v_r)\frac{g(v_r)}{\sigma_0}L\left(1 + \frac{g(v_r)}{\sigma_0 L|s|}\left(e^{-\frac{\sigma_0 L|s|}{g(v_r)}} - 1\right)\right) \qquad (3.3.2)$$

Further using Equation (3.2.4), it can be shown:

$$\int_0^t \delta\dot{z}(\varsigma)d\varsigma = -v_r\frac{g(v_r)}{\sigma_0|s|}\left(e^{-\frac{\sigma_0 L|s|}{g(v_r)}} - 1\right) \qquad (3.3.3)$$

Finally, an expression for F(s) can be obtained in the form:

$$F(s) = \mathrm{sgn}(v_r)F_n g(s)\left(1 + \gamma\frac{g(s)}{\sigma_0 L|s|}\left(e^{-\frac{\sigma_0 L|s|}{g(s)}} - 1\right)\right) + F_n\sigma_2 r\omega s \qquad (3.3.4)$$

with $\gamma = 1 - \sigma_1|v_r|/g(s)$ *and*

$$g(s) = \mu_c + (\mu_s - \mu_c)e^{-\left|\frac{r\omega s}{v_s}\right|^{\frac{1}{2}}}$$

for some constant ω, and s∈[0,1].

3.4 Dynamic Tire/Road Friction Model Under Braking

Subsection 3.2 described the lumped and distributed friction models, and the difference between these two models. An expression for friction force using lumped model was presented in equation (3.2.1). Equation (3.2.3) presents the representation for distributed model in the case of traction. In this subsection, the distributed model is utilized and expanded to derive the expression for friction force under braking. The developed model referred to as dynamic tire/road friction model will be used in the development of ABS controllers in this investigation.

The uncertainty in the road characteristics or the knowledge of the function $g(v_r)$, can be modeled by introducing the parameter θ, as

$$\tilde{g}(v_r) = \theta g(v_r)$$

where $g(v_r)$ is the nominal known function in Eq. (3.2.1), and θ is an unknown parameter of the tire/road conditions, which can suitably describe the changes in the road characteristics.

Equations (3.2.2) and (3.2.3) can thus be rewritten as:

$$\frac{d\delta z}{dt}(\varsigma,t) = v_r - \theta \frac{\sigma_0 |v_r|}{g(v_r)} \delta z \qquad (3.4.1)$$

$$F = \int_0^L (\sigma_0 \delta z + \sigma_1 \delta \dot{z} + \sigma_2 v_r) \delta F_n d\varsigma \qquad (3.4.2)$$

with boundary conditions:

$$\delta z(0,t)=\delta z(L,t)=0, \qquad \forall t \geq 0, \qquad (3.4.3)$$

where $\delta Fn = Fn$ L and L is the length of the patch which is assumed to be constant.

Expressing the PDE in equation (3.4.1) as:

$$\frac{d\delta z}{dt} = \frac{\partial \delta z}{\partial \varsigma}(\varsigma, t)\frac{d\varsigma}{dt} + \frac{\partial \delta z}{\partial t}(\varsigma, t) \qquad (3.4.4)$$

and considering that the linear motion of the differential δF in the patch frame O_p is $\dot{\varsigma} = r\omega$, assuming that v and ω are constant and $\frac{\partial \delta z}{\partial t}(\varsigma, t) = 0$ within a small enough interval of time, an equation for quasi-static condition can be derived as follows:

$$\frac{d\delta z}{dt} = \frac{\partial \delta z}{\partial \varsigma}(\varsigma, t)\frac{d\varsigma}{dt} + \frac{\partial \delta z}{\partial t}(\varsigma, t) = \frac{\partial \delta z}{\partial \varsigma}(\varsigma, t) r\omega + \frac{\partial \delta z}{\partial t}(\varsigma, t) \Rightarrow$$

$$\frac{\partial \delta z}{\partial \varsigma}(\varsigma) r\omega = v_r - \frac{\sigma_0 |v_r|}{g(v_r)}\delta z \Rightarrow$$

$$\frac{d\delta z}{d\varsigma}(\varsigma) = \frac{v_r}{r\omega} - \frac{\sigma_0 |v_r / r\omega|}{g(v_r)}\delta z \qquad \varsigma \in (0, L) \qquad (3.4.5)$$

$$\varsigma(0) = \varsigma(L) = 0$$

Defining $\eta = v_r / r\omega$ and solving the above differential equation leads to:

$$\dot{\delta z} + \frac{\sigma_0 |v_r / r\omega|}{g(v_r)}\delta z - \frac{v_r}{r\omega} = \dot{\delta z} + \frac{\sigma_0 |\eta|}{g(v_r)}\delta z - \eta = 0$$

for $\delta z(\zeta)$ with initial condition $\delta z(\zeta)=\zeta=0$, it can be shown that:

$$\delta z(\varsigma)=\begin{cases}\dfrac{g(v_r)}{\sigma_0}\left(e^{-\frac{\sigma_0|\eta|}{g(v_r)}\varsigma}-1\right) & 0\le\varsigma\le\dfrac{L}{2}\\ \dfrac{g(v_r)}{\sigma_0}\left(e^{-\frac{\sigma_0|\eta|}{g(v_r)}(L-\varsigma)}-1\right) & \dfrac{L}{2}\le\varsigma\le L\end{cases} \qquad (3.4.6)$$

The first term for the friction force can then be obtained by performing the integration of the above functions in the given limits as follws:

$$\int_0^L \delta z(\varsigma)d\varsigma = \int_0^{\frac{L}{2}} \frac{g(v_r)}{\sigma_0}\left(e^{\frac{\sigma_0|\eta|}{g(v_r)}\varsigma} - 1\right)d\varsigma + \int_{\frac{L}{2}}^{L} \frac{g(v_r)}{\sigma_0}\left(e^{-\frac{\sigma_0|\eta|}{g(v_r)}(L-\varsigma)} - 1\right)d\varsigma$$

$$= \frac{g(v_r)}{\sigma_0}\int_0^{\frac{L}{2}}\left(e^{-\frac{\sigma_0|\eta|}{g(v_r)}\varsigma} - 1\right)d\varsigma + \frac{g(v_r)}{\sigma_0}\int_{\frac{L}{2}}^{L}\left(e^{-\frac{\sigma_0|\eta|}{g(v_r)}(L-\varsigma)} - 1\right)d\varsigma$$

$$= \frac{g(v_r)}{\sigma_0}\left(-\frac{g(v_r)}{\sigma_0|\eta|}e^{-\frac{\sigma_0|\eta|}{g(v_r)}\varsigma} - \varsigma\right)_0^{\frac{L}{2}} + \frac{g(v_r)}{\sigma_0}\left(\frac{g(v_r)}{\sigma_0|\eta|}e^{-\frac{\sigma_0|\eta|}{g(v_r)}L}e^{\frac{\sigma_0|\eta|}{g(v_r)}\varsigma} - \varsigma\right)_{\frac{L}{2}}^{L}$$

$$= \frac{g(v_r)}{\sigma_0}\left\{\left[\left(-\frac{g(v_r)}{\sigma_0|\eta|}e^{-\frac{\sigma_0|\eta|}{g(v_r)}\frac{L}{2}} - \frac{L}{2}\right) - \left(-\frac{g(v_r)}{\sigma_0|\eta|}e^{0} - 0\right)\right] + \left[\left(\frac{g(v_r)}{\sigma_0|\eta|}e^{-\frac{\sigma_0|\eta|}{g(v_r)}(L-L)} - L\right) - \left(\frac{g(v_r)}{\sigma_0|\eta|}e^{-\frac{\sigma_0|\eta|}{g(v_r)}(L-\frac{L}{2})} - \frac{L}{2}\right)\right]\right\}$$

$$= \frac{g(v_r)}{\sigma_0}\left\{\left[-\frac{g(v_r)}{\sigma_0|\eta|}\left(e^{-\frac{\sigma_0|\eta|L}{2g(v_r)}} - 1\right) - \frac{L}{2}\right] + \left[\left(\frac{g(v_r)}{\sigma_0|\eta|} - L\right) - \left(\frac{g(v_r)}{\sigma_0|\eta|}e^{-\frac{\sigma_0|\eta|\frac{L}{2}}{g(v_r)}} - \frac{L}{2}\right)\right]\right\}$$

$$= \frac{g(v_r)}{\sigma_0}\left\{\left[-\frac{g(v_r)}{\sigma_0|\eta|}\left(e^{-\frac{\sigma_0|\eta|L}{2g(v_r)}} - 1\right) - \frac{L}{2}\right] + \left[-\frac{g(v_r)}{\sigma_0|\eta|}\left(e^{-\frac{\sigma_0|\eta|L}{2g(v_r)}} - 1\right) - \frac{L}{2}\right]\right\}$$

$$= \frac{g(v_r)}{\sigma_0}\left[-\frac{2g(v_r)}{\sigma_0|\eta|}\left(e^{-\frac{\sigma_0|\eta|L}{2g(v_r)}} - 1\right) - L\right]$$

$$= -\frac{g(v_r)}{\sigma_0}L\left[\frac{2g(v_r)}{\sigma_0|\eta|L}\left(e^{-\frac{\sigma_0|\eta|L}{2g(v_r)}} - 1\right) + 1\right]$$

$$= -\frac{g(v_r)}{\sigma_0}L\left[1 + \frac{2g(v_r)}{\sigma_0|\eta|L}\left(e^{-\frac{\sigma_0|\eta|L}{2g(v_r)}} - 1\right)\right] \qquad (3.4.7)$$

The expressions for the second term of the friction force can be established by substituting Eq.(3.4.6) into Eq.(3.4.4), which yields:

$$\dot{\delta z} = \frac{d\delta z}{dt} = \begin{cases} v_r - \dfrac{\sigma_0|v_r|}{g(v_r)}\dfrac{g(v_r)}{\sigma_0}\left(e^{-\frac{\sigma_0|\eta|}{g(v_r)}\varsigma} - 1\right) & 0 \le \varsigma \le \dfrac{L}{2} \\ v_r - \dfrac{\sigma_0|v_r|}{g(v_r)}\dfrac{g(v_r)}{\sigma_0}\left(e^{-\frac{\sigma_0|\eta|}{g(v_r)}(L-\varsigma)} - 1\right) & \dfrac{L}{2} < \varsigma \le L \end{cases}$$

$$= \begin{cases} v_r - |v_r|\left(e^{-\frac{\sigma_0|\eta|}{g(v_r)}\varsigma} - 1\right) & 0 \le \varsigma \le \dfrac{L}{2} \\ v_r - |v_r|\left(e^{-\frac{\sigma_0|\eta|}{g(v_r)}(L-\varsigma)} - 1\right) & \dfrac{L}{2} < \varsigma \le L \end{cases} \qquad (3.4.8)$$

Following the same approach is the first term, the second term of the friction force is then obtained in the following steps.

$$\int_0^L \delta\dot{z}(\varsigma)d\varsigma = \int_0^{\frac{L}{2}}\left[v_r - |v_r|\left(e^{-\frac{\sigma_0|\eta|}{g(v_r)}\varsigma} - 1\right)\right]d\varsigma + \int_{\frac{L}{2}}^{L}\left[v_r - |v_r|\left(e^{-\frac{\sigma_0|\eta|}{g(v_r)}(L-\varsigma)} - 1\right)\right]d\varsigma$$

$$= \left[v_r\varsigma - |v_r|\left(-\frac{g(v_r)}{\sigma_0|\eta|}e^{-\frac{\sigma_0|\eta|}{g(v_r)}\varsigma} - \varsigma\right)\right]_0^{\frac{L}{2}} + \left[v_r\varsigma - |v_r|\left(\frac{g(v_r)}{\sigma_0|\eta|}e^{-\frac{\sigma_0|\eta|}{g(v_r)}(L-\varsigma)} - \varsigma\right)\right]_{\frac{L}{2}}^{L}$$

$$= \left\{\left[v_r\frac{L}{2} - |v_r|\left(-\frac{g(v_r)}{\sigma_0|\eta|}e^{-\frac{\sigma_0|\eta|\frac{L}{2}}{g(v_r)}} - \frac{L}{2}\right)\right] - \left[0 - |v_r|\left(-\frac{g(v_r)}{\sigma_0|\eta|}e^{0} - 0\right)\right]\right\} +$$

$$\left\{\left[v_rL - |v_r|\left(\frac{g(v_r)}{\sigma_0|\eta|}e^{-\frac{\sigma_0|\eta|}{g(v_r)}(L-L)} - L\right)\right] - \left[v_r\frac{L}{2} - |v_r|\left(\frac{g(v_r)}{\sigma_0|\eta|}e^{-\frac{\sigma_0|\eta|}{g(v_r)}(L-\frac{L}{2})} - \frac{L}{2}\right)\right]\right\}$$

$$= \left[\frac{v_rL}{2} + \frac{|v_r|g(v_r)}{\sigma_0|\eta|}e^{-\frac{\sigma_0|\eta|\frac{L}{2}}{g(v_r)}} + \frac{|v_r|L}{2} - \frac{|v_r|g(v_r)}{\sigma_0|\eta|}\right] +$$

$$\left\{\left[v_rL - \frac{|v_r|g(v_r)}{\sigma_0|\eta|}e^{0} + |v_r|L\right] - \left[\frac{v_rL}{2} - \frac{|v_r|g(v_r)}{\sigma_0|\eta|}e^{-\frac{\sigma_0|\eta|}{g(v_r)}(L-\frac{L}{2})} + \frac{|v_r|L}{2}\right]\right\}$$

$$= \left[-\frac{|v_r|g(v_r)}{\sigma_0|\eta|}\left(1 - e^{-\frac{\sigma_0|\eta|L}{2g(v_r)}}\right) + \frac{L}{2}(v_r + |v_r|)\right] + \left[-\frac{|v_r|g(v_r)}{\sigma_0|\eta|}\left(1 - e^{-\frac{\sigma_0|\eta|L}{2g(v_r)}}\right) + \frac{L}{2}(v_r + |v_r|)\right]$$

$$= -\frac{2|v_r|g(v_r)}{\sigma_0|\eta|}\left(1 - e^{-\frac{\sigma_0|\eta|L}{2g(v_r)}}\right) + L(v_r + |v_r|) \qquad (3.4.9)$$

In braking case, $r\omega < V$, so $Vr = r\omega - v > 0$. Therefore, $|v_r| = -v_r$ *and* $v_r + |v_r| = 0$.

Hence equaion (3.4.9) simplifies to:

$$\delta\dot{z} = -\frac{2|v_r|g(v_r)}{\sigma_0|\eta|}\left(1 - e^{-\frac{\sigma_0|\eta|L}{2g(v_r)}}\right) \qquad (3.4.10)$$

Substituting Eq.(3.4.7) and Eq. (3.4.10) into Eq. (3.4.2), and for constant velocity v, the expression for friction force in braking can be derived as shown in the following steps.

$$
\begin{aligned}
F(\eta,v) &= \int_0^L (\sigma_0\delta\xi + \sigma_1\dot{\delta\xi} + \sigma_2 v_r)\delta F_z d\varsigma \\
&= \int_0^L (\sigma_0\delta\xi + \sigma_1\dot{\delta\xi} + \sigma_2 v_r)\frac{F_z}{L} d\varsigma \\
&= \int_0^L \sigma_0\delta\xi\frac{F_z}{L} d\varsigma + \int_0^L \sigma_1\dot{\delta\xi}\frac{F_z}{L} d\varsigma + \int_0^L \sigma_2 v_r\frac{F_z}{L} d\varsigma \\
&= \frac{\sigma_0 F_z}{L}\int_0^L \delta\xi d\varsigma + \frac{\sigma_1 F_z}{L}\int_0^L \dot{\delta\xi} d\varsigma + \frac{\sigma_2 v_r F_z}{L}\int_0^L d\varsigma \\
&= \frac{\sigma_0 F_z}{L}\left\{-\frac{g(v_r)}{\sigma_0}L\left[1+\frac{2g(v_r)}{\sigma_0 L|\eta|}\left(e^{-\frac{\sigma_0|\eta|L}{2g(v_r)}}-1\right)\right]\right\} + \frac{\sigma_1 F_z}{L}\left[-\frac{2|v_r|g(v_r)}{\sigma_0|\eta|}\left(1-e^{-\frac{\sigma_0|\eta|L}{2g(v_r)}}\right)\right] + \sigma_2 v_r F_z \\
&= -F_z g(v_r)\left[1+\frac{2g(v_r)}{\sigma_0|\eta|L}\left(e^{-\frac{\sigma_0|\eta|L}{2g(v_r)}}-1\right)\right] - \frac{2\sigma_1 F_z|v_r|g(v_r)}{L\sigma_0|\eta|}\left(1-e^{-\frac{\sigma_0|\eta|L}{2g(v_r)}}\right) + \sigma_2 v_r F_z \\
&= -F_z g(v_r)\left[1+\frac{2g(v_r)}{\sigma_0|\eta|L}\left(e^{-\frac{\sigma_0|\eta|L}{2g(v_r)}}-1\right) - \frac{2\sigma_1|v_r|}{L\sigma_0|\eta|}\left(e^{-\frac{\sigma_0|\eta|L}{2g(v_r)}}-1\right)\right] + \sigma_2 v_r F_z \\
&= -F_z g(v_r)\left[1+\left(\frac{2g(v_r)}{\sigma_0|\eta|L}-\frac{2\sigma_1|v_r|}{L\sigma_0|\eta|}\right)\left(e^{-\frac{\sigma_0|\eta|L}{2g(v_r)}}-1\right)\right] + \sigma_2 v_r F_z \\
&= -F_z g(v_r)\left(1+2\gamma\frac{g(v_r)}{\sigma_0 L|\eta|}\left(e^{-\frac{\sigma_0 L|\eta|}{2g(v_r)}}-1\right)\right) + F_n\sigma_2 v_r
\end{aligned}
\qquad (3.4.11)
$$

with $\gamma = 1-\dfrac{\sigma_1|v_r|}{g(v_r)}$ *and*

$\eta = \dfrac{v_r}{r\omega} = -\dfrac{s}{1-s}$, *and skid*, $s = \dfrac{v-r\omega}{v}$

where s is the longitudinal skid under braking. Eq. (3.4.11) is similar to the traction case derived in subsection 3.2 that considers the angular velocity ω to be constant. $\lambda \in [0,1]$ was used in subsection 3.2, while in this case $\eta \in (-\infty,0]$.

In the pseudo-static expression in Eq. (3.4.11), it is assumed that the velocity is constant. If velocity changes, the resulting curve will changes as well. However, by examining the dynamic equation for the internal state z reveals that it changes much faster than vehicle dynamics or velocity. Based on this observation, it is assumed that, for each time step, this formula can be used to calculate the approximated maximum peak value of the braking force produced by the tire/road friction.

The static expression in Eq. (3.4.11) is a function of longitudinal skid ratio s. In the braking case, it has been defined as $s = \frac{v - r\omega}{v}$. When the vehicle's velocity becomes very small, the relationship does not have real physical significance. However, since the interest here is to find a controller strategy for braking the car at fairly high speeds, this approach for large velocities can be utilized with an established lower bound v_{min} to obtain good braking. This translates to selecting an upper bound $\bar{s}$ for the maximum skid ratio $s_{max} \in [0, \bar{s}]$ in Eq. (3.4.11).

A set of parameters used for a static curve of the dynamic friction model of the tire is shown in table 3.1. Simulation results obtained from equation (3.4.11) showing normalized friction force as a function of skid rate is presented in figure 3.3. For different values of road condition parameter θ.

A set of results computed using Magic Formula along with those obtained form friction model are presented in Figure 3.4 for comparison.

Table 3.1. Parameters used for static expression by Eq. (3.4.5)

Parameter	Value	Units
σ_0	40	1/m
σ_1	4.9487	s/m
σ_2	0.0018	s/m
μ_C	0.9	---
μ_S	0.5	---
V_s	12.5	m/s
L	0.25	m

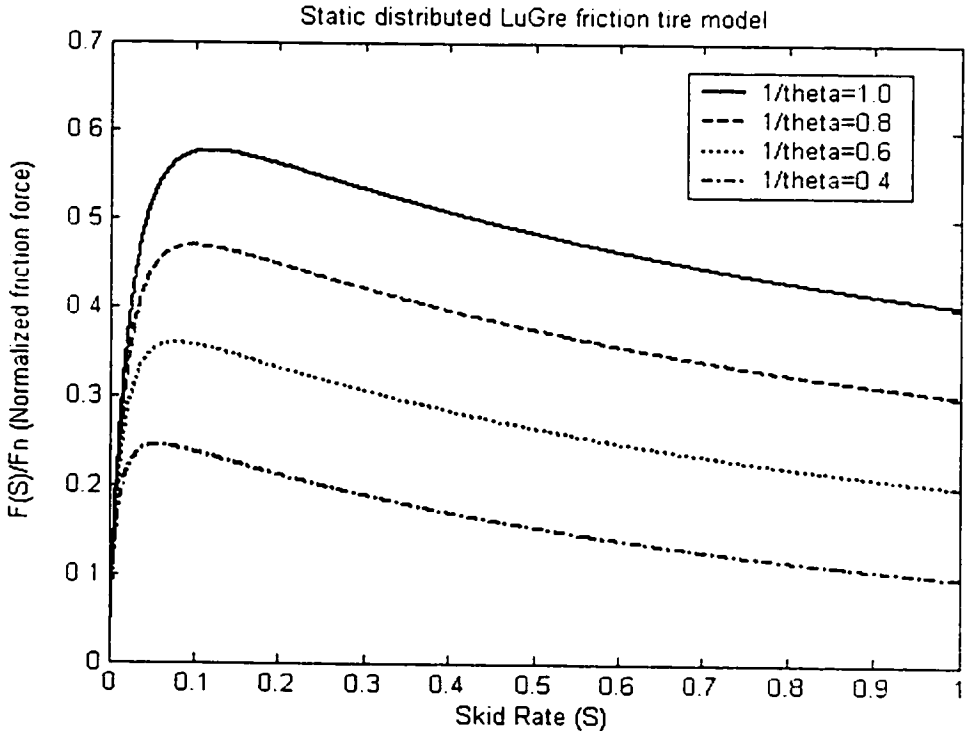

Fig. 3.3 Dynamic model prediction of static normalized friction $\mu=F(s)/Fn$, as a function of the skid rate s, at a velocity v=20 m/s, for different value of θ

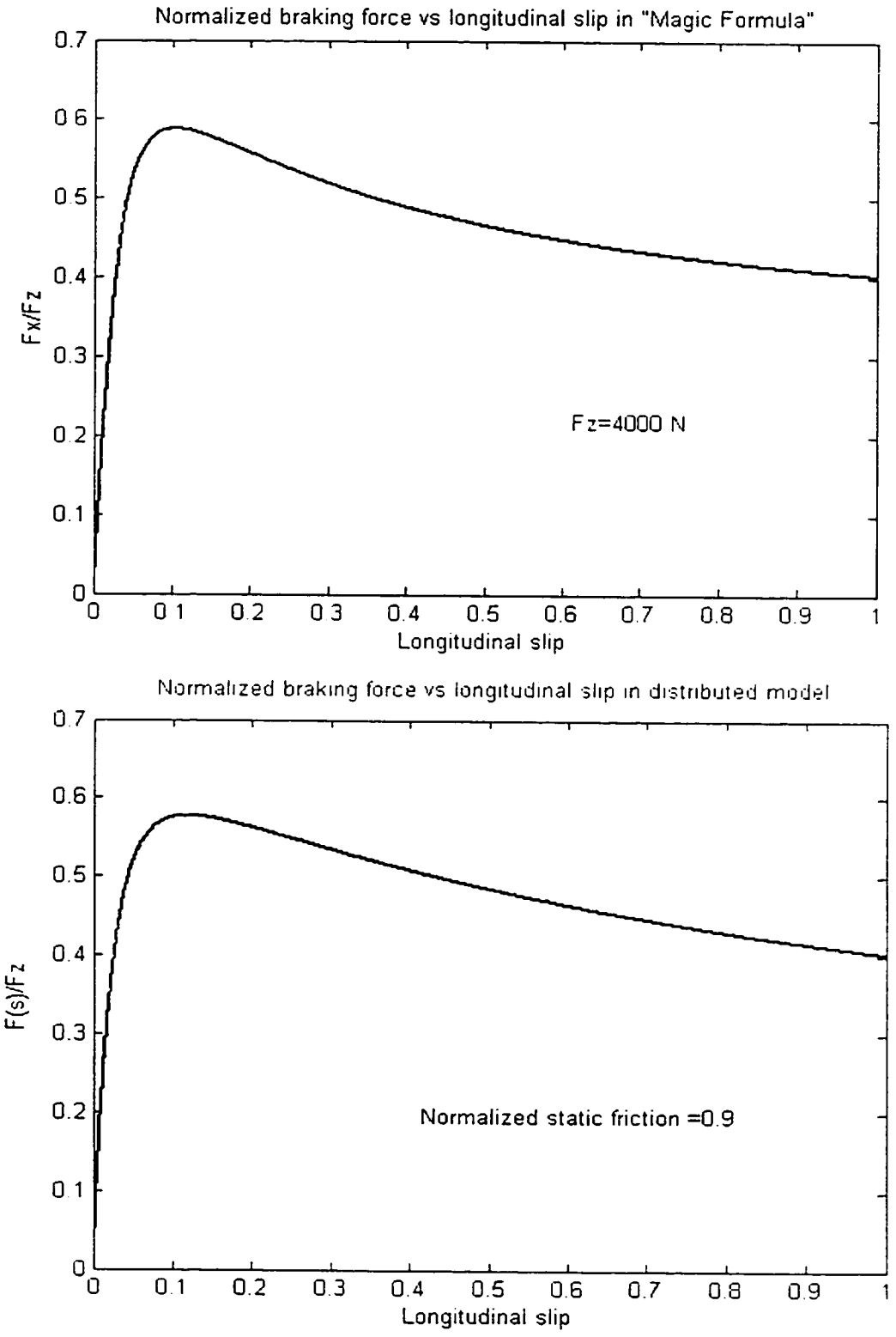

Fig. 3.4 Comparison between the dynamic model and the "magic formula" for a tested tire in brake case

3.5 Vehicle Model

As discussed earlier, a simplified quarter vehicle model is utilized in this investigation to study proposed tire model with ABS controllers. The quarter-vehicle, however, may be assigned either 2 DOFs or 3 DOFs depending on the vehicle modeling and response requirement. In Chapter IV, a 3 DOFs vehicle model is used for an ABS PI controller. The DOF includes vehicle forward velocity, angular velocity of the wheel, and pitch motion of the vehicle to account for the load shift. In Chapter V, a simple 2 DOF vehicle model with forward velocity of the vehicle and angular velocity of the wheel, is used for the development of the robust (slide mode) controller. A quarter vehicle model is the fundamental model, which can provide basic information regarding brake system behavior in order to develop the fundamental controller. Such controller can then be easily extended to multi-DOF vehicle model to study the vehicle performance. For example, a commonly used handling model referred to as "bicycle model" with in plane vehicle mass & two axle can be simply regarded as a model including two quarter models with or without the consideration of the pitch motion. The controller developed from the quarter vehicle model is still valid for such a "bicycle model".

In deriving the equation of motion for the 2 DOF quarter vehicle model, it is assumed that sprung and unsprung masses along with all its component move together as one unit. Furthermore, it is assumed that mass of the vehicle include the effective mass due to rotating inertia of the components. The simplified model also neglects the vertical dynamic of the vehicle and it effect on the braking. A schematic drawing of the quarter vehicle model along with its motion, forces and moments are shown in Fig. 3.5. The most simple expressions for the two equations under braking can be expressed as:

$$\begin{cases} m\dot{v} = -F_x - F_a - F_f \\ J\dot{\omega} = -T_b + RF_x + RF_f \end{cases} \tag{3.5.1}$$

where F_x, F_a and F_f are the braking, aerodynamic and rolling resistance forces, respectively, T_b is the applied braking torque, R is the effective rolling radian of the wheel, V and ω are forward velocity of the vehicle, and angular velocity of the wheel, respectively.

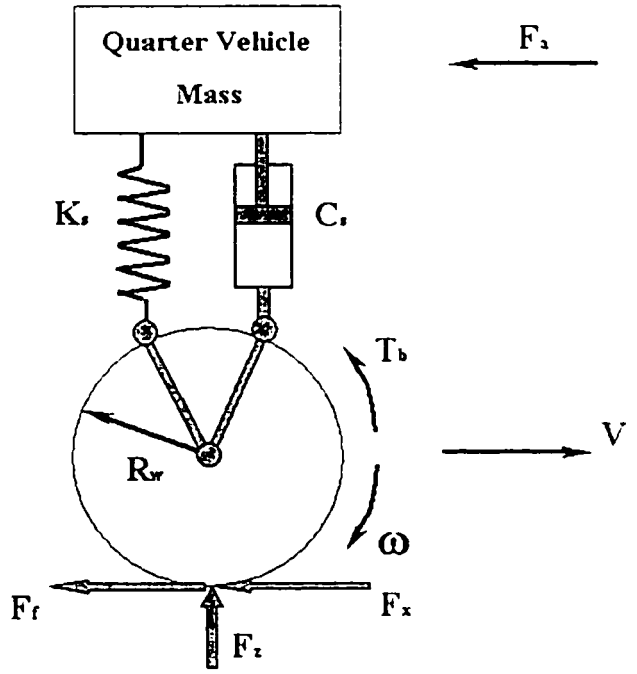

Figure 3.5 The free body diagram for 2 DOFs quarter vehicle model

These equations although very simple, are highly useful to carry out preliminary investigations of straight line braking performance and brake system control strategies. This model can further be easily extended to include important effect of load shift due to

deceleration in pitch plane that has direct influence on brake force limits and braking performance.

Inclusion of the effect of pitch load shift, i.e. a 3-DOF system can be achieved with the two equations described in Eq. (3.5.1), provided the pitch motion itself is of no interest and is negligible. The pitch plane model of the vehicle showing the effect of longitudinal deceleration is shown in Fig. 3.6(a), while the free-body-diagram of the wheel model is shown in Fig. 3.6(b).

As evident, the primary effect of the pitch plane load shift is the change in normal tire force F_z. Neglecting the effect of aerodynamic drag, the expression for normal forces at the front and rear tires can be obtained by taking moments about the two contact patches to yield:

$$F_{zf} = \frac{mgl_r - ma_x h_{cg}}{l_f + l_r} \qquad (3.5.2)$$

$$F_{zr} = \frac{mgl_f + ma_x h_{cg}}{l_f + l_r} \qquad (3.5.3)$$

where m is the vehicle mass, F_{zf} and F_{zr} are the normal forces of front and rear tires, respectively, a_x is the instantaneous longitudinal acceleration, and h_{cg} is the height of the vehicle CG from the ground, l_f and l_r define the location of CG from axles as shown in Figure 3.6(a), where l_f + l_r = wheel base of the vehicle (l).

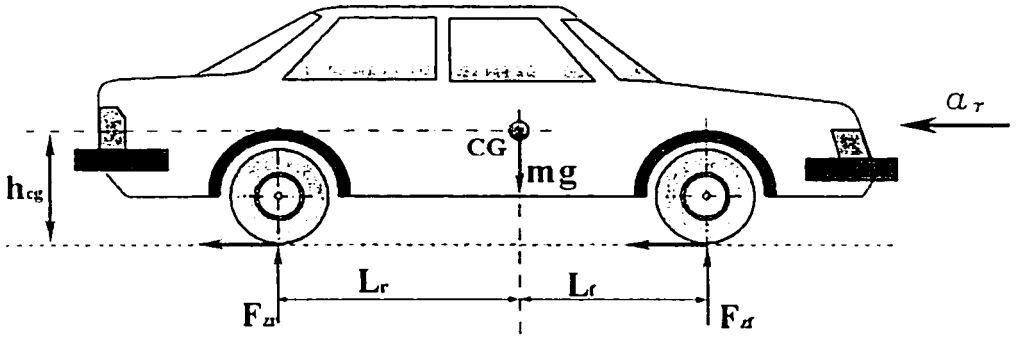

a) **Pitch plane model of vehicle**

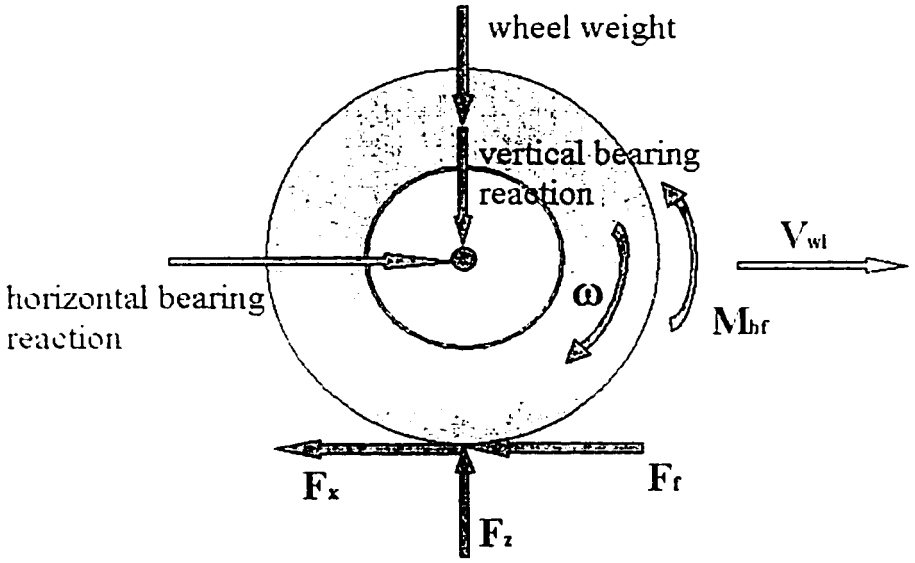

b) **Free body diagram of a wheel model with pitch load shift**

Fig. 3.6 Description of model with pitch load shift

Using the approximate F_z expression from the above equations, one can model the front or rear quarter vehicle model using equation (3.5.1). In the equation, however, F_r and F_f are function of the normal load F_z, and thus must be expressed in terms of a_x as given by equations (3.5.2) and (3.5.3).

The tire and vehicle model developed in this chapter are utilized in Chapter IV for the design of PI controller for ABS. In Chapter V, the model is further used for the design of robust (sliding mode) controller.

CHAPTER IV
PI CONTROLLER DESIGN

4.1 Introduction

Dynamic friction model for tire forces and simplified vehicle model for brake system are presented in Chapter III. These models are incorporated in order to develop controllers for ABS. Two control strategies, namely, PI controller and sliding mode control are utilized to demonstrate the effectiveness of the developed tire model in the design of ABS controllers.

This chapter develops the mathematics for the simulation of ABS using PI controller. Sample simulation results are presented to demonstrate the performance of ABS with the controller. The next chapter is developed to a similar analysis with sliding mode controller.

4.2 Quarter Vehicle Model

A quarter vehicle model describing longitudinal motion of the vehicle and angular motion of the wheel under braking is described in Chapter III. The free body diagram of the quarter vehicle model is shown in Fig. 4.1, where m_{car} represents the vehicle's mass, m_t represents the mass of one wheel assembly, and J_u represents the effective rotating inertia of one wheel assemlby. Two motions of the vehicle are forward

velocity(v) and angular velocity of wheel (ω). Various forces and moments acting on the model under braking operation include:

F_L: Load transfer between axle under deceleration

F_a: Aerodynamic drag force

T_b: Braking torque

F_z: Normal tire force

F_t: Longitudinal force at tire-road interface

F_f: Tire rolling resistance

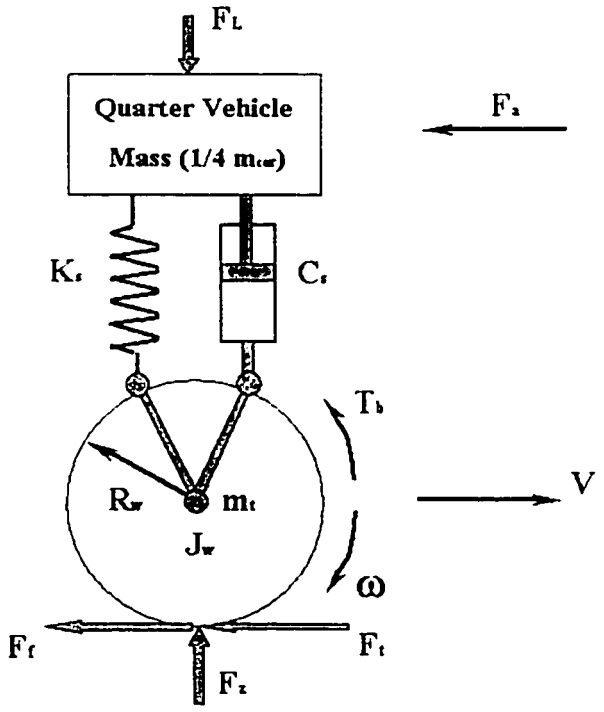

Fig. 4.1 Quarter vehicle model

The equation of motion as derived in Chapter III for rotation of wheel and forward velocity of the vehicle are:

$$\begin{cases} J_w \dot{\omega} = -T_b + R_w F_t + R_w F_f & (4.1) \\ m_{tot} \dot{v} = -F_t - F_a - F_f & (4.2) \end{cases}$$

where R_w is the effective radian of the wheel.

In the above equation (4.1), J_w is the effective wheel inertia which includes the inertia of the wheel assembly (J_t) as well as a component of inertia due to other rotating parts. The effective inertia can be expressed as:

$$J_w = J_t + \frac{1}{2}\xi^2 J_e \qquad (4.3)$$

where J_e is the rotating inertia of the engine & drive, ξ is the total gear ratio and $1/2$ is used to account for contribution to one wheel for a 2 wheel drive vehicle.

The value of m_{tot} in equation (4.2) for a quarter-vehicle is established by adding quarter of the vehicle mass m_{car} to that of one wheel suspension assembly (m_t) as:

$$m_{tot} = m_t + \frac{1}{4} m_{car} \qquad (4.4)$$

The term for rolling resistance in the equation of motion can be expressed by an empirical relationship as [73]:

$$F_f = (f_0 + 3.24 f_s (\frac{K_{mph} v}{100})^{2.5}) F_z \qquad (4.5)$$

where f_1 and f_2 are curve fit parameters to satisfy empirical relationship. K_{mph}=2.237 is a factor introduced with velocity (v) to account for the unit of velocitys, such that v in equation (4.5) can be converted to miles per hour (mph).

The aerodynamic drag force F_a in equation (4.2) can be expressed as:

$$F_a = \frac{\rho}{2} C_d A_f v^2 \qquad (4.6)$$

where ρ is the air density, C_d is the drag coefficient, A_f is the front area and v is the forward velocity of the vehicle. In this investigation, it is assumed that the drag force only act in the longitudinal direction and does not contribute pitching or pitch load transfer.

The force F_t in equation (4.1) and (4.2) is the longitudinal force at the tire road interface which is obtained from dynamic friction tire model expressed as:

$$F_t = \mu(\lambda, \theta) F_z \qquad (4.7)$$

where μ is the dynamic friction coefficient which is a function of skid λ and road condition parameter θ. F_z is the normal load due to vehicle mass and load shift in pitch plane, expressed earlier by:

$$F_z = m_{tot} g \pm \frac{m_{car} h_{cg}}{l} \dot{v} \qquad (4.8)$$

where l is the wheel base ($l_f + l_r$), h_{cg} is the CG height from ground, $\dot{v}$ is the forward acceleration, and m_{car} represents the sprung mass of the vehicle. The second term therefore represents the load shift during braking deceleration from the rear to the

front axle. Hence, for modeling rear wheel, the negative sign will be used in computation of F_z

Substituting the expressions into the right hand side of the equation of motion presented in equation (4.1) and (4.2) will yield:

$$\begin{cases} J_w\dot{\omega} = -T_b + R_w\left(\mu(\lambda)\left(m_{tot}g \pm \frac{m_{car}h_{cg}}{l}\dot{v}\right)\right) + R_w\left(f_0 + 3.24f_s\left(\frac{K_{mph}v}{100}\right)^{2.5}\right)F_z & (4.9) \\ m_{tot}\dot{v} = -\mu(\lambda)\left(m_{tot}g \pm \frac{m_{car}h_{cg}}{l}\dot{v}\right) - \frac{\rho}{2}C_dA_fv^2 - \left(f_0 + 3.24f_s\left(\frac{K_{mph}v}{100}\right)^{2.5}\right)F_z & (4.10) \end{cases}$$

Equation (4.10) can be easily rearranged to obtain an expression for longitudinal acceleration as:

$$\dot{v} = \frac{-\mu(\lambda)m_{tot}g - \frac{\rho}{2}C_dA_fv^2}{m_{tot} \mp \mu(\lambda)\frac{m_{car}h_{cg}}{l}} \qquad (4.11)$$

In the above expression, the effect of rolling resistance (i.e. the last term in Eq.(4.10)) is neglected for simplification of the acceleration expression. The effect of neglecting F_f is considered negligible for the performance of ABS.

Also, equation (4.9) can be rearranged as:

$$\begin{aligned} \dot{\omega} &= -\frac{T_b}{J_w} + \frac{R_w}{J_w}\mu(\lambda)\left(m_{tot}g \pm \frac{m_{car}h_{cg}}{l}\dot{v}\right) + \frac{R_w}{J_w}\left(f_0 + 3.24f_s\left(\frac{K_{mph}v}{100}\right)^{2.5}\right)\left(m_{tot}g \pm \frac{m_{car}h_{cg}}{l}\dot{v}\right) \\ &= -\frac{T_b}{J_w} + \frac{R_w}{J_w}\left(\mu(\lambda) + f_0 + 3.24f_s\left(\frac{K_{mph}v}{100}\right)^{2.5}\right)\left(m_{tot}g \pm \frac{m_{car}h_{cg}}{l}\dot{v}\right) \qquad (4.12) \end{aligned}$$

By defining the following state space variables:

$$x_1 = x,\ x_2 = \dot{x} = v,\ x_3 = \omega,\ m_{eq} = \frac{m_{car} h_{cg}}{l},\ u = T_b,$$

Equation (4.11) and (4.12) can be written as:

$$\begin{cases} \dot{x}_2 = \dfrac{-\mu(\lambda) m_{tot} g - \dfrac{\rho}{2} C_d A_f x_2^2}{m_{tot} \mp \mu(\lambda) m_{eq}} & (4.13) \\ \dot{x}_3 = \dfrac{R_w}{J_w}\left(\mu(\lambda) + f_0 + 3.24 f_s \left(\dfrac{K_{mph}}{100} x_2\right)^{2.5}\right)\left(m_{tot} g \pm \dfrac{m_{car} h_{cg}}{l} \dot{x}_2\right) - \dfrac{u}{J_w} & (4.14) \end{cases}$$

Let

$$A = \begin{bmatrix} 1 & 0 & 0 \\ 0 & 1 & 0 \\ 0 & \pm \dfrac{R_w}{J_w}\left(\mu(\lambda) + f_0 + 3.24 f_s \left(\dfrac{K_{mph}}{100} x_2\right)^{2.5}\right) \dfrac{m_{car} h_{cg}}{l} & 1 \end{bmatrix} \quad (4.15)$$

Then, the quarter vehicle model can take the form in state-space format as following:

$$\begin{bmatrix} \dot{x}_1 \\ \dot{x}_2 \\ \dot{x}_3 \end{bmatrix} = A \begin{bmatrix} x_2 \\ \dfrac{-\mu(\lambda) m_{tot} g - \dfrac{\rho}{2} C_d A_f x_2^2}{m_{tot} \mp \mu(\lambda) m_{eq}} \\ \dfrac{R_w}{J_w}\left(\mu(\lambda) + f_0 + 3.24 f_s \left(\dfrac{K_{mph}}{100} x_2\right)^{2.5}\right) m_{tot} g \end{bmatrix} + \begin{bmatrix} 0 \\ 0 \\ -\dfrac{1}{J_w} \end{bmatrix} u \quad (4.16)$$

Next step, our task is to design proper controller for the derived vehicle system.

The model parameters used for the vehicle system of this study are given in Table4.1: [21], [54].

Table 4.1: Vehicle parameters

g	9.81 m/s^2	gravitational acceleration
l	2.5 m	wheel base
h_{cg}	0.5 m	center of gravity height
m_t	40 kg	tire mass
$¼\ m_{car}$	375 kg	quarter vehicle mass
J_t	1.7 kgm^2	wheel inertia
J_e	0.241 kgm^2	engine inertia
ξ	10.0	transmission gear ratio
R_w	0.326 m	wheel radius
f_0	0.01	basic coefficient
f_s	0.005	speed effect coefficient
A_f	2.04 m^2	vehicle frontal area
C_d	0.539	vehicle drag coefficient
K_{mph}	2.237	speed scaling constant
ρ	1.23 kg/m^3	air density

4.3 Brake System Simulation

The simplified vehicle model for simulation of braking performance developed in section (4.2) is utilized here under application of a braking torque. The study is then extended to ABS with PI control in section (4.4).

In general, application of very large braking torque for a period will cause rapid increase in the longitudinal skid at the tire road interface leading to wheel lock up at 100% skid. A typical braking torque time history that can be applied for simulations, testing and evaluations of braking system are shown in Figure 4.2.

As shown, the braking sequence consists of a very small braking torque of magnitude 200 Nm is exerted for 0.5 seconds, then the braking torque is rapidly increased to a value, 2000 Nm, in 0.1 seconds, and exerted for 0.5 seconds. The braking torque is then completely released, and brought down to 0 in a period of 0.1 seconds and keep this no-braking condition for 0.5 seconds. The braking torque then applied again to reach to 1000 Nm in 0.1 second and keep this value as illustrated in the figure. The total braking sequence as shown lasts for a period of 2.5 seconds.

The vehicle parameters used for the simulation are presented in table 4.1. A first set of braking response simulation is obtained for an initial velocity of 20 m/s. The resulting time history of the vehicle forward velocity for the period is shown in Figure 4.3. As demonstrated in this result, the given braking torque sequence brings the vehicle velocity from 20 m/s to 9 m/s in the 2.5 seconds, where slopes of the curve on effective deceleration is higher corresponding to the period of higher torque. The corresponding angular velocity of the wheel is presented in Figure 4.4. Further results in terms of tire

longitudinal skid and deceleration of the vehicle are obtained and presented in Figure 4.5 and 4.6, respectively. These results can be easily examined for an in-depth understanding and qualitative validation of the simulation results.

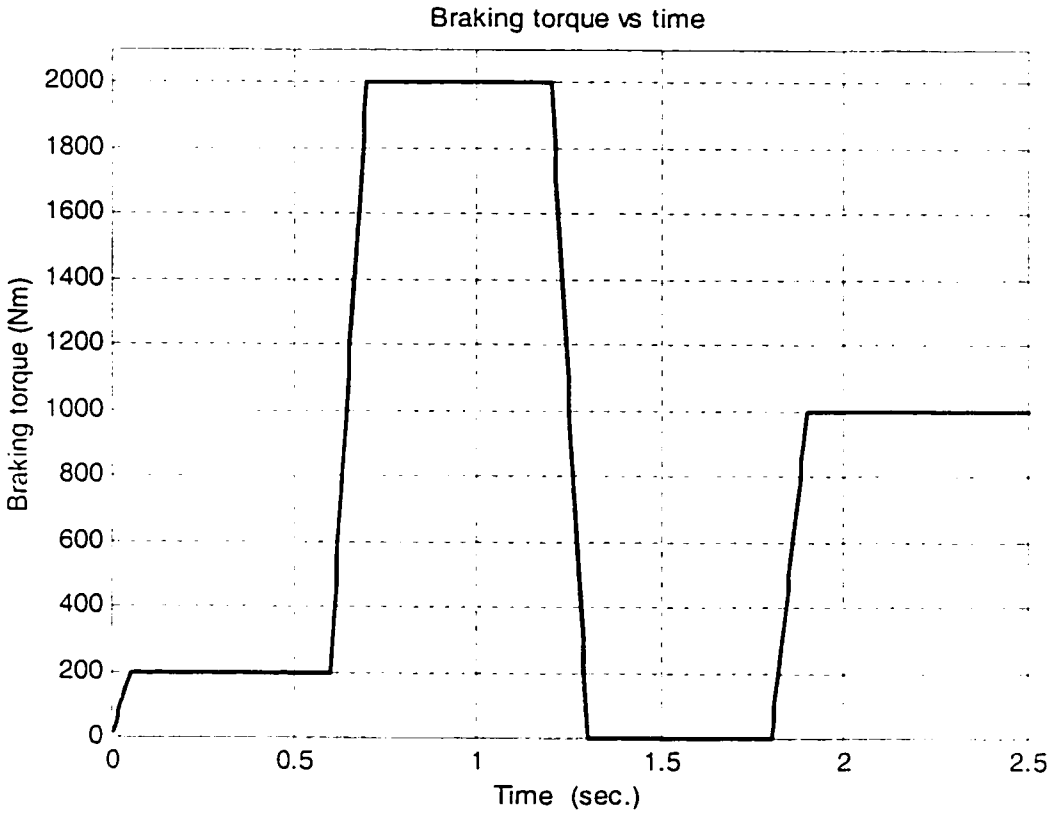

Fig. 4.2 Input braking torque time history

As shown, when the small braking torque for a 0.55 seconds was applied to the vehicle braking system, the velocity reduced slowly, from initial 20 m/s to 19 m/s, while angular velocity of the wheel reduced from initial 62 rad/s to 58 rad/s. The resulting skid of tire as shown in Figure 4.5 was approximately 0.01 or 1%. As shown in Figure 4.6, the deceleration of the vehicle in this period reached from 0 to –0.22 g. The braking torque was then stepped up to 2000 Nm from 0.6 second to 0.7 second, and kept this value until 1.2 second. During this period, the velocity reduced rapidly, from 19 m/s to 13.5 m/s as

shown in Figure 4.3. Because of the very high braking torque, the wheel was fully locked and resulted in angular velocity being reduced from 58 rad/s to 0 rad/s as shown in Figure 4.4. Locking of the wheel results in 100% skid or gross skid of the wheel during the high braking torque, as shown in Figure 4.5. The corresponding vehicle deceleration as shown in Figure 4.6 increases rapidly to its maximum value. It can be easily noted from this result that the peak braking force or deceleration correspond to approximate 20% skid value and is 0.75g. During 100% skid the deceleration as expected reduces to 0.7g, due to sliding friction value. During the next braking segment, starting at 1.2 second, the braking torque was fully released down to 0 Nm at 1.3 second, and kept at this no-braking condition until 1.8 second. During this period, the velocity maintained its value as the locked wheel was released, allowing the angular velocity to climb back to 42 rad/s. The longitudinal skid and braking deceleration also reflected this as both these values reduces to zero during this period. Finally, the braking torque was stepped up to 1000 Nm from 0 at 1.9 second, and kept at this value until the illustration time was over at 2.5 second. Corresponding to this braking torque, the velocity reduced again from 13.5 m/s to 9 m/s, and the angular velocity also reduced from 42 rad/s to 13 rad/s. During this period, the longitudinal skid increased again from 0 to 0.54, causing the braking deceleration to reach its maximum value again. It is again evident that the maximum deceleration corresponds to 20% skid and the deceleration drops slightly as skid level increase gradually.

The above results for application of given braking sequence clearly demonstrate its effect on various variables and leaded confidence on the model as a representative of a real brake system.

Fig. 4.3 Velocity response for PI brake model illustration

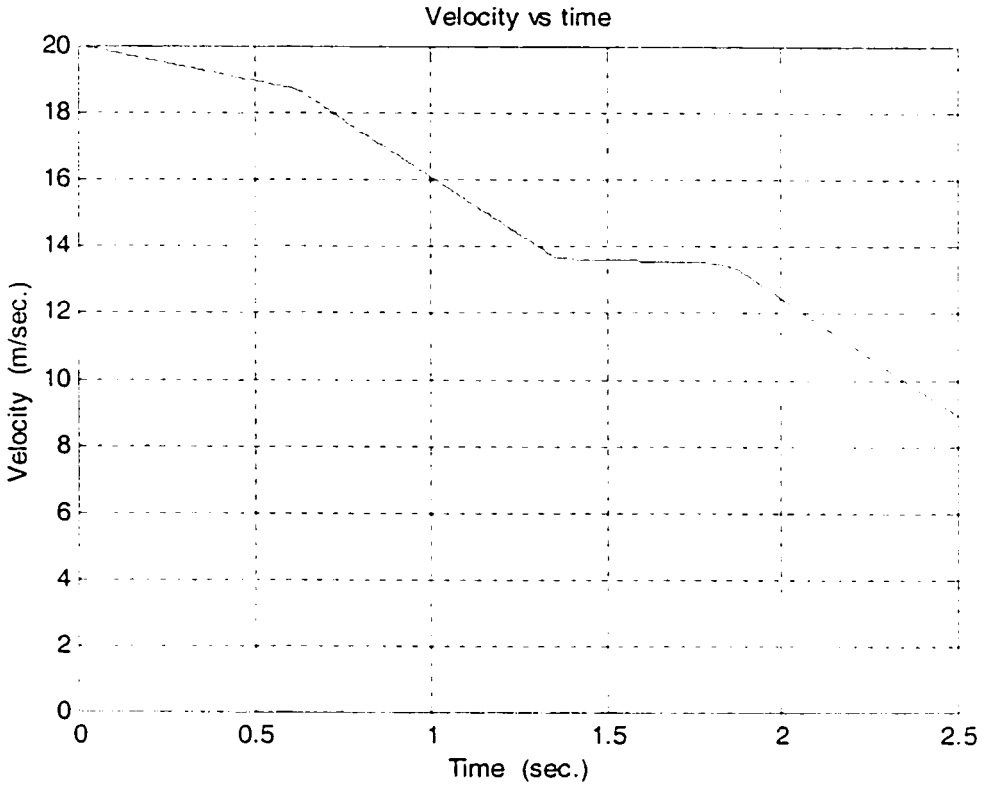

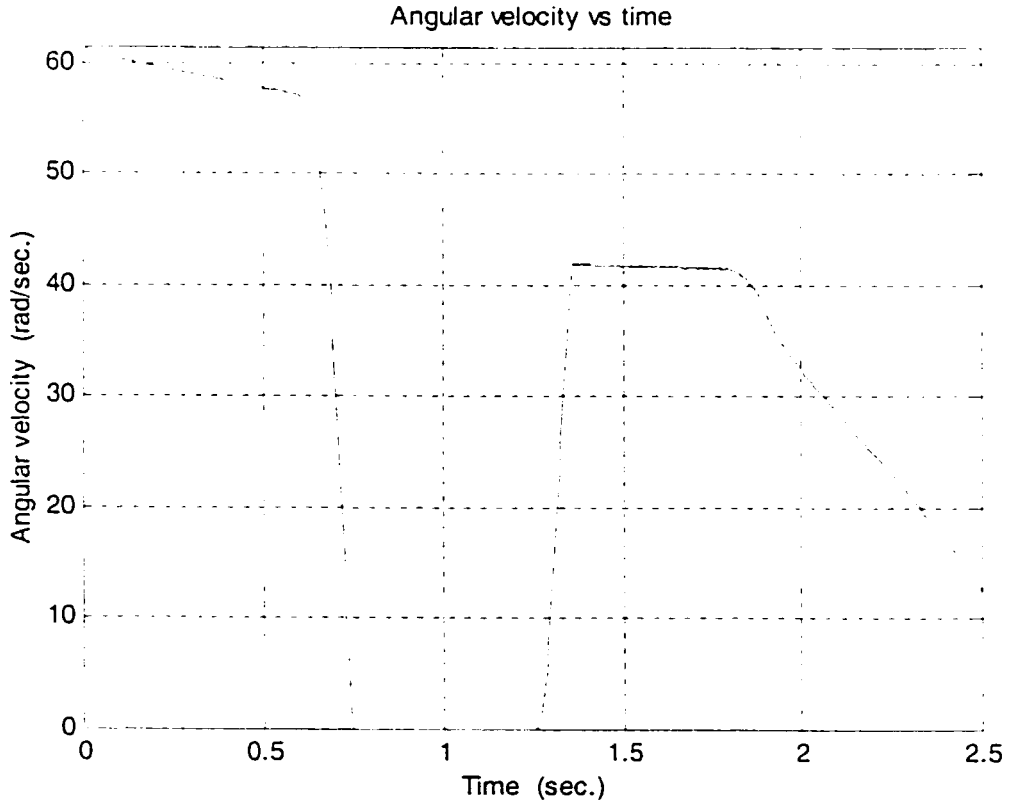

Fig. 4.4 Angular velocity response for PI brake model illustration

Fig. 4.5 Longitudinal skid response for PI brake model illustration

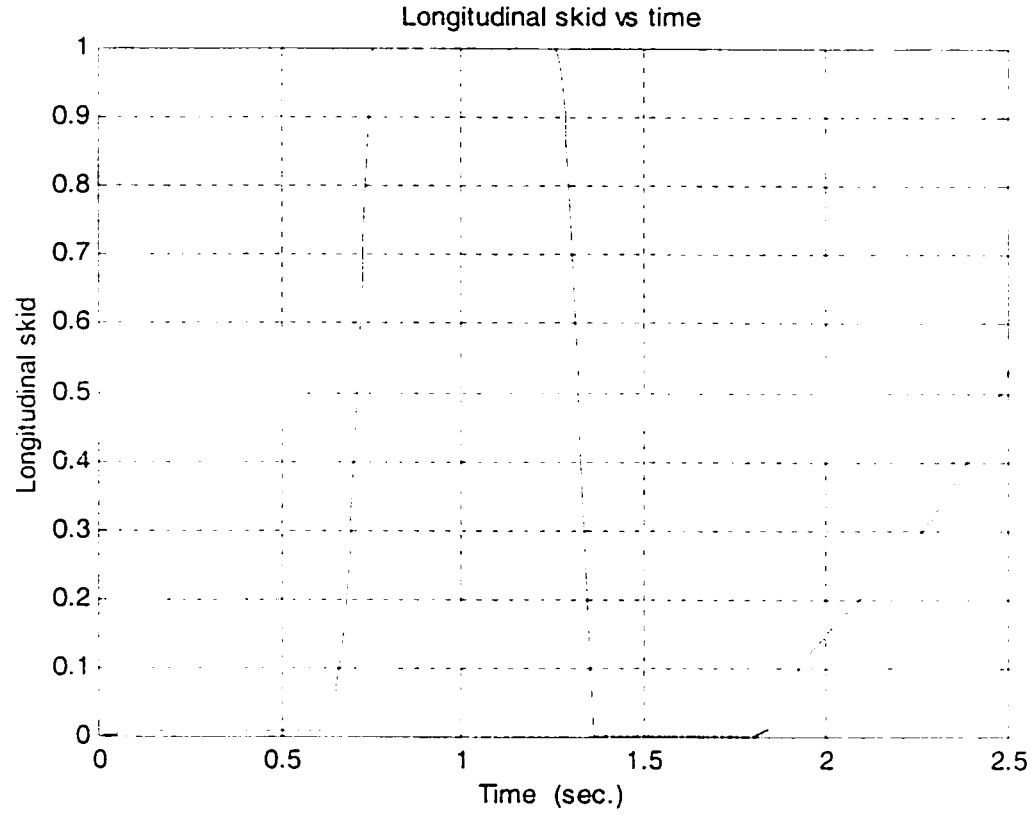

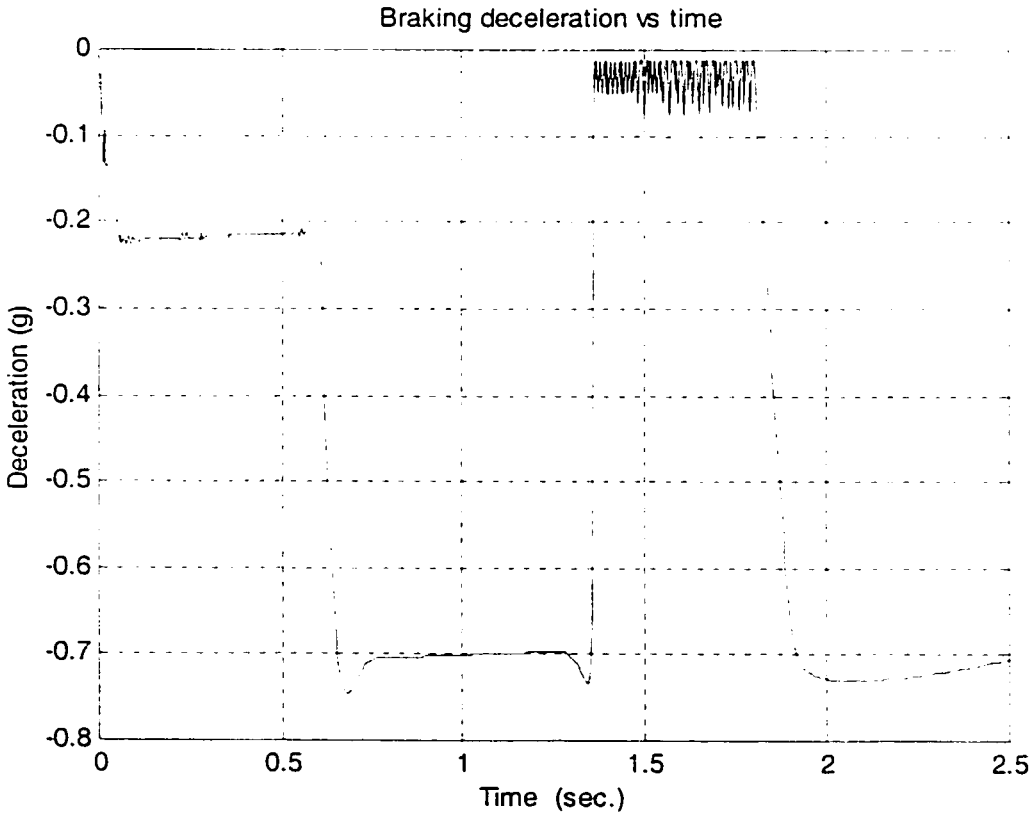

Fig. 4.6 Deceleration response for PI brake model illustration

4.4 PI Controller For ABS Control

The simple vehicle model with dynamic tire friction developed in this investigation for brake system was investigated in the previous section. It was easy to demonstrate the effect of large brake torque which leads to wheel lock and as discussed earlier, consequent loss of divertive control. In this section, a PI controller is introduced for realization of ABS. In general the task for the controller in ABS is to ensure that the skid (λ) level is maintained within a prescribed range during braking. The architecture for the PID controller is shown in Figure 4.7.

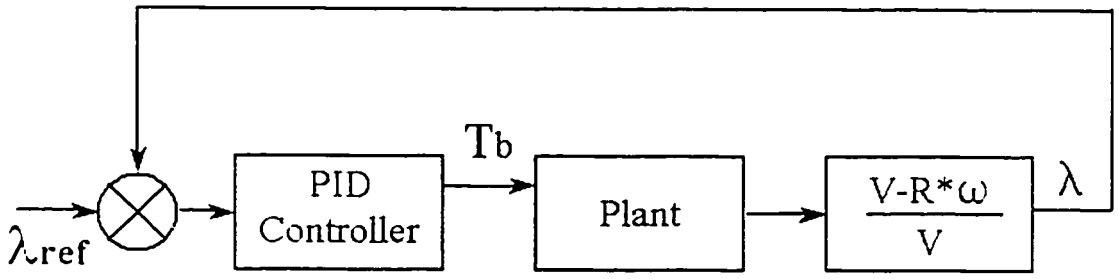

Fig. 4.7 PID Controller

Upon application of brake, the PI controller allows brake line pressure to brake cylinders which generates brake torque T_b at the wheel. As shown in previous section,

depending on μ the T_b leads to brake torque at the tire road interface leading to deceleration and other responses of the vehicle. This in turn generates skid (λ) which influences braking force generated by tires, as well as most importantly the availability of cornering force. With a prior knowledge of optimal skid ($\lambda_{x,f}$) the controller can be designed to apply T_b such that λ is close to $\lambda_{x,f}$. Therefore, as shown in Figure 4.7, the controller is used to control T_b through comparison of λ generated and $\lambda_{x,f}$.

Modern control systems for ABS goes one step further to establish optimal $\lambda_{x,f}$ corresponding to maximum deceleration in a dynamic operating and environmental condition. This can be established in the following manner.

As shown earlier, the vehicle deceleration can be expressed as:

$$\ddot{x} = -\mu(\lambda)\frac{m_{tot}\,g}{m_{tot} - \mu(\lambda)m_{eq}} - \frac{\frac{\rho}{2}c_d A_f \dot{x}^2}{m_{tot} - \mu(\lambda)m_{eq}} \qquad (4.17)$$

where the road adhesion coefficient μ is a function of the wheel slip λ. In genera, -μ is a unimodal function of λ, that is, the function μ(λ) has only one minimizer. Note that the second term in Equation 4.17 helps to decrease $\ddot{x}$ (increase deceleration), which in turn reduces the stopping distance, x. It will be shown that minimizing -μ(λ) leads to the minimization of the first term in equation 4.17. Therefore, the objective here is to minimize the function (equation 4.17) which is equivalent to maximizing its negative which is given by:

$$F = F(\mu(\lambda)) = \mu(\lambda)\frac{m_{tot}\,g}{m_{tot} - \mu(\lambda)m_{eq}} \tag{4.18}$$

differentiating over the skid (λ), i.e., $\frac{dF}{d\lambda}$, yields

$$\frac{dF(\mu(\lambda))}{d\lambda} = \frac{m_{tot}^2\,g}{(m_{tot} - \mu(\lambda)m_{eq})^2}\frac{d\mu(\lambda)}{d\lambda} \tag{4.19}$$

since $m_{tot} - \mu(\lambda)m_{eq} > 0$,

$$\frac{dF}{d\lambda} = 0 \quad \text{if and only if } \frac{d\mu}{d\lambda} = 0, \tag{4.20}$$

which means that F has only one critical point that coincides with the maximizer of μ, which is a minimizer of -μ. By letting λ^* to be the maximizer of μ, one can show that λ^* is also the maximizer of F and applying the second derivative test:

$$\frac{d^2F}{d\lambda^2} = \left(\frac{2m_{eq}m_{tot}^2\,g}{(m_{tot} - \mu(\lambda)m_{eq})^3} + \frac{m_{tot}^2\,g}{(m_{tot} - \mu(\lambda)m_{eq})^2} \right)\frac{d^2\mu}{d\lambda^2} \tag{4.21}$$

where $m_{tot} - \mu(\lambda)m_{eq}$ is greater than zero, hence

$$\frac{d^2F(\mu(\lambda^*))}{d\lambda^2} < 0 \text{ if and only if } \frac{d^2\mu(\lambda^*)}{d\lambda^2} < 0 \qquad (4.22)$$

which means that λ^* is indeed the maximizer of F.

The optimizer for λ incorporated within ABS system with PI controller is presented as a flowchart diagram in Figure 4.8. For such a system, the tire model can only provide the static μ_λ response, and the optimal slip value is unknown for each simulation step. The optimizer, therefore, has to be built to search the optimal skid for the PI controller. This makes the controller a little complex, and is not the best controller for the system due to the errors in optimizing process.

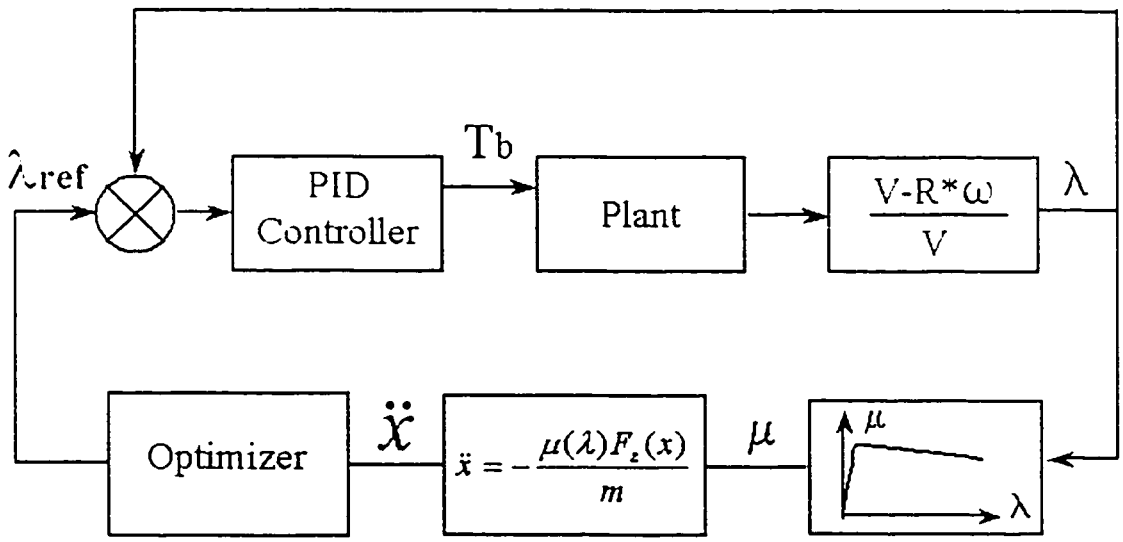

Fig. 4.8 PID controller for static μ_λ response brake system

In this study, it is advocated that if transient μ-λ response can be made available, the optimal skid will be known and hence, the need for optimizer can be avoided from the PI controller. This will in turn lead to much simple and more reliable control system for ABS. The proposed PI controller with transient μ-λ used in establishing vehicle response is presented in Figure 4.9. As shown in this case, the optimal λ established by the plant is used as λ_{ref} .

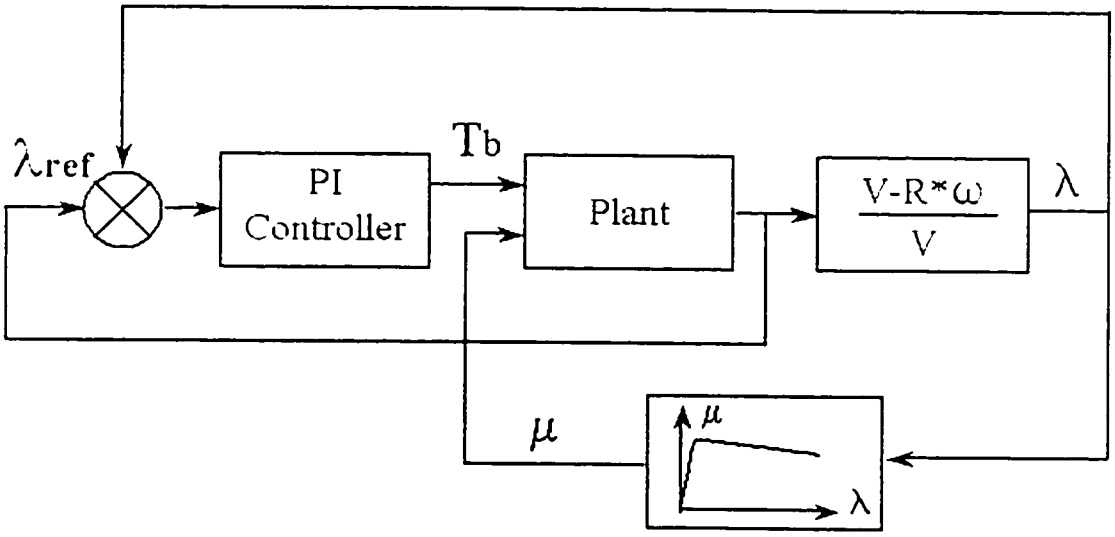

Figure 4.9 PI Controller with transient μ-λ feedback

The strategy for the proposed PI controller can be established utilizing the dynamic friction tire model presented in Chapter III. The expression for tire force using friction tire model describing a pseudo-static relationship was:

$$F(\lambda) = -F_z g(v_r)\left(1 + 2\gamma \frac{g(v_r)}{\sigma_0 L|\eta|}\left(e^{-\frac{\sigma_0 L|\eta|}{2g(v_r)}} - 1\right)\right) - F_z \sigma_2 v_r \qquad (4.23)$$

with $\gamma = 1 - \sigma_1|\lambda| / r\omega g(v_r)$ *and*

$$\eta = \frac{v_r}{r\omega} = -\frac{\lambda}{1-\lambda}, \qquad \lambda = \frac{v - r\omega}{v}$$

The equation can be rewritten to express road adhesion coefficient as:

$$\frac{F(\lambda)}{F_z} = -g(v_r)\left(1 + 2\gamma \frac{g(v_r)}{\sigma_0 L|\eta|}\left(e^{-\frac{\sigma_0 L|\eta|}{2g(v_r)}} - 1\right)\right) - \sigma_2 v_r \qquad (4.24)$$

where $F(\lambda)$ is the friction force, F_z is the tire normal load, hence $F(\lambda) / F_z$ is the road adhesion coefficient of interest.

In the pseudo-static curve in (Equation (4.24)), the velocity is however, assumed to be constant. If the velocity changes, the curve will also changes. However, by examining the dynamic equation for the internal state z , it is established that z changes much faster than the vehicle dynamics. Therefore, it is considered safe to assume that, for each time step, this formula can be used to calculate the approximated maximum peak value for the braking force produced by the tire/road friction.

Table 4.2 gives the parameters used for pseudo-static relationship by Equation (4.26), and Figure 4.10 gives the responses in terms of adhesion as a function of skid for several velocities. These results clearly demonstrate the significant influence of velocity on both tire/road friction coefficient and corresponding skid value. Finally, the maximum value of tire/road friction coefficient under different velocity and corresponding longitudinal skid are summarized in Table 4.3.

Table 4.2 Parameters used for Equation (4.26)

Parameter	Value	Units
σ_0	100	1/m
σ_1	0.7	s/m
σ_2	0.011	s/m
μ_C	0.35	--
μ_S	0.5	---
V_s	10	m/s
L	0.25	m

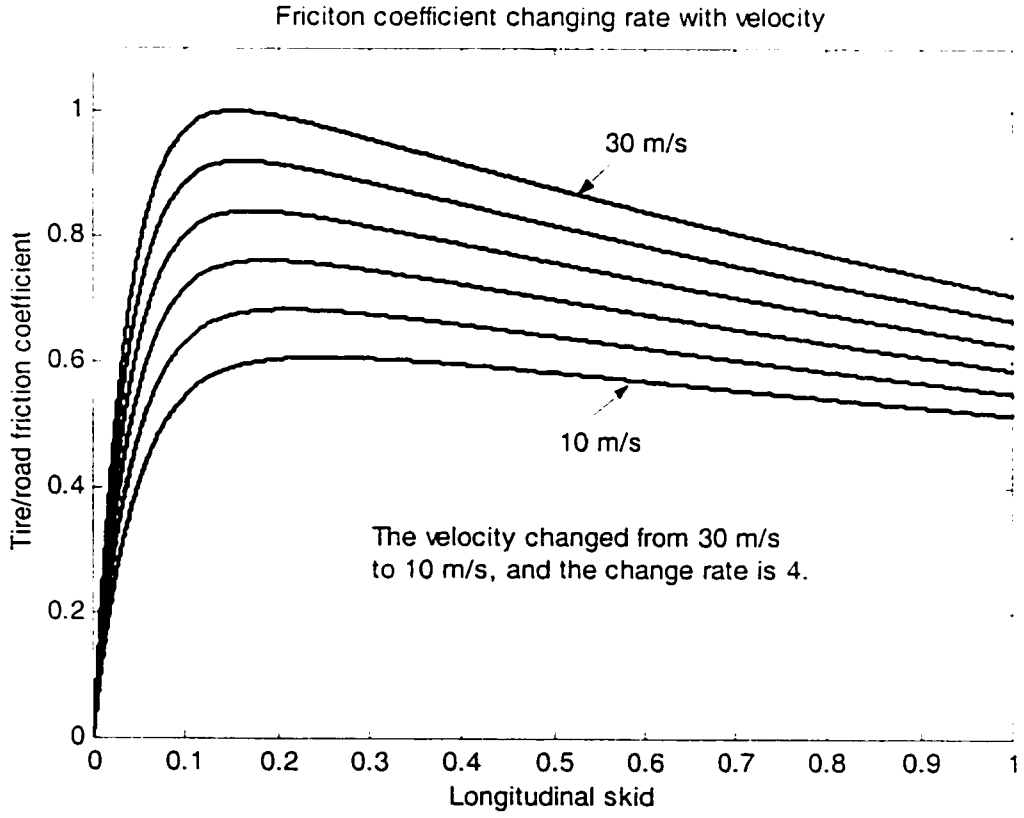

Fig. 4.10 Mu_lambda responses under several velocities

Table 4.3 Max friction coefficient and corresponding longitudinal skid under different velocity

Velocity	30 m/s	26 m/s	22 m/s	18 m/s	14 m/s	10 m/s
Max. mu	1.0000	0.9199	0.8400	0.7608	0.6827	0.6070
Corresponding lambda	0.1533	0.1619	0.1732	0.1895	0.2134	0.2516

Following the above analysis, the optimal value for longitudinal skid (λ) corresponding to max F_l at each velocity can be established. This λ can then be made available to the PI controller in Figure 4.9 at each step of the control loop. This approach has the obvious advantage for simplified controller design with greater accuracy and reliability.

The Matlab program for the designed PI controller is given in Appendix C, which includes both the main codes and member functions.

4.5 Simulation Results and Discussions

The vehicle parameters used for the simulation of ABS with proposed PI controller is same as those presented in Table 4.1 and 4.2.

The first set of simulation results are obtained for initial velocities of 30 and 20 m/s. In these simulations, no brake torque is applied externally. Here it is considered that the controller provides the brake torque to ensure that optimal skid level is maintained through out the brake process. A upper bound for the skid equal to 0.4 was, however, assigned to ensure that the skid level during braking does not exceed 0.4 at any time. The PI controller gains selected for the simulation are: K_P=5800, K_I=320.

The brake torque time history applied by the controller to stop the vehicle from 30 m/s and 20 m/s are shown in Figure 4.11. Once the system is activated, the optimal λ is established and since actual skid is zero, the brake torque is applied and increased within the first fraction of second so that the skid level increases to catch up with the optimal λ established at that speed. The control system then brakes the skid produced, compares it with the calculated optimal λ and varies the braking torque to minimize the error. The resulting time history for the braking torque as shown in Figure 4.11 indicate identical trend for both initial velocities. However, the maximum braking torque applied for 30 m/s is greater than that for 20 m/s. Furthermore, the brake torque is applied for 4.55 seconds when initial velocity was 30 m/s and 3.3 seconds for initial velocity 20 m/s.

The effectiveness of the controller in tracking the skid or maintaining the skid near the optimal value can be see from the results presented in Figure 4.12. This trend can

be easily compared with the applied braking force (Figure 4.11) to appreciate the variation of brake force required to achieve the optimal skid during the operation.

The resulting change in vehicle velocities and wheel angular velocities at the two speeds are presented in Figure 4.13 and 4.14, respectively. These results clearly show the highly smooth change in velocity from the initial value to zero. As it can be seen in Figure 4.14, the angular velocity clearly reflect the drop in braking force applied by the controller between 0.5 and 1 seconds after the application of brake.

The forward motion or the stopping distance of the vehicle corresponding to the two initial velocities are presented in Figure 4.15. These results further endure the performance in terms of smoothness in stopping the vehicle.

These results also show that in order to achieve braking with the proposed PI controller, a distance of 63m will be required to stop from a velocity of 30 m/s, and time to stop is 4.55 seconds. In the case of initial velocity 20 m/s, the stopping distance is 32 m and the time required to stop is 3.3 seconds. First set of results from this simulation showing a deceleration time history for the two initial velocities while braking with the proposed PI controller are presented in Figure 4.15. The results show identical trend for both initial speeds except the peak deceleration corresponding to the peak braking force applied in each case. This is expected since the peak breaking force applied for 30 m/s was 1975 N-m while for 20 m/s it was 1840 N-m.

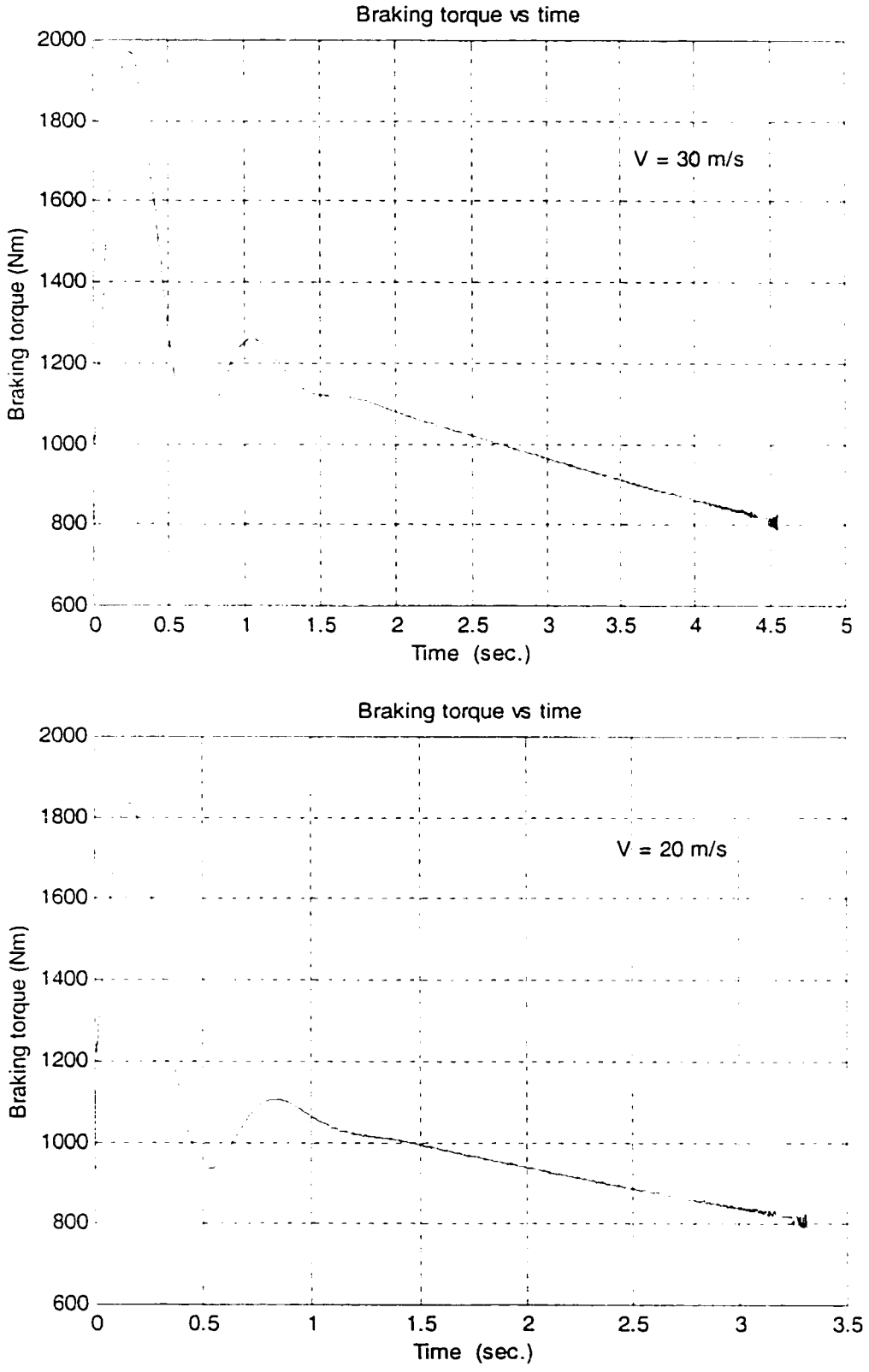

Fig. 4.11 Brake torque response for PI controller

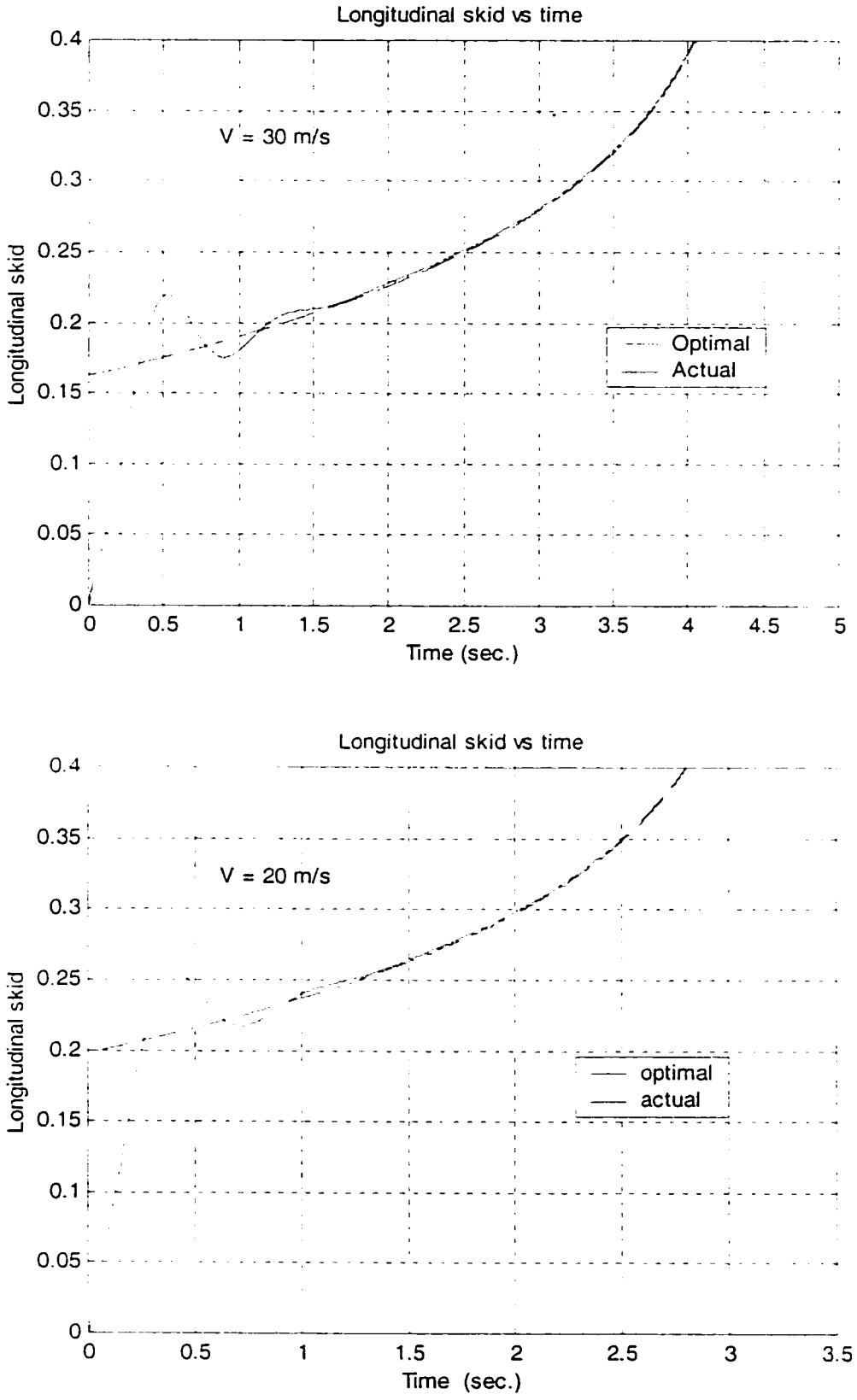

Fig. 4.12 Time history of actual and optimal skid during braking

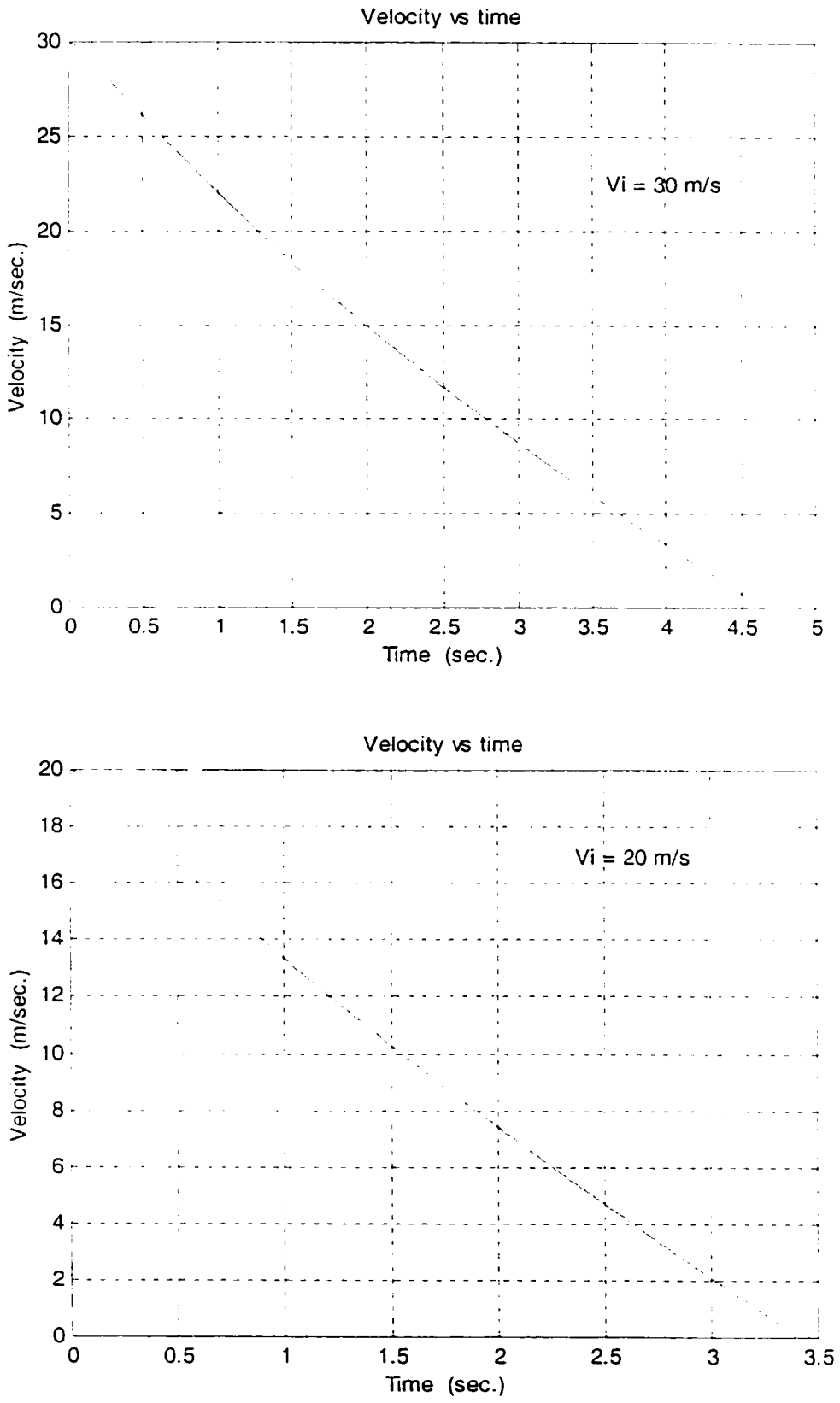

Fig. 4.13 Velocity response for PI controller

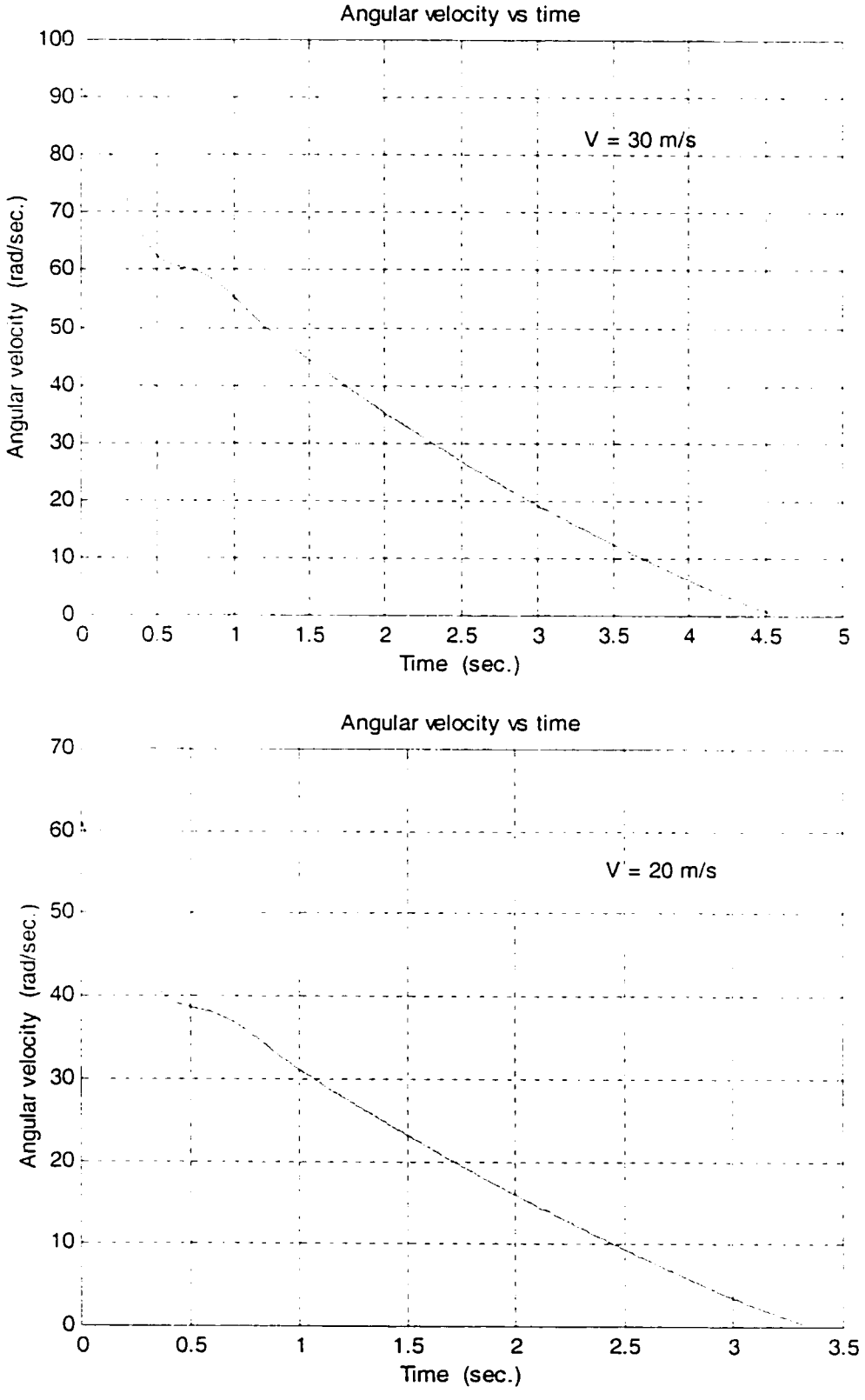

Fig. 4.14 Angular velocity response for PI controller

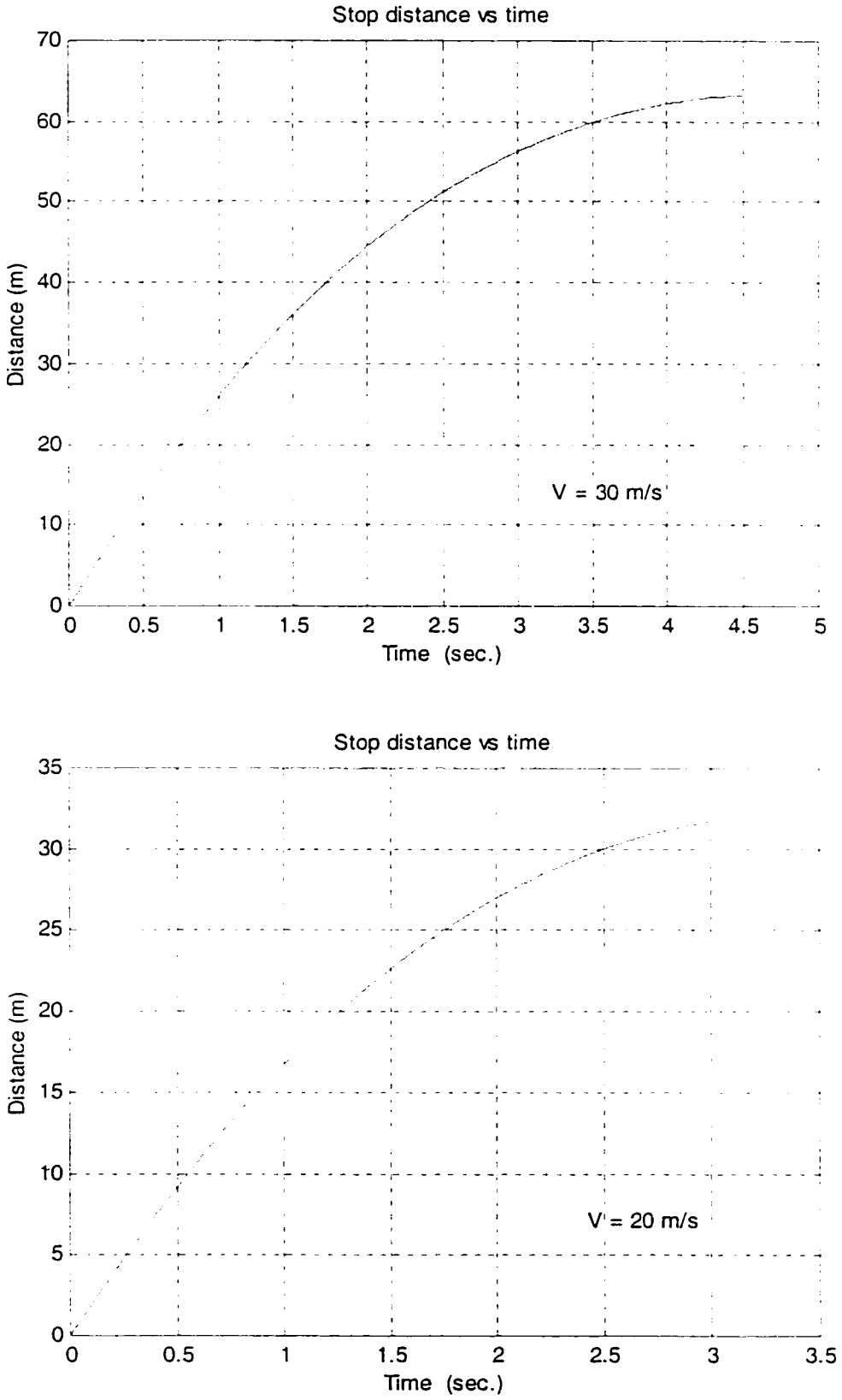

Fig. 4.15 Stopping distance versus time for PI controller

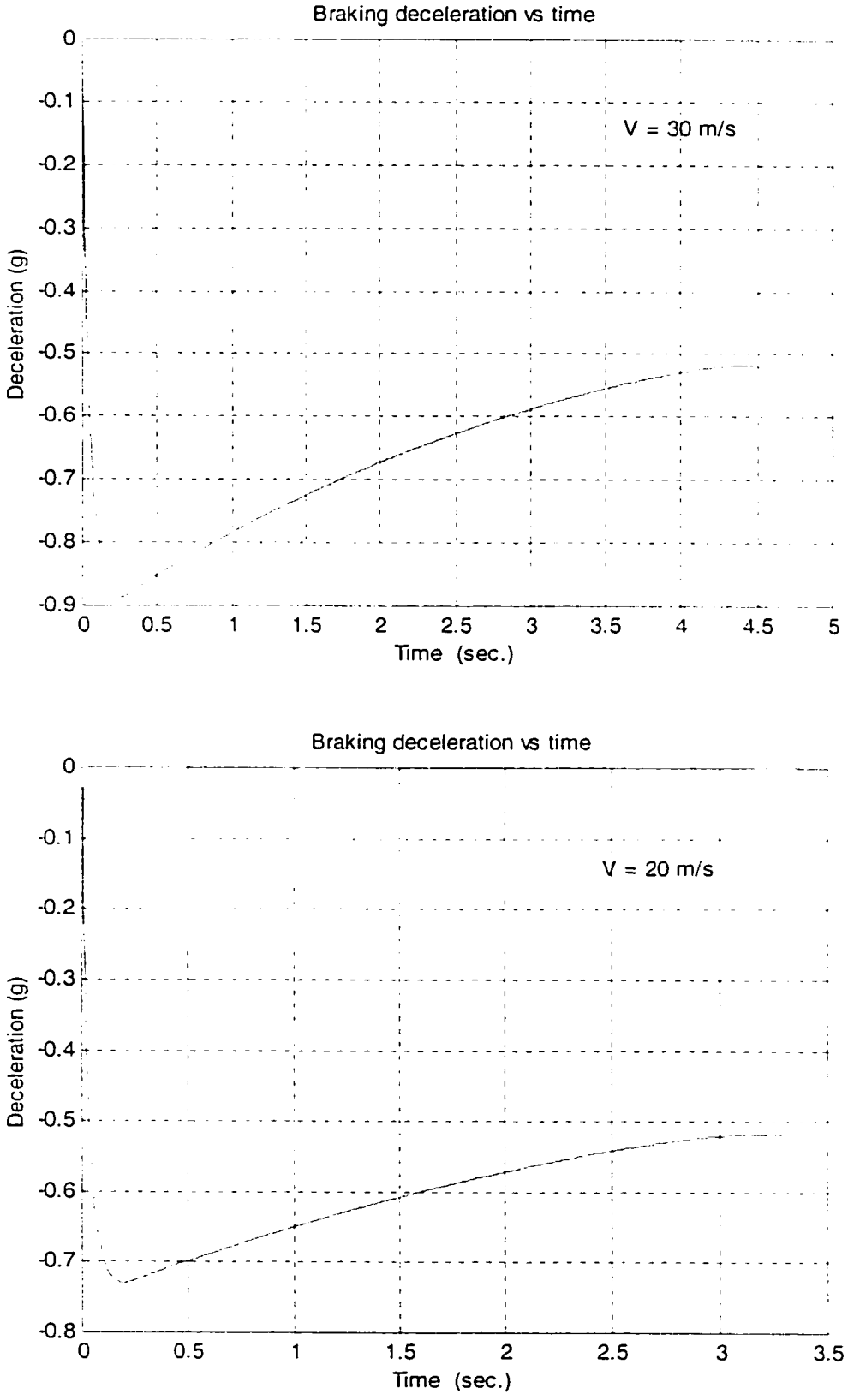

Fig. 4.16 Braking deceleration response for PI controller

4.6 Summary

A quarter vehicle model for evaluation of braking performance developed for this investigation was tested under a given braking torque to establish the braking performance. The model was then integrated with a PI controller for the control of brake system based on skid developed at the tire road interface. The dynamic friction tire model developed in this investigation was utilized to establish optimal skid corresponding to maximum μ at a velocity. In the control loop, the optimal skid was used as the reference to maintain the actual skid close to the optimal value. It is shown that such scheme can replace the need for online optimization that is need in commonly used ABS scheme. A set of simulation is carried out at two different speeds to get in-depth understanding of the proposed controller and its effectiveness in modulating braking force. In this simulation, however, there was no external braking force applied. Here the controller was used to generate braking force in order to establish its effectiveness in such control. In actual ABS for vehicle such controller will only modulate the braking force applied by the operator.

The results obtained in this section of the study with dynamic friction tire model and simple vehicle braking model exhibit promising potential for such system in the design of simple and effective controllers. This section was devoted to the evaluation of control system using PI controller. It is well known that such controller are prone to instability and can not be evaluated for the guaranty of stability. The next section of the study is therefore, devoted to the development and evaluation of a robust (sliding mode) controller that utilizes dynamic friction tire model.

CHAPTER V

ROBUST (SLIDING MODE) CONTROLLER DESIGN

5.1 Introduction

A PI control method for ABS utilizing friction tire model was developed in chapter IV. Simulations were also carried out to demonstrate the effectiveness of the proposed control in braking performance of simplified vehicle model.

Stability of PI controllers and problems associated with establishing the stability of such controller is well known. This part of the study with control of ABS is, therefore, directed toward design and evaluation of a robust controller.

This chapter of the thesis focus on the development of robust (sliding mode) controller for application to ABS utilizing friction tire model. The simplified vehicle model utilized for PI controller study in the previous chapter is adapted here for the study of robust controller design and analysis of braking performance with such controller.

This chapter starts with vehicle model used in this part of the study. The model is then simulated for response to a typical brake input to ensure that the model response is qualitatively valid. The design of the robust controller is then presented and developed. Finally, the performance of vehicle brake system with the controller is obtained and discussed.

5.2 Vehicle Model

The quarter vehicle model with longitudinal vehicle motion and angular wheel motion with effect of load shift in pitch plane was developed and utilized in the investigation of PI controllers. For the robust controllers, same model is utilized with further simplification in order to facilitate simple primary investigation of new concept. Here it is assumed that there is no load shift and that the weight of the vehicle is distributed evenly on the four wheels. The dynamic friction tire model developed for the investigation in chapter III, and used for PI controller in chapter IV is also adapted for the study of robust controller.

The equations for the model are derived here starting with the LuGre friction model and basic equation for vehicle motion derived earlier as:

$$\begin{cases} \dot{z} = v_r - \theta \dfrac{\sigma_0 |v_r|}{g(v_r)} z \\ J\dot{\omega} = -rF_t - \sigma_\omega \omega - T_b \\ m\dot{v} = F_t - F_a \end{cases} \qquad (5.1)$$

where the coefficient σ_ω is introduced to represent viscous resistance moments experienced by the wheels, $F_a = \dfrac{\rho}{2} C_d A_f v^2$ is the aerodynamic force, C_d is the drag coefficient, A_f is the front area of the vehicle, T_b is the traction/braking torque, and F_t is the traction/breaking force generated at the tire/road contact, z is the internal friction state, $g(v_r)$ corresponds to the Stribeck effect. The term for braking force F_t can be expressed as a function of normal load:

$$F_t = F_z(\sigma_0 z + \sigma_1 \dot{z} + \sigma_2 v_r) \qquad (5.2)$$

where σ_0 is the normalized rubber longitudinal lumped stiffness, σ_1 the normalized rubber longitudinal lumped damping, σ_2 the normalized viscous relative damping.

Defining the state variables as:

$$x_1 = z, \quad x_2 = v, \quad x_3 = v_r = r\omega - v$$

The LuGre friction model in Eq. (5.1) can be expressed as:

$$\dot{x}_1 = \dot{z} = x_3 - \theta \frac{\sigma_0 |x_3|}{g(x_3)} x_1 = x_3 - \theta f(x_3) x_1 \qquad (5.3)$$

where

$$f(x_3) = \frac{\sigma_0 |x_3|}{g(x_3)},$$

and as discussed earlier in chapter III, the Stribeck effect in terms of the coefficient of friction and velocities can be expressed as follows:

$$g(x_3) = \mu_C + (\mu_S - \mu_C) e^{-\left|\frac{x_3}{v_S}\right|^{1/2}}$$

Similarly, the longitudinal equation of motion in (5.1) can be rewritten as:

$$\dot{x}_2 = \dot{v} = (F_t - F_a)/m = (F_z(\sigma_0 x_1 + \sigma_1 \dot{x}_1 + \sigma_2 x_3) - \frac{\rho}{2} C_d A_f x_2^2)/m \qquad (5.4)$$

Assuming that there is no load shift, (ie. $F_z = mg$), and substituting for $\dot{x}_1$ from equation (5.3), equation (5.4) can be expressed as:

$$\dot{x}_2 = g[\sigma_0 x_1 + \sigma_1 (x_3 - \theta f(x_3) x_1 + \sigma_2 x_3] - C_{av} x_2^2 \qquad (5.5)$$

where g is the acceleration due to gravity, and $C_{av} = \frac{\rho}{2} \frac{C_d A_f}{m}$.

The equation describing wheel angular motion in (5.1) can be expressed in term of state variable x_3 defined earlier by using the following relations:

$$\dot{x}_3 = \dot{v}_r = r\dot{\omega} - \dot{v} = r\dot{\omega} - \dot{x}_2 \qquad (5.6)$$

Further, from $x_3 = v_r = r\omega - v$, the angular velocity ω is:

$$\omega = \frac{x_3 + v}{r} = \frac{x_3 + x_2}{r}$$

Substituting the above and equation (5.2) for F_t, the equation for angular motion in (5.1) can be expanded as:

$$\begin{aligned}\dot{\omega} &= (-rF_t - \sigma_\omega\omega - u_T)/J \\ &= (-r(F_z(\sigma_0 x_1 + \sigma_1\dot{x}_1 + \sigma_2 x_3) - \sigma_\omega\frac{x_2 + x_3}{r} - T_b)/J \\ &= (-r(F_z(\sigma_0 x_1 + \sigma_1(x_3 - \theta f(x_3)\dot{x}_1 + \sigma_2 x_3)) - \sigma_\omega\frac{x_2 + x_3}{r} - T_b)/J \qquad (5.7)\end{aligned}$$

Since σ_2 in the above equation is very small as indicated in table 4.2, it can be neglected to simplify the equation as:

$$\dot{\omega} = -\frac{rF_z}{J}(\sigma_0 x_1 + \sigma_1(x_3 - \theta f(x_3)\dot{x}_1)) - \frac{\sigma_\omega}{J}\frac{x_2 + x_3}{r} - \frac{T_b}{J} \qquad (5.8)$$

Substitute Equation (5.8) into Equation (5.6), then

$$\begin{aligned}\dot{x}_3 &= -\frac{r^2F_z}{J}(\sigma_0 x_1 + \sigma_1(x_3 - \theta f(x_3)\dot{x}_1)) - \frac{\sigma_\omega}{J}(x_2 + x_3) - \frac{rT_b}{J} \\ &\quad - g[\sigma_0 x_1 + \sigma_1(x_3 - \theta f(x_3)\dot{x}_1) + \sigma_2 x_3] + C_{av}x_2^2 \\ &= -(g + \frac{r^2F_z}{J})(\sigma_0 x_1 + \sigma_1(x_3 - \theta f(x_3)\dot{x}_1)) - g\sigma_2 x_3 - \frac{\sigma_\omega}{J}(x_2 + x_3) + C_{av}x_2^2 \\ &\quad - \frac{r}{J}K_b P_b \qquad (5.9)\end{aligned}$$

in the above equation, an expression we use the formula $T_b = K_b P_b$ is used, where K_b is the brake coefficient gain and P_b is the brake pressure which is the controlled variable.

Finally, the equations derived in term of these state variables are summarized as follows:

$$\begin{cases} \dot{x}_1 = x_3 - \theta f'(x_3)\dot{x}_1 \\ \dot{x}_2 = g[\sigma_0 x_1 + \sigma_1(x_3 - \theta f(x_3)x_1) + \sigma_2 x_3] - C_{av}x_2^2 \\ \dot{x}_3 = -(g + \frac{r^2 F_z}{J})[\sigma_0 x_1 + \sigma_1(x_3 - \theta f(x_3)x_1] - g\sigma_2 x_3 - \frac{\sigma_w}{J}(x_2 + x_3) + C_{av}x_2^2 - \frac{r}{J}K_b P_b \end{cases} \tag{5.10}$$

By defining the following expression:

$$\alpha = -\left[g + \frac{r^2 F_z}{J}\right],$$
$$f_1(X) = f(x_3)\dot{x}_1,$$
$$f_2(X) = g[\sigma_0 x_1 + (\sigma_1 + \sigma_2)x_3] - C_{av}x_2^2,$$
$$f_3(X) = \alpha\sigma_0 x_1 + (\alpha\sigma_1 - g\sigma_2)x_3 + C_{av}x_2^2 - \frac{\sigma_w}{J}(x_2 + x_3)$$

The above equation (5.10) can be easily rearranged as:

$$\begin{cases} \dot{x}_1 = x_3 - f_1(X)\theta \\ \dot{x}_2 = f_2(X) - [g\sigma_1 f_1(X)]\theta \\ \dot{x}_3 = f_3(X) - [\alpha\sigma_1 f_1(X)]\theta - \frac{r}{J}K_b P_b \end{cases} \tag{5.11}$$

When emergency braking control is to be achieved, the estimation of the braking system gain K_b is important. This gain is uncertain and changes with temperature, vehicle velocity, physical wear and other parameters. If K_b is properly estimated, braking control can be realized using the pressure in the master cylinder as the control input.

The vehicle and tire model parameters used in this part of the investigation are same as these used in Chapter IV. The basic parameters are presented here in Table 5.1, along with calculated values for the model parameters.

Table 5.1 Vehicle parameters for sliding mode controller

g	9.81 m/s^2	gravitational acceleration
m_t	40 kg	tire mass
$\frac{1}{4} m_{car}$	375 kg	quarter vehicle mass
J_t	1.7 kgm^2	wheel inertia
J_e	0.241 kgm^2	engine inertia
ξ	10.0	transmission gear ratio
R_w	0.326 m	wheel radius
A_f	2.04 m^2	vehicle frontal area
C_d	0.539	vehicle drag coefficient
ρ	1.23 kg/m^3	air density

$m = m_t + \frac{1}{4} m_{car} = 40 + 375 = 415\ kg$

$C_{av} = ((\rho/2)C_d A_f)/m = ((1.23/2)*0.539*2.04)/415 = 0.0016\ m^{-1}$

$J = J_t + \frac{1}{2} \xi^2 J_e = 1.7 + \frac{1}{2} *10*0.241 = 2.905\ Kgm^2$

In summarization, $\boldsymbol{m = 415\ kg}$, $\boldsymbol{C_{av} = 0.0016\ m^{-1}}$, $\boldsymbol{J = 2.905\ Kgm^2}$

5.3 Vehicle System Response To Brake

In Chapter IV, the vehicle model developed for PI controller was first tested for response to an applied braking torque that was varied in time. The model developed in this chapter for the application of robust controller is although similar to that of PI controller, the model was simplified and a different approach, namely state variable was adapted.

In the development of vehicle dynamic model for sliding mode method, the internal state z is included in the motion equation, and the braking force F_t can not be directly evaluated from the function $F_t = F_z * \mu(\lambda)$. Instead, F_t is related to internal state z which is presented in Equation (5.2). It should be pointed out that regardless of the approach used in developing the models, the two methods are essentially the same, which in the present model, it is assumed that all wheels carry equal load and that there is no load shift. It is therefore expected that simulated response for both model under same braking torque will be very similar. A time variant braking torque time history used previously in Figure 4.2 is also used in this simulation. In the present model, however, the control variable is pressure and the braking torque $T_b = K_b P_b$. For this simulation, the braking pressure time history is shown in Figure 5.1 and the gain $K_b = 0.9\ m^3$ is selected such that the brake torque time history is identical to that presented in Figure 4.2.

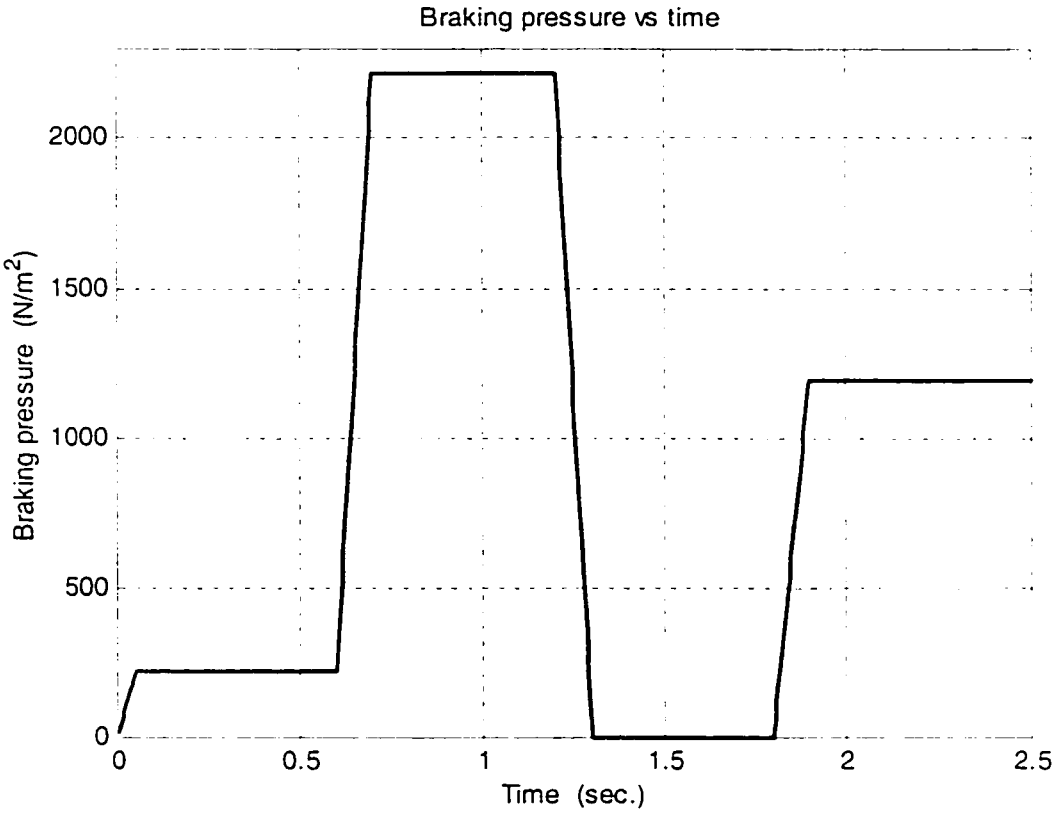

Fig. 5.1 Brake pressure input for slide mode brake model illustration

The simulation of vehicle response to the described brake torque is carried out using Matlab. The vehicle response time history in terms of vehicle forward velocity and wheel angular velocity are shown in Figures 5.2 and 5.3, respectively. As shown, the velocity drops slowly with the application of brake until a very large pressure or torque is

developed at which point the velocity drops rapidly. As shown in Figure 5.3, the corresponding angular velocity during the application of large torque is zero indicating wheel lockup during this period. The results also show that the angular velocity returns to a large value at the release of brake pressure since the forward velocity is not zero. Finally further application of brake causes further reduction in both forward and angular velocities. These results can be further verified by examining the response time history in terms of longitudinal skid and deceleration presented in Figures 5.4 and 5.5, respectively. These results clearly indicate that when wheel is locked in braking, the longitudinal skid is 100%. Furthermore, on the approach to lock up, maximum deceleration is achieved well before 100% skid is reached and the 100% skid resulted in a slight loss of deceleration. The trends of the results obtained here are identical to those obtained in Chapter IV for the model developed for PI controller. The magnitude of the results, however, are very slightly different in this case, as models are not identical. In this model, the pitch motion and resulting load shift is neglected for the shake of simplicity. Furthermore, here the equations are derived based on internal state z and relative velocity. The change in these variables are small in the presence of low brake pressure and hence show low effect on the skid. Whereas, the brake torque was a function of tire/road friction coefficient in the case of model developed for PI controller. There difference, however, are very small and negligible for a study where the main focus is the performance of controller in braking.

Fig. 5.2 Velocity response for slide mode brake model illustration

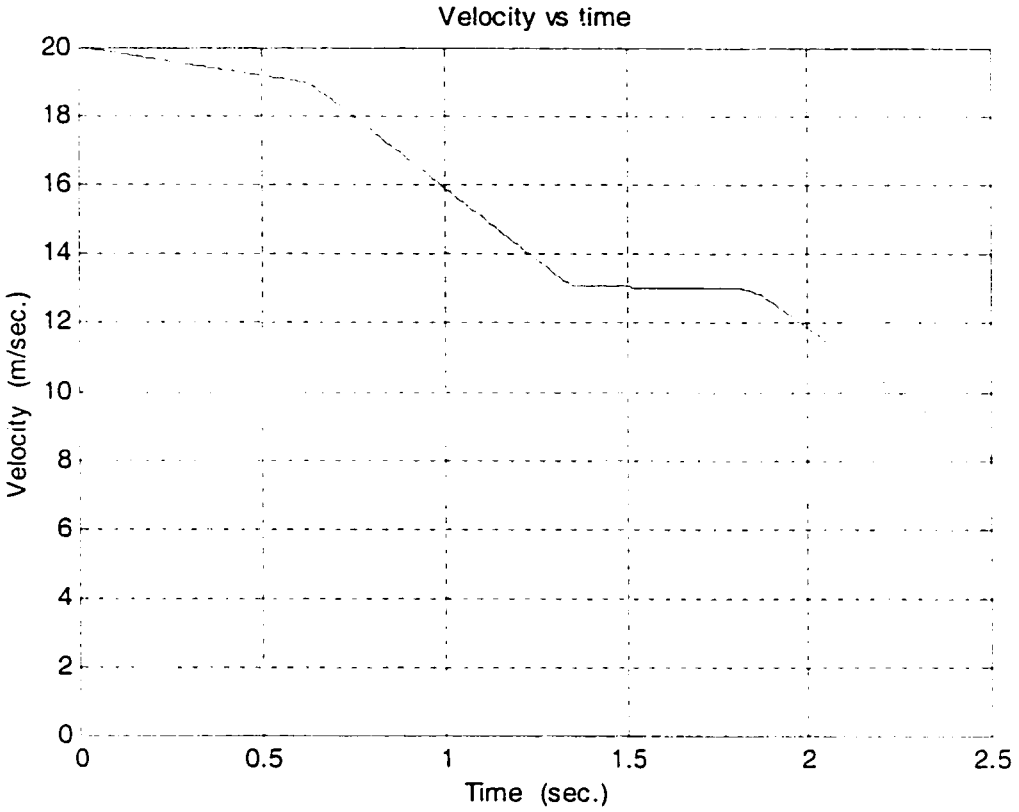

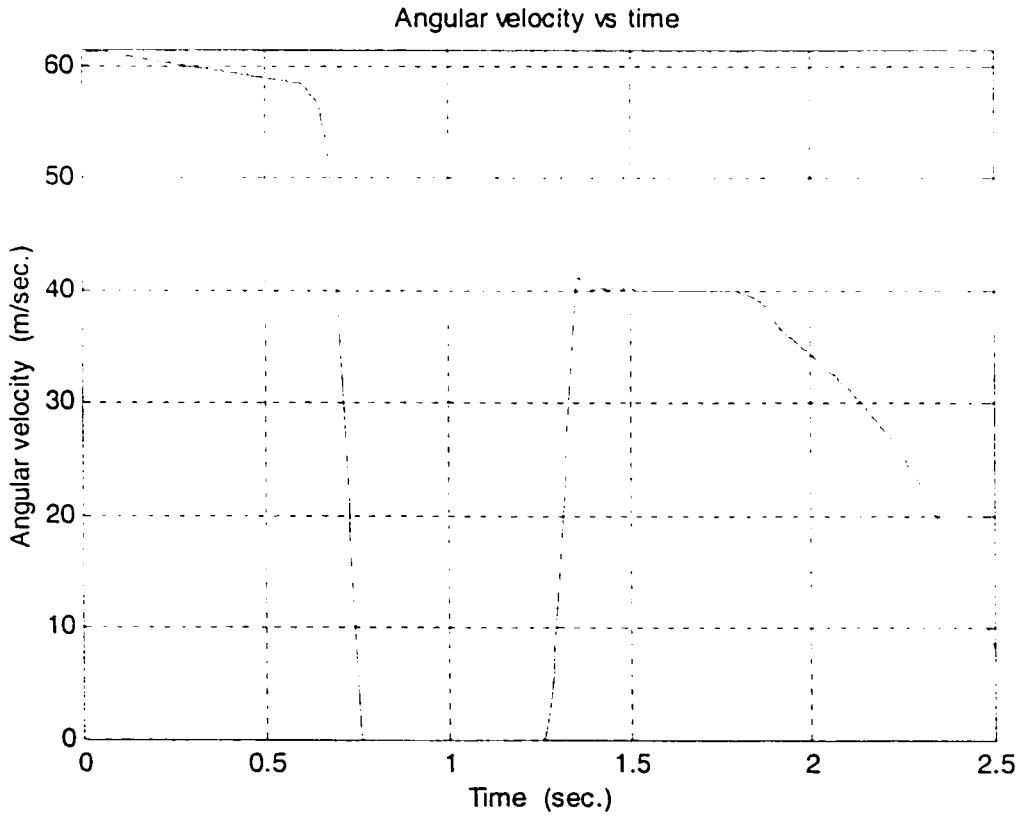

Fig. 5.3 Angular velocity response for slide mode brake model illustration

Fig. 5.4 Longitudinal skid response for slide mode brake model illustration

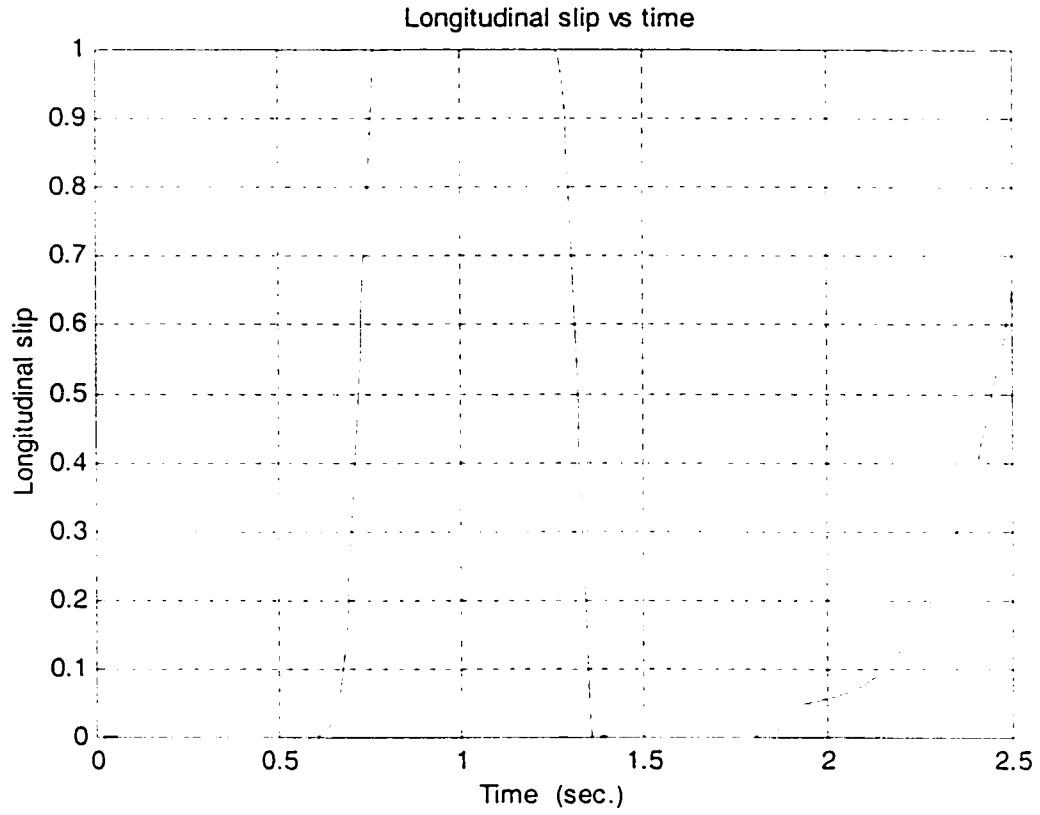

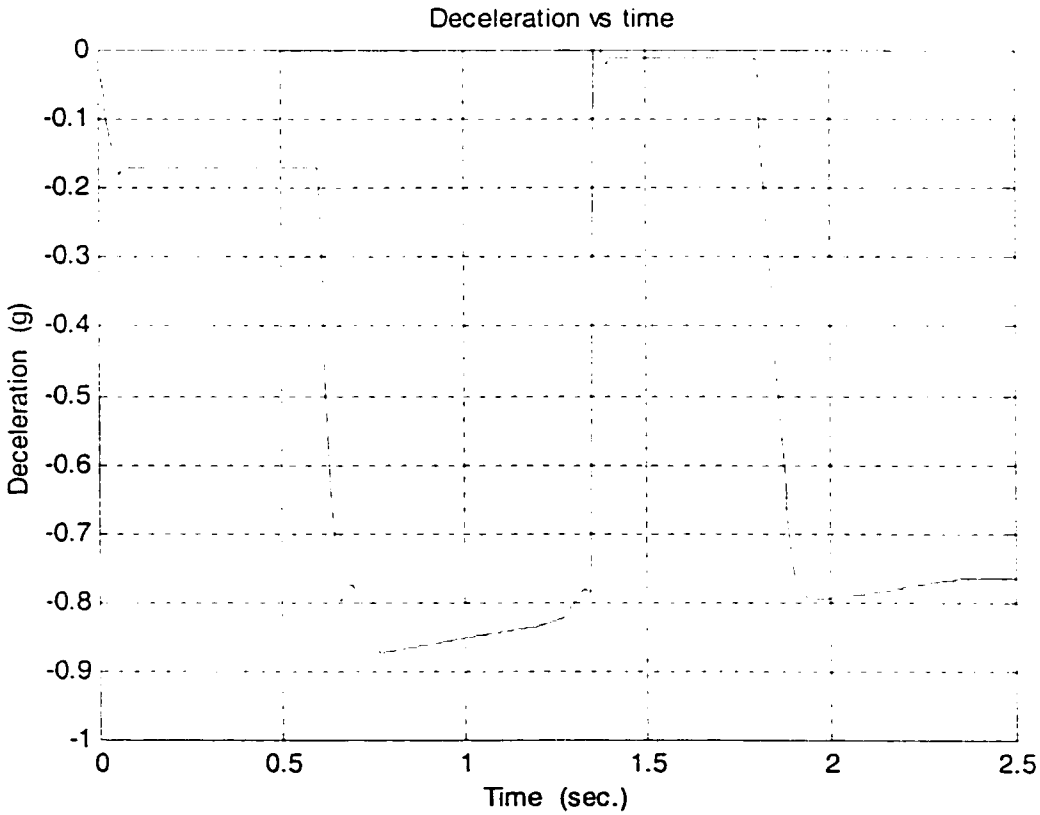

Fig. 5.5 Deceleration response for slide mode brake model illustration

5.4 Design of Robust (Slide Mode) Controller

The vehicle model developed in subsection 5.3 in terms of state variable z_i is next integrated with a slide mode controller for an application to ABS. A scheme of the controller architecture is presented in Figure 5.6. It clearly shows that the robust (slide mode) controller controls the state of braking and vehicle systems (namely plant in this architecture) to act along the sliding surface, which is built dynamically by utilizing maximum longitudinal skid (λ_{max}) and the variables achieved from the performance of the vehicle system in each step. The maximum longitudinal skid can be evaluated through the dynamic friction tire model which is established through the road condition. The sliding surface will be analyzed in further detail in the following investigation of robust slide mode controller.

Recalling the state variables defined as:

x_1 : internal state

x_2 : forward velocity

x_3 : relative velocity $v_r = r\omega - v$,

the longitudinal skid can be expressed in terms of state variables as:

$$\lambda = \frac{-x_3}{x_2} \qquad (5.12)$$

therefore, the relative velocity can have the expression as following:

$$x_3 = -\lambda x_2 \qquad (5.13)$$

Since controlled variables in the design of robust (slide mode) controller are the forward motion and relative velocity, the control goal is to achieve $x_2 \rightarrow 0$, and $x_3 \rightarrow x_{3d}$,

where x_{3d} is the unknown relative velocity corresponding to maximum skid. Hence, control goal can be achieved when $\lambda \rightarrow \lambda_{max}$.

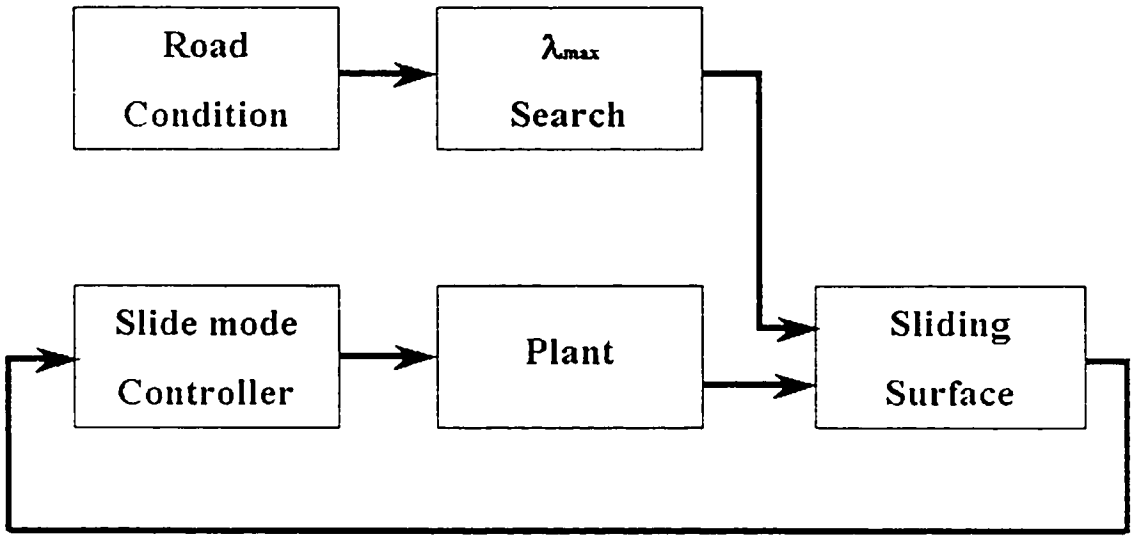

Fig. 5.6 Slide mode controller architecture

The formulation for the controller can be achieved by starting with the relationship between x_2, x_3, and λ and expressing as:

$$x_{3d}(\hat{\theta}) = -\lambda_{max}(\hat{\theta}) x_2 \qquad (5.14)$$

where $\hat{\theta}$ is the road condition parameter as presented in subsection 3.4 of Chapter III.

The longitudinal skid $\lambda_{max}(\hat{\theta})$ can be further be expressed as:

$$\lambda_{max}(\hat{\theta}) = \begin{cases} \arg\max_{\lambda \in [0, \bar{\lambda}]} F_t & when \ \ v \geq v_{min} \\ \bar{\lambda} & when \ \ 0 \leq v < v_{min} \end{cases} \qquad (5.15)$$

According to the above equation (5.12), λ is assigned a value corresponding to maximum F_t when the forward velocity is less than a preassigned minimum velocity v_{min}.

Otherwise, λ is assigned a constant value $\bar{\lambda}$. This is adapted to ensure that when v is small and skid is large, the maximum value of λ is restricted to $\bar{\lambda}$.

λ_{max} can be established from the dynamic friction tire model. As presented earlier, the dynamic friction tire model can be expressed as:

$$F(\lambda) = -F_z g(v_r)\left(1 + 2\gamma \frac{g(v_r)}{\sigma_0 L|\eta|}\left(e^{-\frac{\sigma_0 L|\eta|}{2g(v_r)}} - 1\right)\right) - F_z \sigma_2 v_r \qquad (5.16)$$

$$with\ \ \gamma = 1 - \sigma_1|\lambda|/r\omega g(v_r)\ \ and$$

$$\eta = \frac{v_r}{r\omega} = -\frac{\lambda}{1-\lambda}, \qquad \lambda = \frac{v - r\omega}{v}$$

Note that form subsection 3.4 in Chapter III, the equation (5.14) can produces a static curve for an infinitesimal time, ie., constant velocity hold. Thus, here this equation can be utilized as an approximation for λ_{max} when v is large enough, because the internal friction model dynamics is much faster than the vehicle dynamics. During each time step Δt, we assume that, for the vehicle braking control system, the internal state of the friction dynamic model converges to its steady-state. Thus, the maximum deceleration can be approximated well by equation (5.12). When v is small, we just bound v by v_{min}

From the above analysis, the sliding surface in this investigation can be defined as:

$$\tilde{s} = x_3 - x_{3d}(\hat{\theta}) = x_3 + \lambda_{max}(\hat{\theta}).x_2 \qquad (5.17)$$

where $\lambda_{max}(\hat{\theta})$ is the peak value of the longitudinal skid which can be evaluated from equation (5.14) under current conditions based on the estimated parameter $\hat{\theta}$ given by Eq. (5.13).

Differentiating $\tilde{s}$ in order to obtain the control input:

$$\dot{\tilde{s}} = \dot{x}_3 - \dot{x}_2\lambda_{max} + x_2\dot{\lambda}_{max} \tag{5.18}$$

Substituting $\dot{x}_2$, $\dot{x}_3$ which have been derived in equations of motion in equation (5.11) into above equation (5.18), $\dot{\tilde{s}}$ can be expressed as following:

$$\begin{aligned}\dot{\tilde{s}} &= -\frac{r}{J}K_b P_b - [\alpha\sigma_1 f_1(X) + g\sigma_1 f_1(X)\lambda_{max}]\theta + [f_3(X) + x_2\dot{\lambda}_{max} + \lambda_{max} f_2(X)] \\ &= dK_b P_b + \beta_1(X)\theta + \beta_2(X)\end{aligned} \tag{5.19}$$

where

$$d = -\frac{r}{J},$$
$$\beta_1(X) = -[\alpha\sigma_1 f_1(X) + g\sigma_1 f_1(X)\lambda_{max}],$$
$$\beta_2(X) = f_3(X) + x_2\dot{\lambda}_{max} + \lambda_{max} f_2(X)$$

Define $M_b = \frac{1}{k_b d}$ (5.20)

$$\theta_b = \frac{\theta}{k_b d} \tag{5.21}$$

It is reasonable to assume that the upper bounds for M_b and θ_b are known, denoted as ρ_1 and ρ_2, satisfying

$$\theta_b \le \rho_1$$

and $M_b \le \rho_2$

Then, the sliding mode control law can be synthesis as,

$$P_b = K_a \tilde{s} + \beta_1(\mathrm{X})\psi_1 + \beta_2(\mathrm{X})\psi_2 \qquad (5.22)$$

where

$$\psi_1 = \rho_1 \operatorname{sgn}(\tilde{s}\beta_1(\mathrm{X}))$$

$$\psi_2 = \rho_2 \operatorname{sgn}(\tilde{s}\beta_2(\mathrm{X}))$$

and K_a is a control gain, and $Ka > 0$.

One of the primary reason for development of slide mode controller is to ensure the stability of the controller in ABS application. The stability of the proposed slide mode model can be established by Lyapunov function. It is well known that by Lypunov's theorem, if the differentiation of the Lyapunov candidate can be proved to be less than zero in any condition, the stability of the control system can be achieved.

With the above definitions, the equation (5.19) can be re-written as,

$$M_b \dot{\tilde{s}} = -P_b + \beta_1(\mathrm{X})\theta_b + \beta_2(\mathrm{X})M_b$$

Consider the following Lyapunov candidate,

$$V = \frac{1}{2} M_b \tilde{s}^2$$

The derivative with respective to time t is

$$\dot{V} = M_b \tilde{s} \dot{\tilde{s}}$$

$$= \tilde{s}(-P_b + \beta_1(\mathrm{X})\theta_b + \beta_2(\mathrm{X})M_b)$$

$$= \tilde{s}(-\eta\tilde{s} - \beta_1(\mathrm{X})\psi_1 - \beta_2(\mathrm{X})\psi_2 + \beta_1(\mathrm{X})\theta_b + \beta_2(\mathrm{X})M_b)$$

$$= -\eta\tilde{s}^2 - \rho_1 |\tilde{s}\beta_1(\mathrm{X})| - \rho_2 |\tilde{s}\beta_2(\mathrm{X})| + \tilde{s}\beta_1(\mathrm{X})\theta_b + \tilde{s}\beta_2(\mathrm{X})M_b$$

$$\leq -\eta\tilde{s}^2$$

So the stability of the above controller has been proved.

Since the sliding mode controller has been designed by choosing the proper sliding surface and the stability of the designed controller has been proved clearly, the Matlab can be used to conduct the simulation, and make a detailed analysis for the results obtained from the simulations in the following section.

The Matlab program for the designed robust (slide mode) controller is given in the Appendix D, which included both main program codes and member functions.

5.5 Simulation Results Discussion

The vehicle parameters used for the simulation of ABS with proposed robust (slide mode) controller is same as those presented in Table 5.1. The dynamic friction tire model is still utilized in the investigation of robust (slide mode) controller to search the maximum longitudinal skid at each step, hence the parameters for the dynamic tire model are same as those presented in Table 4.2.

Before starting the simulations of slide mode controller, several points should be mentioned. First of all, a smooth function has to be added to the simulation, because when the slide mode control method is utilized in the simulation, the controller will

switch along the sliding surface, resulting control chatters, the smoothed function can be utilized to eliminate the control chatters in order to achieve analytical results. Second, a value of 3000 psi is assigned to limit the braking pressure, because due to the capacity of the braking systems in the real vehicle system, the brake pressure cannot exceed maximum value.

The first set of simulation results are obtained for initial velocities of 30 and 20 m/s, which are the same as those in Chapter IV. In these simulations, no brake torque is applied externally. Here it is considered that the controller provides the brake pressure to ensure that the slide motion along the sliding surface is maintained through out the brake process. A upper bound for the skid equal to 0.4 was, however, assigned to ensure that the skid level during braking does not exceed 0.4 at any time.

The brake pressure time history applied by the controller to stop the vehicle from 30 m/s and 20 m/s are shown in Figure 5.7. Once the system is activated, the maximum λ and sliding surface are established and since the relative velocity is zero, and the initial velocity is large, the sliding surface is in the up bound position, the brake pressure is therefore, applied and increased fast within the first fraction of second so that the sliding surface can be pushed to around zero as soon as possible. The control system then brakes the skid produced, varies the braking pressure so that the state of the vehicle system can be moved along the sliding surface and minimize the error. Once the sliding surface tends to zero, the braking pressure can be kept a stable value of 1100 N/m^2 for both initial velocities corresponding the sliding surface established. When the vehicle tends to stop, and the relative velocity tends to zero, the forward velocity is small, it is not necessary to keep a high pressure for the braking, so the braking pressure drops down quickly

corresponding to the sliding surface established at this moment. The resulting time history for the braking pressure as shown in Figure 5.7 indicate identical trend for both initial velocities. The brake pressure is applied for 3.8 seconds when initial velocity was 30 m/s and 2.4 seconds for initial velocity 20 m/s.

The effectiveness of the sliding surface can be seen from the results presented in Figure 5.8. This trend can be easily compared with the applied braking pressure (Figure 5.7) to appreciate the variation of brake pressure required to control the state of the vehicle system to trace the sliding surface during the operation.

The resulting change in vehicle velocities and wheel angular velocities at the two speeds are presented in Figure 5.9 and 5.10, respectively. These results clearly show the highly smooth change in velocity from the initial value to zero. As it can be seen in Figure 5.10, the angular velocity clearly reflect the fast increment in braking pressure applied by the controller between 0 and 0.1 seconds after the application of brake.

The resulting change in relative velocities at the two initial speeds are presented in Figure 5.11. Since the high braking pressure applied by the controller makes the reduction in the angular velocity of the wheel much faster than that in forward velocity, the relative velocity reaches its maximum value within the first fraction of second, while the sliding surface drops down from the up bound position. The constant pressure then control the state of the system to trace the steadily change in sliding surface, the relative velocity therefore, smoothly reaches its zero value 0.2 seconds earlier than the time when the vehicle fully stopped. Starting at this moment, the sliding surface and the braking pressure are released by the controller.

The forward motion or the stopping distance of the vehicle corresponding to the two initial velocities are presented in Figure 5.11. These results further endure the performance in terms of smoothness in stopping the vehicle.

These results also show that in order to achieve braking with the designed robust (slide mode) controller, a distance of 58m will be required to stop the vehicle from a velocity of 30 m/s, and time to stop is 3.8 seconds. In the case of initial velocity 20 m/s, the stopping distance is 26 m and the time required to stop is 2.5 seconds. First set of results from this simulation showing a deceleration time history for the two initial velocities while braking with the proposed PI controller are presented in Figure 5.13. The results show identical trend for both initial speeds except the peak deceleration corresponding to the peak braking pressure applied in each case. Furthermore, the response of the deceleration also clearly reflect the drop in braking pressure applied by the controller after decrement of sliding surface.

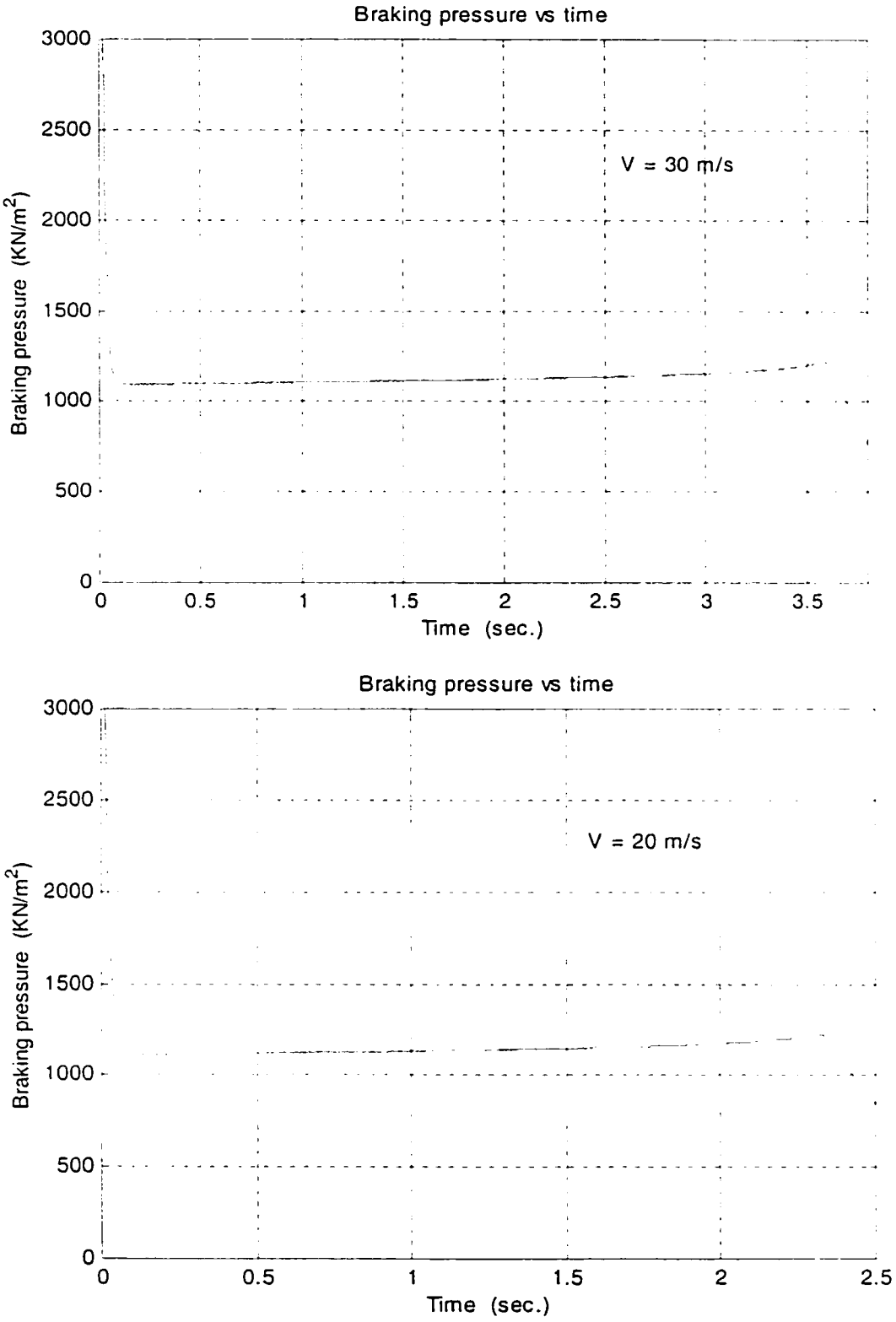

Fig. 5.7 Braking pressure response for slide mode controller

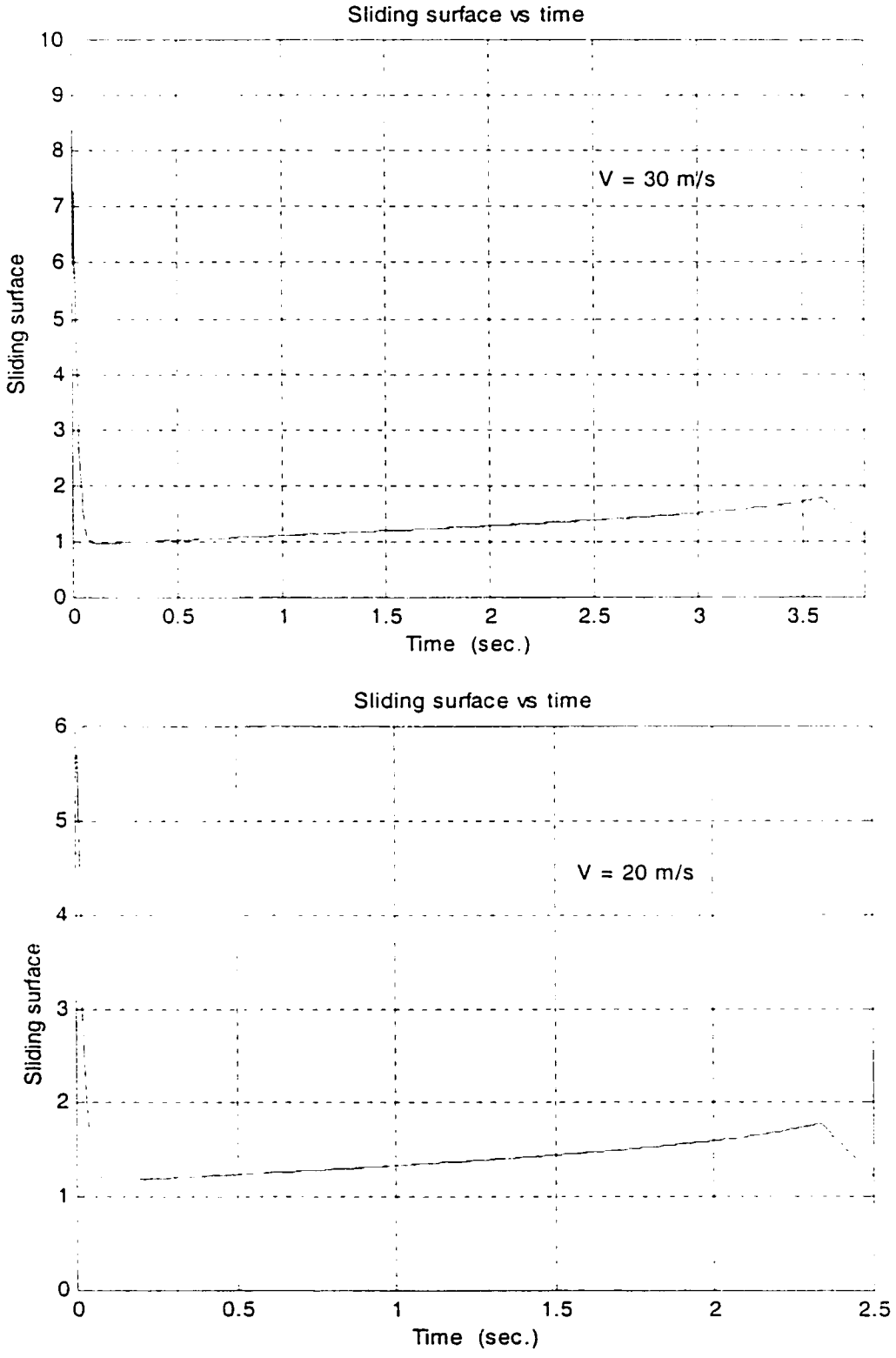

Fig. 5.8 Sliding surface response for slide mode controller

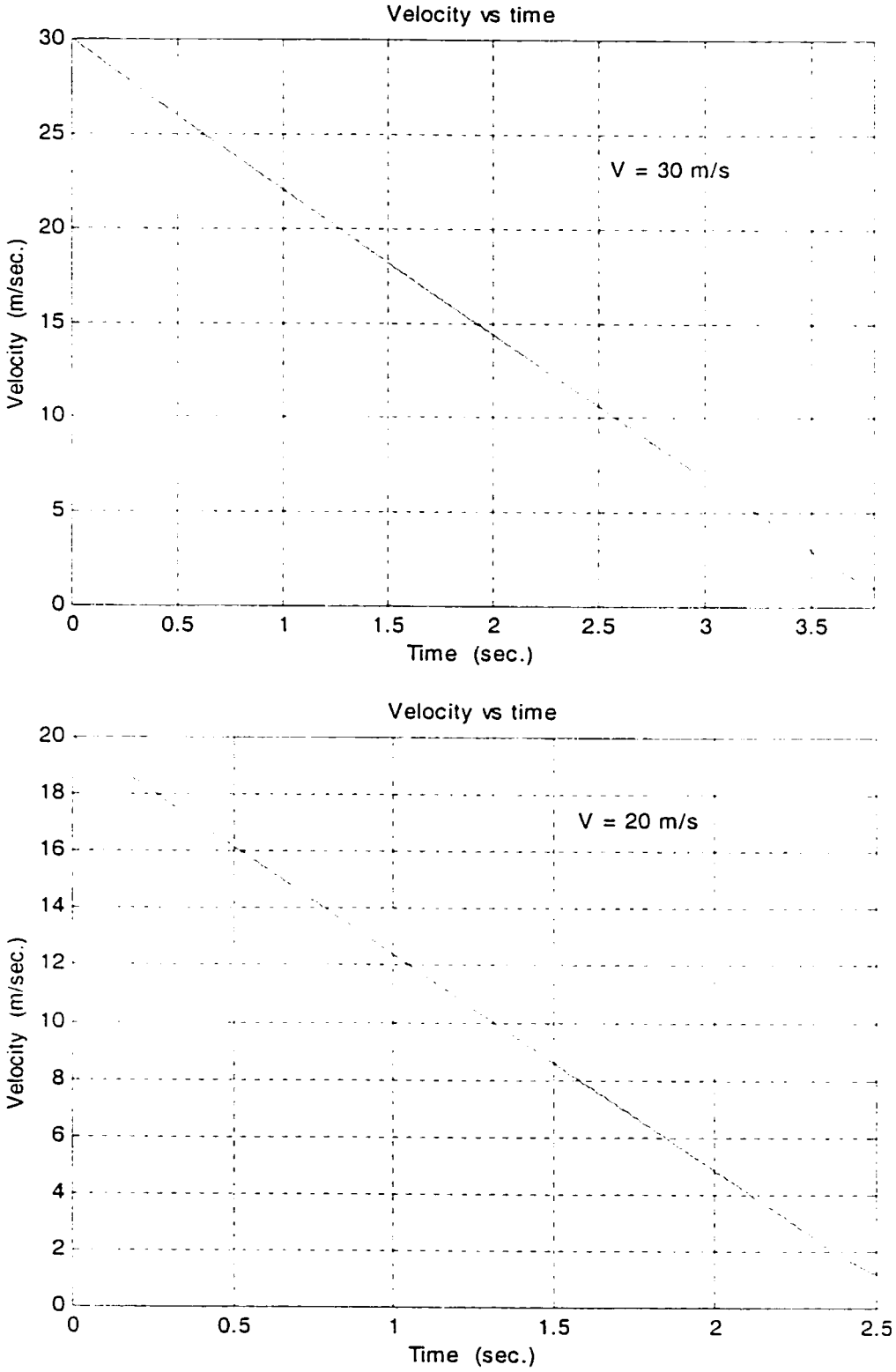

Fig. 5.9 Velocity response for slide mode controller

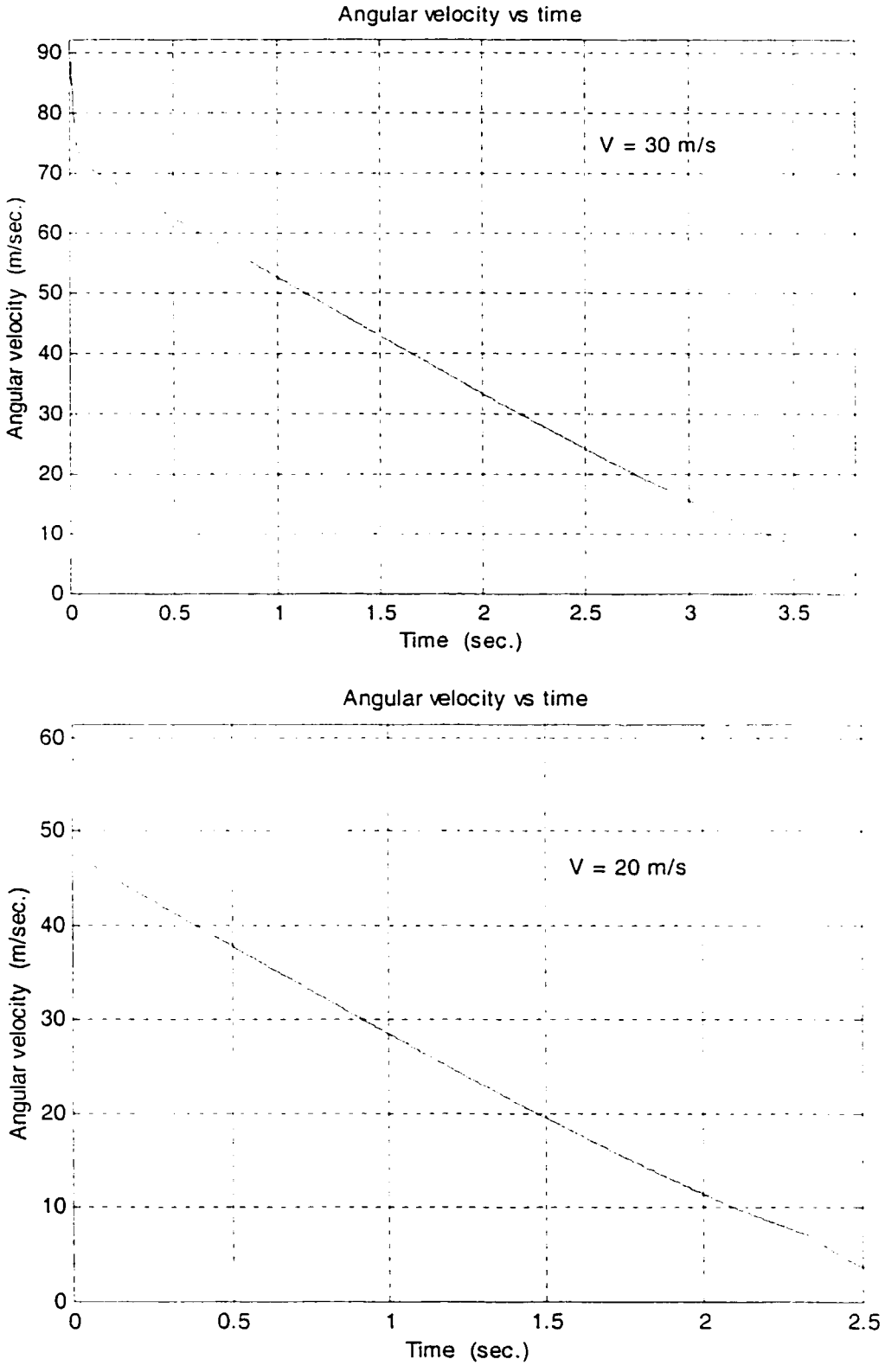

Fig. 5.10 Angular velocity response for slide mode controller

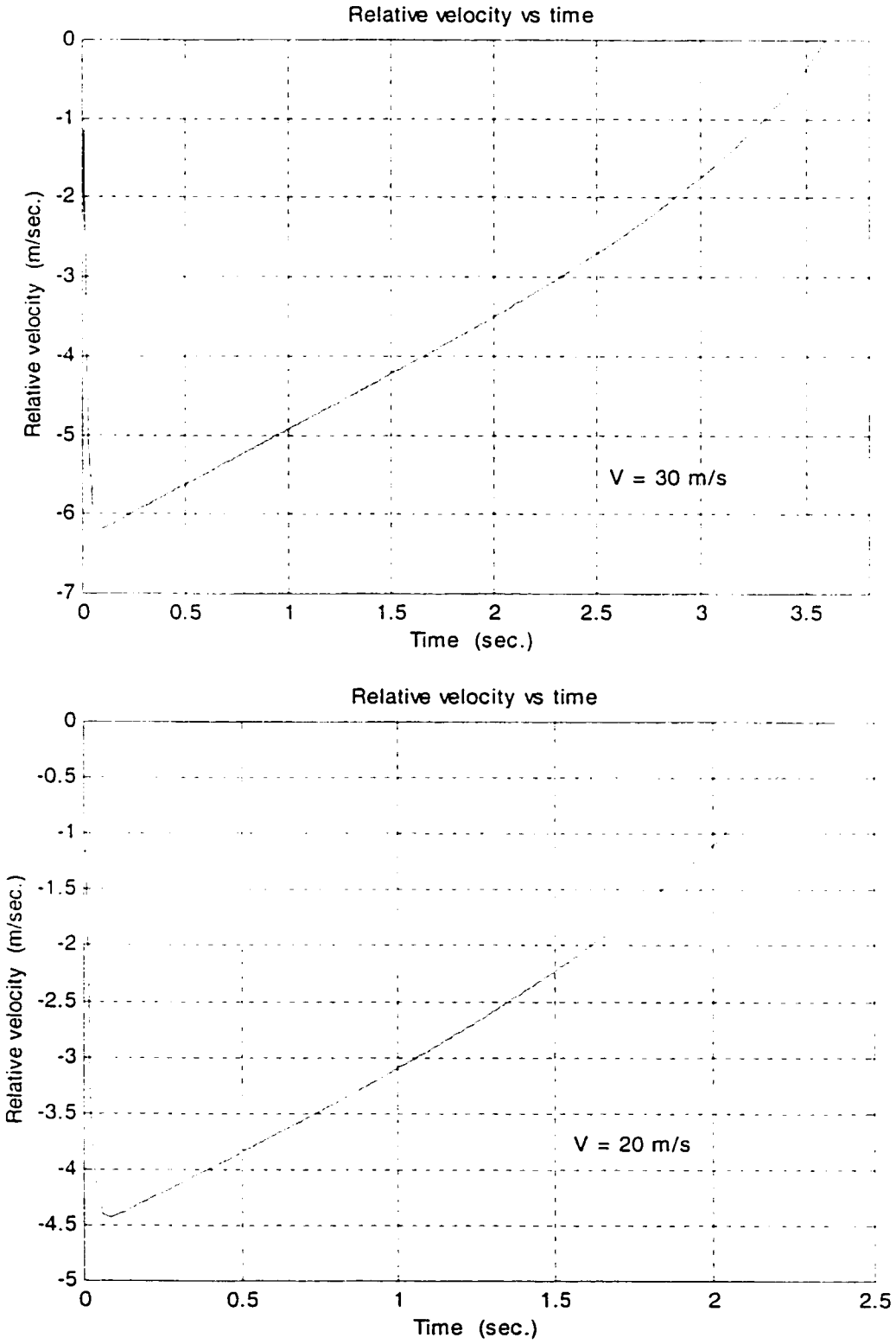

Fig. 5.11 Relative velocity response for slide mode controller

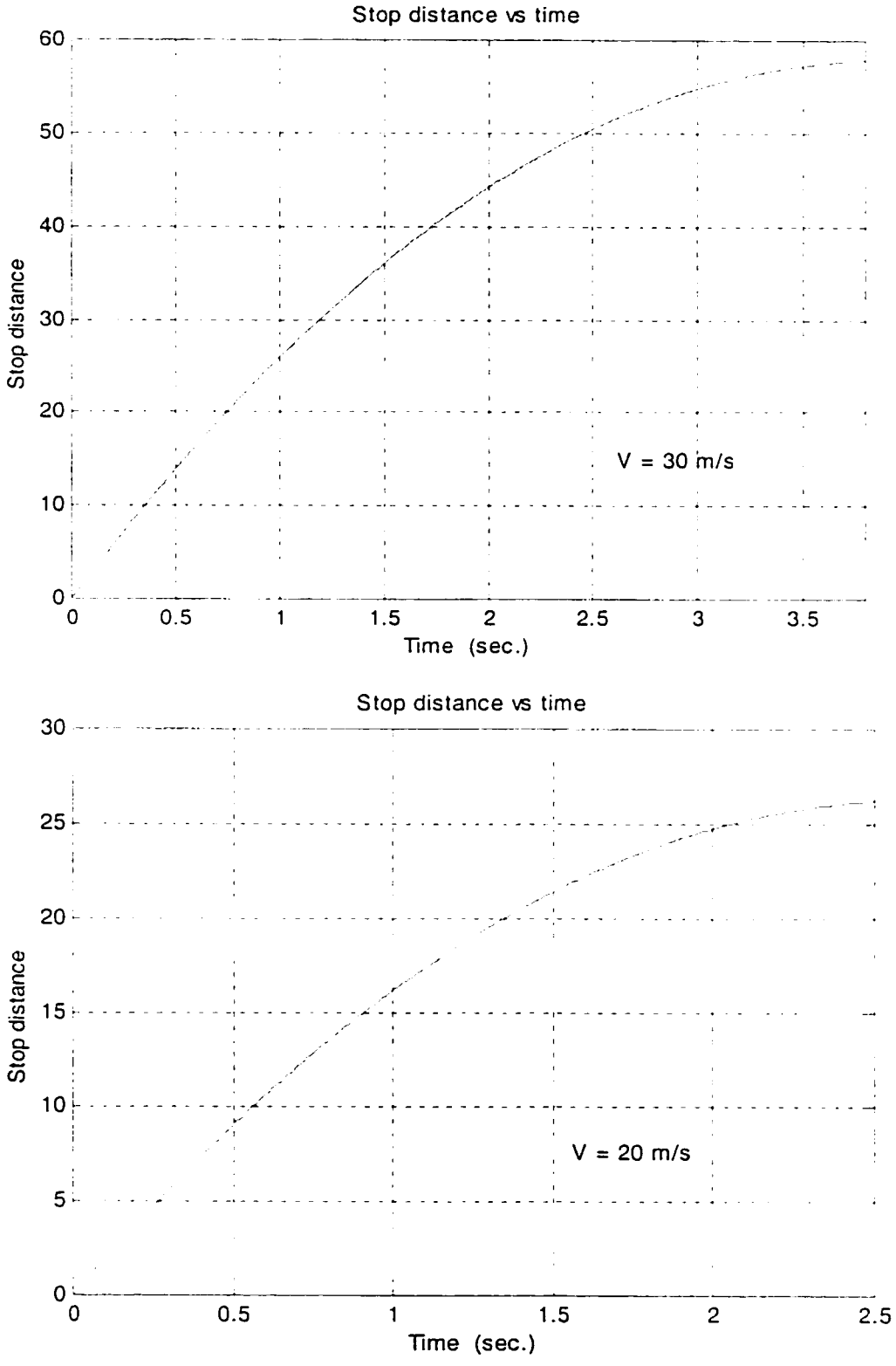

Fig. 5.12 Stop distance versus time for slide mode controller

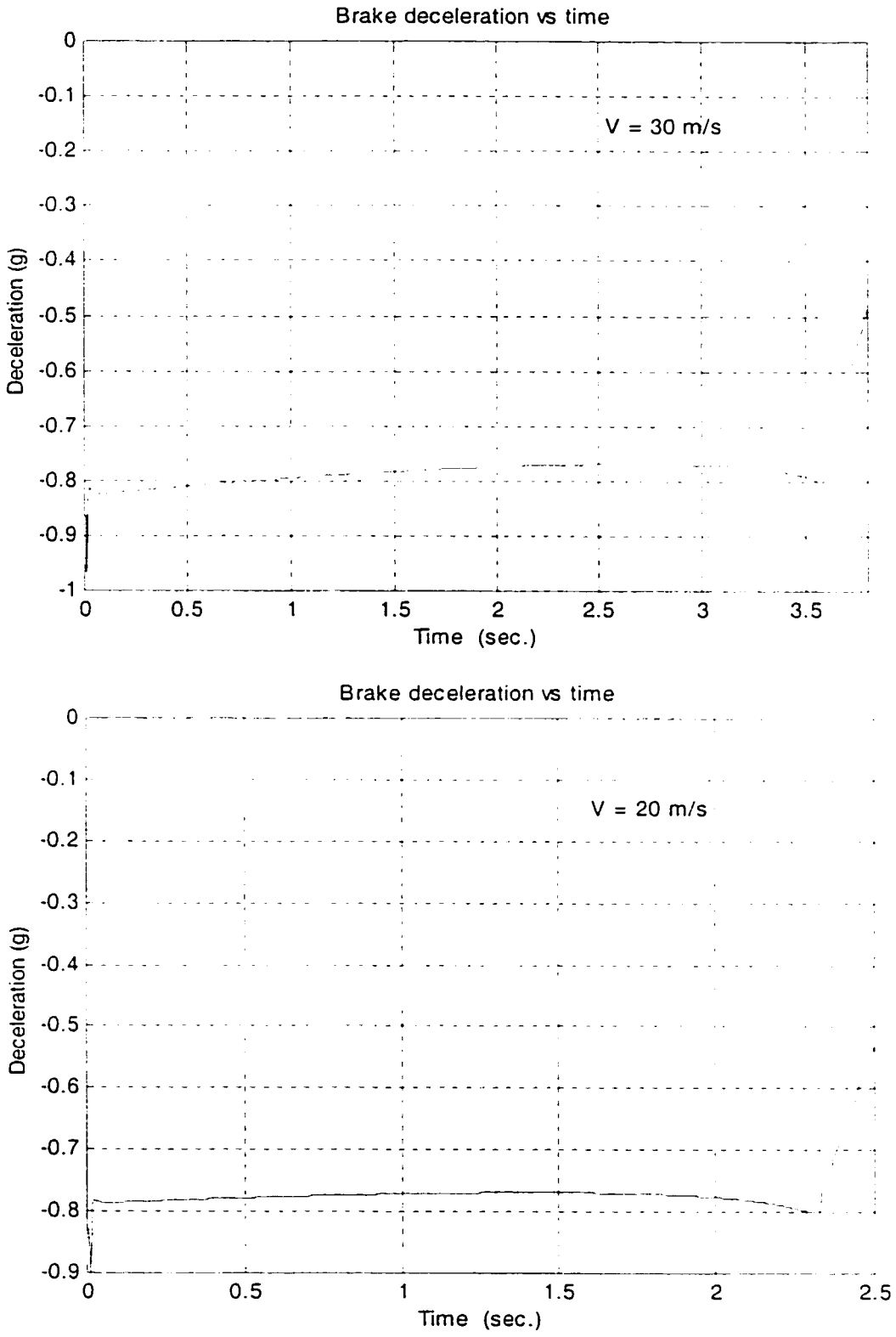

Fig. 5.13 Braking deceleration response for slide mode controller

5.6 Summary

Same as what has been done in Chapter IV, a quarter vehicle model for evaluation of braking performance developed for this investigation was tested under a given braking pressure to establish the braking performance. The model was then integrated with a robust (slide mode) controller for the control of brake system based on established sliding surface and assuming that the vehicle velocity and internal state are measurable. The dynamic friction tire model developed in this investigation was utilized to establish maximum skid as the input to establish the sliding surface.

The results obtained in this section of the study with dynamic friction tire model and simple vehicle braking model exhibit promising potential for such system in the design of stable and effective controllers, through which a better approximate maximum deceleration in a faster and more stable manner can be achieved. This section was devoted to the evaluation of control system using robust (slide mode) controller. Furthermore, the stability of the designed controller has been proved by means of Lyapunov theorem, which overcame the drawback of the PI controller discussed in Chapter IV.

`CHAPTER VI

CONCLUSIONS AND FUTURE WORKS

6.1 Conclusions

In this research, a dynamic friction tire model is developed based on the LuGre model for generating the dynamic (transient) tire/road interaction. This provides an opportunity to search for the optimal longitudinal skid corresponding to maximum braking force at each velocity during the braking. The methodology, however, assume that the velocity is constant for each simulation step. The study also provides a new method for the modeling of the vehicle braking system and simplifies the design of the ABS controller. It should be noted that the static tire/road response is commonly used in the design of controller for conventional ABS. The major problem is that the designed controllers need a method to find the optimal longitudinal skid. From the control point of view, the PI method and sliding mode method are same regardless of the tire models. However, when they are applied to the different tire models, (the static tire model or dynamic tire friction model), the control algorithms are quiet different. The dynamic friction tire model can give the simplified controller design process to produce stable and reliable performance of ABS.

A quarter vehicle model is used in this investigation, which is convenient for fundamental dynamic analysis of any vehicle systems. For the PI control method, the load shift is also considered together with the quarter vehicle model. In this case, the

effect of pitch motion and resulting load shift is incorporated within the quarter vehicle model. For the slide mode control method, this quarter vehicle model is simplified by neglecting the effect of pitch load transfer in order to simplify the initial investigations. Both the quarter vehicle models are derived from the Newton's second law, however, for the quarter vehicle model used in the slide mode control method, a new variable, namely internal state representing the relative deformation of the tire at the ground contact is introduced. The introduction of the new internal state provides a new approach to represent the tire/road friction force, which is no longer the traditional function of the $\mu(\lambda)$, instead, it is the new function of the internal state. Two controllers designed based on different approach to modeling allow a means to validate each other as well as provide some indepth understanding of the control steps.

Both the models were tested for response to a time varying brake torque. The simulated responses showed very reasonable quantitive and qualitative response of the vehicle to braking. A close examination of all the response variable from the simulation provided the in site and confidence in using the model for development and study of controller for ABS.

The quarter vehicle model was first integrated with a PI controller for the control of brake system based on skid developed at the tire road interface. The dynamic friction tire model was utilized to establish optimal skid corresponding to maximum skid at a velocity. In the control loop, the optimal skid was used as the reference to maintain the actual skid close to the optimal value. It is shown that such scheme can replace the need for online optimization that is need in commonly used ABS scheme

The robust slide mode controller is developed with an innovative representation of vehicle dynamics through state variables of internal state. In this formulation, the braking force is no longer a function of $\mu(\lambda)$. Instead, it is the function of the internal state, which is a new variable included in the development of the model. In the case of PI controller and conventional ABS controllers, velocity and angular velocity are used as controlled variable which is a direct measure of skid. In the present investigation with sliding mode controller, the control variables are velocity and relative velocity at tire road contact, where the control goal is to achieve $v=0$, while relative velocity approach maximum. The proposed sliding surface is therefore, chosen to include the velocity, relative velocity and the optimal longitudinal skid which can be obtained from the dynamic friction tire model. The simulation results show that the vehicle can be stopped as quickly as possible by application of the designed robust controller.

In summary, the development of the dynamic friction tire model, the design of the PI controller based on the combination of such tire model with the common vehicle model, and realization of a control scheme without the need for online optimization are some of the contributions made in this thesis. The research makes further contributions in the development of slide mode controller through the use of innovative state variable approach. The limited simulation results presented in this thesis is to demonstrate the effectiveness of the proposed controllers in application to ABS for vehicle. The models used for vehicle dynamics here are highly simplified and are not adequate to demonstrate the dynamic behavior of vehicle under braking or combined maneuvers. Significant further work is necessary for though exploration of the proposed concepts. A brief recommendations and possible future works are listed in the following subsection.

6.2 Recommendations and Future Works

In this study, two different control methods are investigated for the vehicle ABS coupled with the dynamic friction tire model. The following future works to further explore the performance of the braking system upon the proposed control methodologies are recommended.

In this investigation, both of the two controller are developed from the quarter vehicle model, with longitudinal and wheel angular motions. These models neglect import influence of pitch motion and yaw motion where lateral tire force play important role. A major function of ABS is to ensure that wheels are not locked and that sufficient lateral force is present for stability and handling. In this case , a multi-DOF vehicle model with 4 wheels must be studied under combined braking and steering maneuvers.

The present investigation considered only one wheel and a fixed road condition. A study should focus on the performance of ABS with the controllers for real-time change in road condition form dry to wet or snow, as well as vice versa. Furthermore, the road condition for 4 wheels of a vehicle may be different and its effect is needed to be evaluated under a proposed control system.

For a complete vehicle system, the performance should also be investigated for one controller per axle to one controller per wheel.

The brake system model in this study assumes a torque applied to the wheels. In reality the hydraulic and air brake system are complex system with their own dynamics.

A realistic model of vehicle brake performance should include the brake system dynamics and possibly a driver model.

Finally, once the controller are presented through analytical investigation, a prototype may be tested in laboratory and in field.

REFERENCES

[1] *Automotive Brake Systems*, Robert Bosch GmbH, 1995

[2] Rudolf Limpert, *Brake Design and Safety*, 2nd ed, Society of Automotive Engineers, Inc, 1999

[3] Guntur, R. R., and Ouwerkerk, H., "Adaptive Brake Control System," *Proceedings of the Institution of Mechanical Engineers*, vol. 186, 1972.

[4] Guntur, R. R., and Ouwerkerk, H., "Anti-lock reselection," *Automotive Design Engineering*, pp. 13-15, 1973

[5] Fling, R. T., and Fenton, R. E., "A describing-function approach to antiskid design," *IEEE Transactions on Vehicular Technology*, vol. VT_30, no. 3. pp.134-144, 1981

[6] Zeller, J. W., "An analytical approach to antilock brake system design," *SAE Paper 840249*, 1984

[7] Athan, T. W. (1994), "A Quasi-Monte Carlo Approach to Multicriteria Optimization," *Doctoral Dissertation, Dept. of Mechanical Engineering and Applied Mechanics, University of Michigan*, Ann Arbor, Michigan

[8] Athan, T. W. and Papalambros, P.Y. (1996), "A Quasi-Monte Carlo method for multicriteria design optimization," *Engineering Optimization.*

[9] Tan, H. –S. and Tomizuka, M. (1990), "Discrete-time controller design for robust vehicle traction," *IEEE Control Systems Magazine*, 10(3), pp.107-113

[10] Lin, W. C. and Chin, Y. –K. (1986), "Variable-structure brake control for anti-skid and anti-spin," *Report No. EG-275. General Motors Research Laborotories*, Warren, Michigan.

[11] H. S. Tan and M. Tomizuka, "An adaptive sliding mode vehicle traction controller design," in *Proc. 1989 Amer. Contr. Conf.*, 1989

[12] Y. K. Chin et al., "Sliding-mode ABS wheel slip control," in *Proc. 1992 ACC*, Chicago, IL, June 24-26, 1992, pp. 1-6

[13] S. Drakunov, Ü. Özgüner, P. Dix, and B. Ashrafi, "ABS Control Using Optimum Search Via Sliding Modes," *IEEE Transactions on Control Systems Technology*, Vol. 3, No.1, pp. 79-85, 1995.

[14] Kachroo and Tomizuka, "Sliding mode control with chattering reduction and error convergence for a class of discrete nonlinear systems with application to vehicle control," *ASME Int. Mech. Eng. Congr. Expo*, San Fransisco, CA, 1995

[15] T. L. Lasky and B. Ravani, "A review of research related to automated highway system (AHS)," Univ. California, Davis, Interm Rep. FHWA, Contract DTFH61-93-C-00189, Oct. 25, 1993.

[16] C. Ünsal, and P. Kachroo, "Sliding Mode Measurement Feedback Control for Antilock Braking Systems," *IEEE Transaction on Control Systems Technology*, vol. 7, no. 2, 1999

[17] S. V. Drakunov, B. Ashrafi, and A. Rosiglioni, "Yaw Control Algorithm via Sliding Mode Control," in *Proc. Amer. Contr. Conf.*, Chicago, IL, pp. 569-573, June, 2000.

[18] Tan, H. –S. (1988), "Adaptive and Robust Controls with application to Vehicle Traction Control," *Doctoral Dissertation, Dept. of Mechanical Engineering , University of California, Berkeley*

[19] Gilbson, J. E. (1963), *Nonlinear Automatic Control*, McGraw-Hill, New York

[20] Kawabe, T., Nakazawa, M., Notsu, I. and Watanabe, Y., "A sliding mode controller for wheel slip ratio control system," *Proceedings of AVEC'96*, vol. 2, 1996, pp. 797-804

[21] A. B. Will, S. Hui, and S. H. Zak, "Sliding mode wheel slip controller for an antilock braking system," *Vehicle Design*, vol. 19, no. 4, pp. 523-539, 1998

[22] S. Choi, and D. W. Cho, "Control of Wheel Slip Ratio Using Sliding Mode Controller with Pulse Width Modulation," *Vehicle System Dynamics*, Vol. 32 (1999), pp. 267-284

[23] H. B. Pacejka, "Analysis of the dynamic response of a rolling string-type tire model to lateral wheel-plane vibrations," *Vehicle Dynamics*, vol. 1, pp. 37-66, 1972

[24] Loeb, J. S. et al., "Lateral stiffness, cornering stiffness of relaxation length of the pneumatic tire," *SAE Technical Paper*, 900129, 1990

[25] Van Zanten, A., Ruf, W. D., and Lutz, A., "Measurement and simulation of transient tire forces," *SAE Technical Paper*, 890640, 1989

[26] Segel, L., "An overview of development in road-vehicle dynamics: past present, and future," *Proceedings of the Institution of Mechanical Engineers*, Automobile Division, 1993

[27] Szostak, H. T. et al, "Analytical Modeling of Driver Response in Crash Avoidance Maneuvering, Volume I: Technical Background", *U. S. Dept. of Transportation Report NHTSA DOT HS-807-270*, April 1988

[28] Allen R. T. et al, "Analytical Modeling of Driver Response in Crash Avoidance Maneuvering, Volume II: Interactive Tire Model for Driver/Vehicle Simulation", *U. S. Dept. of Transportation Report NHTSA DOT HS-807-271*, April 1988

[29] Schallamack, A., "Tire Traction and Wear", Chapter 6 in *Mechanics of Pneumatic Tires*, Dot HS-805 952, August 1981, pp. 365-474

[30] Pacejka, H., "Analysis of Tire Properties", Chapter 9 in *Mechanics of Pneumatic Tires*, DOT HS-805 952, August 1981, pp. 721-870

[31] Shuring, D. J., " Tire Parameter Determination. Volume I: Summary", *U. S. Dept. of Transportation Report NHTSA DOT HS-802-086*, November,1976

[32] Shuring, D. J., " Tire Parameter Determination. Volume II: Technical Report ", *U. S. Dept. of Transportation Report NHTSA DOT HS-802-087*, November,1976

[33] Ray, L. R., "Nonlinear tire force estimating and road friction identification: field results," *SAE Technical Paper* 960181, 1996

[34] Eichhorn, U., and Roth, J., "Prediction and monitoring of tire/road friction," *XXIV. FISTA Congress*, London, Great Britain, 1992

[35] Bakker, E., Nyborg, L., and H. B. Pacejka, "Tire modeling for use in vehicle dynamics studies," *SAE paper* 870421, 1987

[36] H. B. Pacejka, and R. S. Sharp, "Shear Force Development by Pneumatic Tyres in Steady State Conditions: A Review of Modeling Aspects," *Vehicle System Dynamics*, Vol. 20 (1991), pp. 121-176

[37] W. R. Pasterkamp, and H. B. Pacejka, "The Tyre as a Sensor to Estimate Friction," *Vehicle System Dynamics*, Vol. 27 (1997), pp. 409-422

[38] P. Van der Jagt, and A. W. Parsons, "Road surface correction of tire test data," *Vehicle System Dynamics*, vol. 25, pp. 147-165, 1996

[39] P. Dahl, "A solid friction model," *Aerospace Corp.*, El Segundo, CA. Tech. Rep. TOR-0158 (3107-18)-1, 1968.

[40] P. -A. Bliman, "Mathematical study of the Dahl's friction model," *European J. Mechanics. A/Solids*, vol. 11, no. 6, pp835-848, 1992

[41] P. -A. Bliman and M. Sorine, "Friction modeling by hysteresis operators. Application to Dahl, Sticktion, and Stribeck effects," in *Proc. Conf. Models of Hysteresis*, Trento, Italy, 1991

[42] C. Walrath, "Adaptive bearing friction compensation based on recent knowledge of dynamic friction," *Automatica*, vol. 20, no. 6, pp. 717-727, 1984

[43] N. Ehrich Leonard and P. Krishnaprasad, "Adaptive friction compensation for bi-directional low-velocity position tracking," in *Proc. 31th Conf. Decis Contr*, 1992, pp. 267-273

[44] B. Armstrong-Hélouvry, *Control of Machines with Friction*, Boston, MA: Kluwer, 1991

[45] J. R. Rice and A. L. Ruina, "Stability of steady frictional slipping," *J. Applied Mechanics*, vol. 50, no.2, 1983

[46] P. Dupont, "Avoiding stick-slip through PD control," *IEEE Trans. Automat. Contr.*, vol 39, pp. 1094-1097, 1994

[47] C. Canudas de Wit, H. Olsson, K.J. Åström, and P. Lischinsky, (March, 1995), "A New Model for Control of Systems with Friction," *IEEE TAC*, (1995) Vol. 40, No. 3, pp419-425

[48] C. Canudas de Wit, P. Tsiotras, "Dynamic Tire Friction Models for Vehicle Traction Control," in *38th IEEE Conf. Decision and Contr.*, Phoenix, AZ, pp. 3746-3751, Dec. 1999.

[49] C. Canudas de Wit, R. Horowitz, "Observers for Tire/road Contact Friction using only wheel angular velocity information," in *38th IEEE Conf. Decision and Contr.*, pp.3932-3937, Phoenix, AZ, Dec. 1999.

[50] P. Tsiotras, C. Canudas de Wit, "On the Optimal Braking of Wheeled Vehicles," in *Proc. Amer. Contr. Conf.*, Chicago, IL, pp. 569-573, June, 2000.

[51] Jingang Yi, L. Alvarez, R. Horowitz, and C. Canudas de Wit, "Adaptive Emergency Braking Control Using a Dynamic Tire/Road Friction Model," in *Proc. Of 39th IEEE Conf. Decision and Contr.*, Australia, pp456-461.

[52] M. Sugai, H. Yamaguchi, M. Miyashita, T. Umeno, and K. Asano, "New Control Technique for Maximizing Braking Force on Antilock Braking System," *Vehicle System Dynamics*, Vol. 32 (1999), pp. 299-312

[53] C. L. Clover, and J. E. Bernard, "Longitudinal Tire Dynamics," *Vehicle System Dynamics*, Vol. 29 (1998), pp. 231-259

[54] Wang, J. Y., "*Theory of Ground Vehicle*", 2nd ed. John Wiley & Sons, Inc., New York, 1993

[55] R. D. Lister, " Retention of Directional Control When Braking," *SAE paper* 650092,1965

[56] W. W. Olson, and D. Milacic, "Development of anti-lock braking traction and control systems of the advanced technology demonstrator II using DADS simulation code", *Vehicle Design*, vol. 17, no. 3 pp. 295-317, 1996

[57] Larry Michaels, "The use of a graphical modeling environment for real-time hrdware-in-the-loop simulation of automotive ABS systems", *SAE Technical paper* 930907, 1993

[58] M. J. Schneider, "Use of a Hazard and Operability study for evaluation of ABS control logic", *SAE paper* 970815, 1997

[59] R. Srinivasa, R. R. Gunter, and J. Y. Wong, "Evaluation of the anti-lock brake systems using laboratory simulation techniques", *Vehicle Design*, vol. 1, no. 5, pp. 467-485, 1980

[60] Bliman, P. A., T. Bonald, and M. Sorine, "Hysteresis Operators and Tire Friction Models: Application to Vehicle Dynamic Simulator", *Prof. Of ICIAM*. 95, Hamburg, Germany, 3-7 July, 1995

[61] H. B. Pacejka, "In-Plane and Outt-Plane Dynamics of Pneumatic Tyres," *Vehicle System Dynamics*, Vol. 10 (1981), pp. 221-251

[62] P. M. Leucht, "The Directional Dynamics of the Commercial Tractor-Semitrailer Vehicle During Braking," *SAE paper* 700371,1970

[63] Barbara E. Sabey, T. Williams, and G. N. Lupton, "Factors Affecting the Friction of Tires on Wet Roads," *SAE paper* 700376, 1970

[64] H. Dugoff, P. S. Fancher, and L. Segel, "An Analysis of Tire Traction Properties and Their Influence on Vehicle Dynamic Performance," *SAE paper* 700377,1970

[65] H. Leiber, and A. Czinczel, "Four Years of Experience with 4-Wheel Antiskid Brake Systems (ABS)," *SAE paper* 830481, 1983

[66] M. Satoh, and S. Shiraishi, "Performance of Antilock Brakes with Simplified Control Technique," *SAE paper* 830484, 1983

[67] M. Watanabe, N. Noguchi, "New Algorithm for ABS to Compensate for Road-Disturbance," *SAE paper* 900205, 1990

[68] J. Eric Bowman, and E. H. Law, "A Feasibility Study of an Automotive Slip Control Braking System," *SAE paper* 930762, 1993

[69] A. Sitchin, "Acquisition of Transient Tire Force and Moment Data for Dynamic Vehicle Handling Simulations", *SAE Paper* No. 831790, November 7-10, 1983

[70] H. B. Pacejka, "Modeling of the Tyre as a Vehicle Component with Applications", Lehrgang V2.01, Carl-Cranz-Gesellschaft, 1982

[71] P. Lugner, R. Lorenz, E. Schindler, "The Connection of Theoretical Simulation and Experiments in Passenger Car Dynamics", *Proc. 8th IAVSD Symp. On the dynamics of vehicles*, Cambridge, Mass, August 15-19, 1983, ed. J. K. Hedrick, Swets & Zeitlinger B. V., Lisse Neth, 1984.

[72] X.B. Yang , "A Closed-Loop Driver/Vehicle Directional Dynamics Predictor", *Ph. D. Thesis*, Concordia University, Montreal, Canada, 1999

[73] Gillespie, T.D. (1992) *Fundamentals of Vehicle Dynamics*, Warrendale, PA: Society of Automotive Engineers, Inc.

APPENDIX

Appendix A
Nonlinear Tire Model

The nonlinear tire model described in this Appendix is based on the very comprehensive work described in [28]. The work in [28] was based, in turn, on the work done by previous investigators in [29] and [30]. As explained in [28], the "...basic objective was not to develop a new tire model, but to consolidate the work of others into a convenient computational form which could be easily applied in a vehicle dynamics simulation. They had no desire to invent new unmeasurable parameters, but instead strived to work with parameters available from the tire test data such as the comprehensive Calspan model and data [31],[32]."

The basic input parameters to this tire model are: tire normal load, tire camber angle, tire velocity, lateral slip angle, and longitudinal slip ratio. The outputs of the model are aligning torque and the normalized lateral and longitudinal forces.

The procedure used in calculating the tire forces is shown schematically in Figure A.1. First, the parameters K_s, K_c, μ_0, and a_p are calculated. These are, respectively, the lateral and longitudinal stiffness coefficients, the ration of the peak tire to road coefficient of adhesion, and the length of the contact patch. These parameters are defines in Table A.1 in terms of other parameters that are given in Table A.3.

The next step involves calculating the composite slip and force saturation function, σ and $f(\sigma)$. These are defined in Table A.2.

The third step involves modifying the longitudinal stiffness coefficient and defining the coefficient of friction to account for the transition from the slip to the sliding

regime. The modified longitudinal stiffness coefficient is K'_c and the coefficient of friction is μ as listed in Table 3.2. The final step results in the calculation of the aligning torque, Mz, and the normalized lateral and longitudinal forces, F_y/F_z, and F_x/F_z.

Sample plots of the predicted longitudinal and lateral force versus longitudinal slip and slip angle, respectively, have been shown in Figure 2.4 (Chapter II) for the P185/70 R 13 wide section The Tire parameters are listed in Table A.3. The tire force nonlinearity and interaction of the lateral and longitudinal forces are also in Figure 2.4. These curves were generated for a speed of 48.3 km/h (30mph).

In the simulation, a subroutine based on the procedure described above was used to calculate the tire forces at each time step based on the instantaneous values of speed, tire normal force, longitudinal slip, and slip angle. Inflation pressure and nominal coefficient of adhesion are parameters that are input to the tire model. However, the time delay of tire side force generation was not included in this stage.

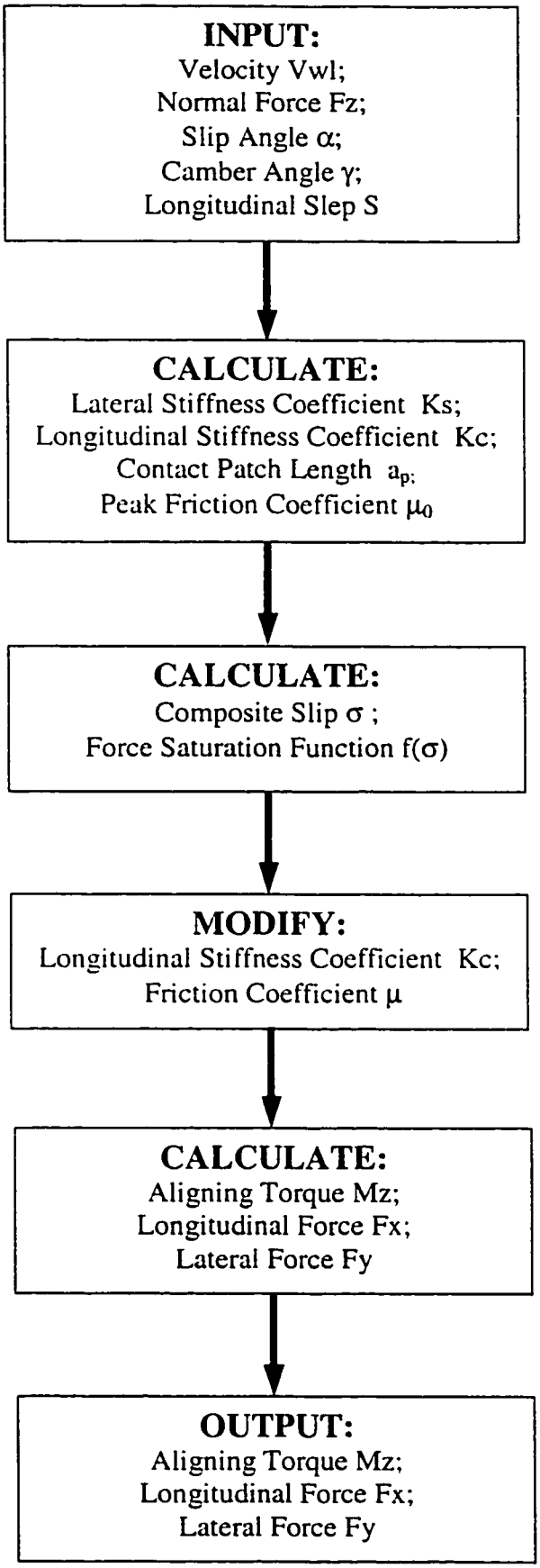

Figure A.1 Procedure for Tire Forces and Moments Calculation

Table A.1 Tire Model Parameters

1. Lateral Stiffness Coefficient of the tire

$$K_{\alpha} = \frac{2.0}{a_{p0}^2}(A_0 + A_1 F_z - \frac{A_1}{A_2} F_z^2)$$

2. Longitudinal Stiffness Coefficient of the tire

$$K_{\kappa} = \frac{2.0}{a_{p0}^2} F_z (\frac{CS}{FZ})$$

3. Camber Thrust Stiffness

$$Y_{\gamma 0} = A_3 F_z - \frac{A_3}{A_4} F_z^2$$

4. Peak Tire to Road Coefficient of Friction

$$\mu_0 = 1.176 \mu_{NOM} (B_1 F_z + B_3 + B_4 F_z^2)$$

5. Tire Contact Patch Length

$$a_p = a_{p0}(1.0 - K_{\alpha} \frac{F_{\alpha}}{F_z})$$

$$Where \ a_{p0} = \frac{0.0768\sqrt{F_z F_{zs}}}{T_w (T_p + 5)}$$

6. Aligning Torque Coefficient

$$K_m = K_1 F_z$$

Table A.2 The Slip and Force Calculations

1. Composite Slip

$$\sigma = \frac{\pi a_p^2}{8\mu_0 F_z}\sqrt{K_x^2 \tan^2\alpha + K_c^2(\frac{s}{1-s})^2}$$

2. Force Saturation Function

$$f(\sigma) = \frac{C_1\sigma^3 + C_2\sigma^2 + \frac{4}{\pi}\sigma}{C_1\sigma^3 + C_3\sigma^2 + C_4\sigma + 1}$$

3. Normalized Lateral Force

$$\frac{F_y}{\mu F_z} = \frac{1}{\mu F_z}[\frac{f(\sigma)K_x \tan\alpha}{\sqrt{K_x^2 \tan^2\alpha + K_c'^2 S^2}} + Y_\gamma \gamma]$$

Where $K_c' = K_c + (K_x - K_c)\sqrt{\sin^2\alpha + S^2\cos^2\alpha}$

$$\mu = \mu_0(1 - K_\mu\sqrt{\sin^2\alpha + S^2\cos^2\alpha})$$

$$Y_\gamma = Y_{\gamma 0}[1.0 - f(\sigma)]$$

$$K_\mu = \frac{0.25\sqrt[3]{V_{wl}}}{11}$$

4. Normalized Longitudinal Force

$$\frac{F_x}{\mu F_z} = \frac{1}{\mu F_z}[\frac{-f(\sigma)K_c' S}{\sqrt{K_x^2 \tan^2\alpha + K_c'^2 S^2}}]$$

5. Aligning Torque

$$M_z = \frac{K_m a_p^2 \tan\alpha}{(1+G_1\sigma^2)^2}\frac{K_x}{2} - G_2 K_c \frac{S}{1-S}(2+\sigma^2)$$

Table A.3 Parameter Description

MATTHEMATICAL SYMBOLS	DEFINATION
a_{p0}	: tread length with zero longitudinal force
$A_0, A_1, A_2, A_3, A_4, B_1, B_3, B_4$	: coefficients obtained by Calspan tests
$\frac{CS}{FZ}$	: Calspan coefficient for the slope of the normalized longitudinal force vs. longitudinal slip curve at zero longitudinal slip
Fz	: the instantaneous value of normal load on the tire
Fx	: the instantaneous value of the longitudinal force on the tire.
Fy	: the instantaneous value of the lateral force on the tire
Fzt	: the tire design load at the operating tire pressure
Ka	: the proportion that the tread length a_{p0} changes with longitudinal Load
S	: longitudinal slip
Tw	: nominal tread width
Tp	: tire pressure
α	: tire side slip angle
μ_{NOM}	: nominal tire to road adhesion coefficient
γ	: tire camber angle

Table A.4 Tire Parameters

PARAMETER	TIRE		
	WIDE SECTION (RADIAL)	STANDARD CROSS (SECTION RIDIAL)	BIAS PLY
Tire Designation	P185/70R13	155 SR 13	P155/80 D 13
Tire Width, in	7.3	6	6
Tire Pressure, psi	24	24	24
Design Load, lb	980	810	900
A_0	1068	914.02	817
A_1	11.3	12.9	7.48
A_2	2442.73	2028.24	2455
A_3	0.31	1.19	1.857
A_4	-1877	-1019.2	3643
Ka	0.05	0.05	0.2
K_1	-8.0E-4	-1.22E-4	-1.95E-4
B_1	-1.69E-4	3.396E-4	-2.57E-4
B_3	1.04	1.19	1.19
B_4	1.69E-8	4.98E-8	2.64E-8
$\frac{CS}{FZ}$	17.91	18.7	15.22
μ_{NOM}	0.85	0.85	0.85
C_1	1.0	1.0	1.0
C_2	0.34	0.34	0.34
C_3	0.57	0.57	1.15
C_4	0.32	0.32	0.8
G_1	1.0	1.0	1.0
G_2	1.0	1.0	1.0
K_{T1}	1.38	1.38	1.38

Appendix B

Magic Formula

The most common tire friction models used in the literature are those of slip/force maps. One of the most well-known models of this type is Pacejka's model [36], also known as the "magic formula". This model has been shown to suitably match experimental data, obtained under particular conditions of constant linear and angular velocity, which was fully described in [35]. The work in [35] was based, in turn, on the work done by previous investigators in [69], [70], and [71]. As explained in [35], "The method makes use of a formula with coefficients which describe some of the typifying quantities of a tyre, such as slip stiffnesses at zero slip and force and torque peak values. The formula is capable of describing the characteristics of side force, brake force, and self aligning torque with great accuracy. This mathematical representation is limited to steady-state conditions during either pure cornering or pure braking and forms the basis for a model describing tyre behaviour during combined braking and cornering."

First, the parameters' descriptions which used in [35] are given in Table B.1, then the proposed tire formulae for brake force, self aligning torque, and side force were summarized in Table B.2, B.3, and B.4, respectively. We may see that each equation have four basic coefficients, which was able to describe all the measured characteristics. The four coefficients were stiffness factor, shape factor, peak factor, and curvature factor. Moreover, in order to fit the measured tire property data, as many as 13 parameters, which was from a_1 to a_{13} in this appendix, were introduced into those tire formulae. Due to ply steer, conicity and rolling resistance, the characteristics would be shifted in the

horizontal and/or vertical directions, these shifts were also included in the equations of side force and self aligning torque. Besides that, the vehicle vertical load is another important coefficient used in these three equations, which mainly decided the peak values of all the three tire forces. The formulae obtained which describe the pure cornering and braking conditions, can be further used in a mode which describes the behavior of the tire at zero camber angle when a combination of cornering and braking takes place.

The proposed formula turns out to be not only accurate in describing the measured data, it also characterizes some of the typifying quantities of the tire such as slip stiffnesses and peak values and permits the calculation of forces and torque in conditions which deviate from those imposed during the actual measurements.

Finally, the values of the coefficients a_1 to a_{13} were given in the Table B.5, and Table B.6.

Table B.1 Parameter descriptions for magic formula

MATTHEMATICAL SYMBOLS	DEFINATION
a_1 -- a_{13}:	coefficients for tire formula
B:	stiffness factor
C:	shape factor
D:	peak factor
E:	curvature factor
S_h:	horizontal shift
S_v:	vertical shift
α:	slip angle
γ:	camber angle
λ:	Longitudinal slip
F_z:	Vehicle vertical load

Table B.2 Brake force equation for magic formula

Brake Force	$F_x = D \sin (C \arctan (B\phi))$
with	$\phi = (1-E)\lambda + (E/B)\arctan(B\lambda)$ $D=a_1F_z^2 + a_2F_z$ $C=1.65$ $B = \frac{a_3F_z^2 + a_4F_z}{CDe^{a_5F_z}}$ $E= (a_6 F_z^2 + a_7F_z+a_8)/(1-a_{12}\lvert\gamma\rvert)$

Table B.3 Self aligning torque equation for magic formula

Self Aligning Torque	$M_z = D \sin (C \arctan (B\phi)) + \Delta S_v$
with	$\phi = (1\text{-}E) (\alpha + \Delta S_h) + (E/B)\arctan(B(\alpha + \Delta S_h))$ $D=a_1F_z^2 + a_2F_z$ $C=2.4$ $B = \left(\frac{a_3F_z^2 + a_4F_z}{CDe^{a_5F_z}} \right)(1 - a_{12}\lvert\gamma\rvert)$ $E= (a_6 F_z^2+ a_7F_z+a_8)/(1\text{-}a_{12}\lvert\gamma\rvert)$ $\Delta S_h=a_9\gamma$ $\Delta S_v=(a_{10} F_z^2 + a_{11} F_z)\gamma$

Table B.4 Side force equation for magic formula

Side Force	$F_y = D \sin (C \arctan (B\phi)) + \Delta S_v$
with	$\phi = (1\text{-}E) (\alpha + \Delta S_h) + (E/B)\arctan(B(\alpha + \Delta S_h))$ $D=a_1F_z^2 + a_2F_z$ $C=1.3$ $B = \left(\frac{a_3\sin(a_4\arctan(a_5F_z))}{CD} \right)(1 - a_{12}\lvert\gamma\rvert)$ $E= a_6 F_z^2+ a_7F_z+a_8$ $\Delta S_h=a_9\gamma$ $\Delta S_v=(a_{10} F_z^2 + a_{11} F_z)\gamma$

Table B.5 Coefficients for magic formula
(with load influence. F_z (kN))

	a_1	a_2	a_3	a_4	a_5	a_6	a_7	a_8
F_y	-22.1	1011	1078	1.82	0.208	0.000	-0.354	0.707
M_z	-2.72	-2.28	-1.86	-2.73	0.110	-01070	0.643	-4.04
F_x	-21.3	1144	49.6	226	0.069	-0.006	0.056	0.486

Table B.6 Coefficients for magic formula (continued)
(connected with camber influence. γ(deg.))

	a_9	a_{10}	a_{11}	a_{12}	a_{13}
F_y	0.028	0.000	14.8	0.022	0.000
M_z	0.015	-0.066	0.945	0.030	0.070

Appendix C

Matlab Program for PID Controller

C.1 Main Program

```
%************** PID controller development  **************
%****All the vehicle parameter come from the paper
%"Sliding mode wheel slip controller for an antilock
braking system"****
%-------------------------------------------------------------

%define global parameters for vehicle systems
global g;          %gravitational acceleration
global l;          %wheelbase
global hcg;        %centre of gravity height
global mt;         %tyre mass
global mc;         %quarter vehicle mass
global Jt;         %wheel inertia
global Je;         %engine inertia
global zeta;       %transmission gear ratio
global R;          %wheel radius
global f0;         %basic coefficient
global fs;         %speed effect coefficient
global Af;         %vehicle front area
global Cd;         %vehicle drag coefficient

global Kmph;       %converts m/s to miles per hour

global m;          %total quarter vehicle mass
global meq;        %equivalent mass
global Jw;

%getting braking acceleration from the function
%"motionequation_PID"
global deceleration;

%vehicle systems description
g=9.81;          %unit:m/s^2
l=2.5;                %m
hcg=0.5;              %m
mt=40;                %kg
mc=375;               %kg
Jt=1.7;               %kgm^2
```

```
Je=0.241;              %kgm^2
zeta=10;
R=0.326;               %m
f0=0.01;
fs=0.005;
Af=2.04;               %m^2
Cd=0.539;

Kmph=2.237;

m=mt+mc;               %m is mtot in paper
meq=mc*hcg/l;
Jw=Jt+0.5*(zeta^2*Je);

%define initial condition for developed system
V=30;                  %initial velocity
W=V/R;                 %initial angular velocity

%define matrix
tt = [];    %time
VV = [];    %velocity
WW = [];    %angular velocity
PP = [];    %brake pressure
VVr= [];    %relative velocity
XX0= [];    %stop distance;
ACC= [];    %acceleration;

%define initial condition for differential equation (motion
%equation)
%x1: stop distance; x2=velocity; x3=angular velocity.
x0=[0 V V/R];
slip=(V-R*W)/V;


%define time sample
t0=0;
interval=0.005;

term0=0;

K=1;

while x0(2)>=0.5,

t=t0+interval;

Slip_max=longitudinal_slip_max(V);
```

```
slip=(x0(2)-R*x0(3))/x0(2);
Delta=Slip_max-slip;

%PID controller design: Delta is the input of the PID
%controller.

KP=5800;
KI=320;
term=term0+KI*Delta;
Tb=KP*Delta+term;

%calculating the real friction coefficient
mu_real=calculation_mu_real(V,slip);

%solve the differential equation
options=odeset('RelTol',1e-4,'AbsTol',1e-4);
[T,x]=ode45('motionequation_PID',[t0 t], x0, options,
mu_real,Tb);

t0=t;
x0=x(length(x),:);
V=x0(2);
Vr=R*x0(3)-x0(2);

term0=term;
Delta_in=Delta;

%time vector
tt = [tt t0];
%velocity vector
VV = [VV x0(2)];
%angular speed vector
WW = [WW x0(3)];
%brake torque vector
PP = [PP Tb];
%relative velocity vector
VVr= [VVr Vr];
%stop distance;
XX0= [XX0 x0(1)];
%braking deceleration
ACC= [ACC deceleration];

end


%plotting the response curves
```

```
figure(1);
plot(tt,VV);
title('Velocity vs time');
xlabel('Time  (sec.)');
Ylabel('Velocity  (m/sec.)');
%axis([0 5 0 VC]);
grid;

figure(2);
plot(tt,WW);
title('Angular velocity vs time');
xlabel('Time  (sec.)');
Ylabel('Angular velocity  (rad/sec.)');
%axis([0 5 0 WC]);
grid;

figure(3);
plot(tt,PP);
title('Braking Pressure vs time');
xlabel('Time  (sec.)');
Ylabel('Braking Pressure (N/m^2.)');
grid;

figure(4);
plot(tt,VVr);
title('Relative velocity vs time');
xlabel('Time  (sec.)');
Ylabel('Relative velocity');
grid;

figure(5);
plot(tt,XX0);
title('Stop distance vs time');
xlabel('Time  (sec.)');
Ylabel('Distance (m)');
grid;

figure(6);
plot(tt,ACC);
title('Braking deceleration vs time');
xlabel('Time  (sec.)');
Ylabel('Deceleration (g)');
grid;

%-------------------------------------------------------------
```

C.2 Member Functions

C.2.1 Motion Equation Function

```
%solve differential equation for PID controller
function dx=motionequation_PID(t,x,flag,mu_real,Tb);

%define global parameters
global g;       %gravitational acceleration
global l;       %wheelbase
global hcg;        %centre of gravity height
global mt;         %tyre mass
global mc;         %quarter vehicle mass
global Jt;         %wheel inertia
global Je;         %engine inertia
global zeta;    %transmission gear ratio
global R;       %wheel radius
global f0;         %basic coefficient
global fs;         %speed effect coefficient
global Af;         %vehicle front area
global Cd;         %vehicle drag coefficient

global Kmph;       %converts m/s to miles per hour

global m;       %total quarter vehicle mass (mtot in paper)
global meq;        %equivalent mass
global Jw;

global deceleration;

dx=zeros(3,1);   %a column vector

dx(1)=x(2);
dx(2)=(-mu_real*m*g-0.25*Cd*Af*(x(2)^2))/(m-mu_real*meq);
dx(3)=(-mu_real*meq*R/Jw)*(-mu_real*m*g-
0.25*Cd*Af*(x(2)^2))/(m-mu_real*meq)...
+(R/Jw)*(mu_real*m*g-f0-3.24*fs*(Kmph*x(2))^2.5)-Tb/Jw;

deceleration=dx(2)/g;
```

C.2.2 Finding the Maximum Lambda Function

```
function lambda_max=longitudinal_slip_max(V);

%Vehicle system inputs%
R=0.326;

%define angular velocity input for calculating the maximum
%lambda
omega=((V-0.0001)/R):-0.01:0;

%Tire model inputs%
sigma0=100;
sigma1=0.7;
sigma2=0.011;
mu_s=0.5;
mu_c=0.35;
Vs=10.0;
L=0.25;

%Tire model
Vr=R.*omega-V;
h_Vr=mu_c+(mu_s-mu_c)*exp(-sqrt(abs(Vr./Vs)));

%-----------------------------------------------
lambda=1-(R.*omega)./V;
eta=-lambda./(1-lambda);
gamma=1-(sigma1*abs(Vr)./h_Vr);


easy1=(sigma0*L).*abs(eta);
easy2=exp(-easy1./(h_Vr))-1;

first_term=h_Vr.*(1+(gamma).*(h_Vr./easy1).*easy2);
second_term=sigma2.*Vr;

mu=first_term-second_term;

mu_max=max(mu);
[mu_max,I]=max(mu);
lambda_max=lambda(I);
```

C.2.3 Finding the Real Friction Coefficient Function

```
function mu_real=calculation_mu_real(V,slip);

%Vehicle system inputs%
R=0.326;

%define angular velocity input for calculating the maximum
%lambda
omega=((V-0.0001)/R):-0.01:0;

%Tire model inputs%
sigma0=100;
sigma1=0.7;
sigma2=0.011;
mu_s=0.5;
mu_c=0.35;
Vs=10.0;
L=0.25;

%tire model
Vr=R.*omega-V;
h_Vr=mu_c+(mu_s-mu_c)*exp(-sqrt(abs(Vr./Vs)));

%-------------------------------------
lambda=1-(R.*omega)./V;
eta=-lambda./(1-lambda);
gamma=1-(sigma1*abs(Vr)./h_Vr);

easy1=(sigma0*L).*abs(eta);
easy2=exp(-easy1./(h_Vr))-1;

first_term=h_Vr.*(1+(gamma).*(h_Vr./easy1).*easy2);
second_term=sigma2.*Vr;

mu=first_term-second_term;

if slip <= 0.001,
   mu_real=0;
   else
III = 5;
rate = 1;
while (III > 4 )
   rate = rate/5;
   I=find(lambda<slip*(1+rate) &lambda>slip*(1-rate));
   II=size(I);
```

```
   III=II(2);
end
j=I(1);
mu_real=mu(j);
end
```

Appendix D

Matlab Program for Slide Mode Controller

D.1 Main Program

```
%********** Slide mode controller development  ***********
%****All the vehicle parameters are same as those used in
%Chapter IV ****
```

```
%define global variables
global mu_max;
global deceleration;

global M;
global Ca;
global J;
global R;
global sigma_omega;
global theta;
global Kb;
global g;

global sigma0;
global sigma1;
global sigma2;
global mu_s;
global mu_c;
global Vs;
global L;

global Cav;
global Fn;
global alpha;


%simulation sampling time
t0=0;
interval=0.005;

%Vehicle system inputs%
M=415.0;
Ca=0.2749;
```

```
J=2.905;
R=0.326;
sigma_omega=0;
theta=0.6;
Kb=0.9;
g=9.81;

%initial velocity value
V0=30;
V=V0;
W=V/R;
W0=W;

%Tire model inputs%
sigma0=100;
sigma1=0.7;
sigma2=0.011;
mu_s=0.5;
mu_c=0.35;
Vs=10.0;
L=0.25;

%define parameters for vehicle dynamics
Cav=Ca/M;
Fn=M*g;
alpha=-(g+Fn*(R^2)/J);

%designed controller constant
Ka=675;

%define rho (designed contrller constant)
rho1=0.285;
rho2=0.155;

%define delta
delta=1.58;

%define matrix
tt = [];    %time
VV = [];    %velocity
ww = [];    %angular velocity
ff = [];    %brake force
PP = [];    %brake prssure
VVr= [];    %relative velocity
SS = [];    %sliding surface
Dee= [];    %deceleration;
XX = [];    %stop distance
```

```
%define initial condition for differential equation
x0=[0 V R*W-V 0];
lam_in=calculate_lambda_max(V);

%simulation loop
while x0(2)>=0.5,
   t=t0+interval;

%tire model
h_Vr=mu_c+(mu_s-mu_c)*exp(-sqrt(abs(x0(3)/Vs)));

lambda=1-(R*W)/x0(2);
eta=-lambda/(1-lambda);

%define lambda_max
  lam_out=calculate_lambda_max(V);

%define sliding mode
sliding=x0(3)+delta*lam_out*x0(2);

%define beta1 and beta2
f0=sigma0*abs(x0(3))/h_Vr;
f1=f0*x0(1);
f2=g*(sigma0*x0(1)+(sigma1+sigma2)*x0(3))-Cav*(x0(2)^2);
f3=alpha*sigma0*x0(1)+(alpha*sigma1-g*sigma2)*x0(3)...
+Cav* (x0(2)^2)-sigma_omega*(x0(2)+x0(3))/J;

beta1=-(alpha*sigma1*f1+delta*g*sigma1*f1*lam_out);
beta2=f3+delta*lam_out*f2+delta*x0(2)*((lam_out-...
lam_in)/interval);

%define psi
sat1=sliding*beta1;
if gt(sat1,1)
   sat1=1;
end
if lt(sat1,-1)
   sat1=-1;
end

psi1=rho1*sat1;

sat2=sliding*beta2/;

if gt(sat2,1)
   sat2=1;
```

```
end
if lt(sat2,-1)
   sat2=-1;
end

psi2=rho2*sat2;

%brake pressure
Pb=Ka*sliding+beta1*psi1+beta2*psi2;

if Pb>3000
   Pb=3000;
end


%solve the differential equations
options=odeset('RelTol',1e-4,'AbsTol',1e-4);
[T,x]=ode45('motionequation_slidemode',[t0 t], x0,
options, Pb);

t0=t;
x0=x(length(x),:);
V=x0(2);
W=(x0(3)+x0(2))/R
lam_in=lam_out;

%calculating the brake force
Fx=Fn*(sigma0*x0(1)+sigma1*(x0(3)-(sigma0*abs(x0(3))/ ...
h_Vr)*x0(1)*theta)+sigma2*x0(3));

%time vector
tt = [tt t0];
%velocity vector
VV = [VV x0(2)];
%angular speed vector
ww = [ww W];
%brake pressure vector
PP = [PP Pb];
%relative velocity vector
VVr= [VVr x0(3)];
%sliding surface vector
SS = [SS sliding];
%deceleration vector
Dee = [Dee deceleration];
%stop distance vector;
XX = [XX x0(4)];
```

```
end

time=3.8;

%plotting the response curves
figure(1);
plot(tt,VV);
title('Velocity vs time');
xlabel('Time  (sec.)');
Ylabel('Velocity  (m/sec.)');
axis([0 time 0 V0]);
grid;

figure(2);
plot(tt,ww);
title('Angular velocity vs time');
xlabel('Time  (sec.)');
Ylabel('Angular velocity  (m/sec.)');
axis([0 time 0 W0]);
grid;

figure(3);
plot(tt,VVr);
title('Relative velocity vs time');
xlabel('Time  (sec.)');
Ylabel('Relative velocity  (m/sec.)');
axis([0 time -5 0]);%axis([0 time -7 0]);
grid;

figure(4);
plot(tt,PP);
title('Braking pressure vs time');
xlabel('Time  (sec.)');
Ylabel('Braking pressure  (N/m^2)');
axis([0 time 0 3000]);
grid;

figure(5);
plot(tt,SS);
title('Sliding surface vs time');
xlabel('Time  (sec.)');
Ylabel('Sliding surface ');
axis([0 time 0 6]);%axis([0 time 0 10]);
grid;

figure(6);
plot(tt,Dee);
```

```
title('Brake deceleration vs time');
xlabel('Time  (sec.)');
Ylabel('Deceleration (g) ');
axis([0 time -0.9 0]);%axis([0 time -1 0]);
grid;

figure(7);
plot(tt,XX);
title('Stop distance vs time');
xlabel('Time  (sec.)');
Ylabel('Stop distance ');
axis([0 time 0 30]);%axis([0 time 0 60]);
grid;


clear;
```

D.2 Member Functions

D.2.1 Motion Equation Function

```
function dx=correct_motionequation(t,x,flag,Pb);

%define global vehicle model inputs
global M;
global Ca;
global J;
global R;
global sigma_omega;
global theta;
global Kb;
global g;

%global tire model inputs%
global sigma0;
global sigma1;
global sigma2;
global mu_s;
global mu_c;
global Vs;
global L;
```

```
global Fn;
global Cav;
global alpha;

global deceleration;

dx=zeros(4,1);  %a column vector

%define parameters%
%notice: f0=f(x3), f1=f1(X), f2=f2(X), f3=f3(X) in paper%
h_Vr=mu_c+(mu_s-mu_c)*exp(-sqrt(abs(x(3)/Vs)));
f0=sigma0*abs(x(3))/h_Vr;
f1=f0*x(1);
f2=g*(sigma0*x(1)+(sigma1+sigma2)*x(3))-Cav*(x(2)^2);
f3=alpha*sigma0*x(1)+(alpha*sigma1-g*sigma2)*x(3) ...
+Cav*(x(2)^2)-sigma_omega*(x(2)+x(3))/J;

%differential equation
dx(1)=x(3)-f1*theta;
dx(2)=f2-(g*sigma1*f1)*theta;
dx(3)=f3-(alpha*sigma1*f1)*theta-R*Kb*Pb/J;
dx(4)=x(2);

deceleration=dx(2)/g;
```

D.2.2 Finding the Maximum Lambda Function

```
function lambda_max=calculate_lambda_max(V);

%Vehicle system inputs%
R=0.326;

%define angular velocity input for calculating the maximum
%lambda
omega=(V/R-0.01):-0.01:0;

%Tire model inputs%
sigma0=100;
sigma1=0.7;
sigma2=0.011;
mu_s=0.5;
mu_c=0.35;
```

```
Vs=10.0;
L=0.25;

%tire model
Vr=R.*omega-V;
h_Vr=mu_c+(mu_s-mu_c)*exp(-sqrt(abs(Vr./Vs)));

lambda=1-(R.*omega)./V;
eta=-lambda./(1-lambda);
gamma=1-(sigma1*abs(Vr)./h_Vr);

easy1=(sigma0*L).*abs(eta);
easy2=exp(-easy1./(2.*h_Vr))-1;

first_term=h_Vr.*(1+(2.*gamma).*(h_Vr./easy1).*easy2);
second_term=sigma2.*Vr;
mu=first_term-second_term;

mu_max=max(mu);
lambda_max=lambda(I);
```